Study of the Thermal Performance of Metal Foam and PCM Composite for Thermal Energy Storage

Xusheng Hu

▶ **To cite this version:**

Xusheng Hu. Study of the Thermal Performance of Metal Foam and PCM Composite for Thermal Energy Storage. Materials. Université de Technologie de Troyes, 2021. English. NNT : 2021TROY0003 . tel-03808728

HAL Id: tel-03808728

https://theses.hal.science/tel-03808728

Submitted on 10 Oct 2022

HAL is a multi-disciplinary open access archive for the deposit and dissemination of scientific research documents, whether they are published or not. The documents may come from teaching and research institutions in France or abroad, or from public or private research centers.

L'archive ouverte pluridisciplinaire **HAL**, est destinée au dépôt et à la diffusion de documents scientifiques de niveau recherche, publiés ou non, émanant des établissements d'enseignement et de recherche français ou étrangers, des laboratoires publics ou privés.

Thèse
de doctorat
de l'UTT

Xusheng HU

Study of the Thermal Performance of Metal Foam and PCM Composite for Thermal Energy Storage

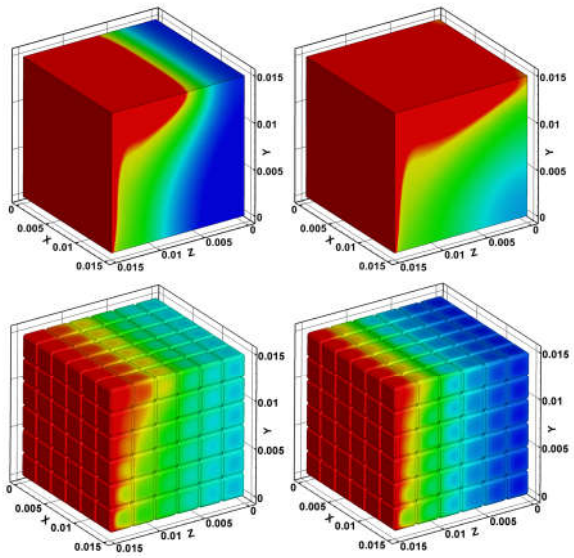

Champ disciplinaire :
Sciences pour l'Ingénieur

2021TROY0003

Année 2021

utt
UNIVERSITÉ DE TECHNOLOGIE
TROYES

THESE

pour l'obtention du grade de

DOCTEUR
de l'UNIVERSITE DE TECHNOLOGIE DE TROYES

en SCIENCES POUR L'INGENIEUR

Spécialité : MATERIAUX, MECANIQUE, OPTIQUE, NANOTECHNOLOGIE

présentée et soutenue par

Xusheng HU

le 19 janvier 2021

Study of the Thermal Performance of Metal Foam and PCM Composite for Thermal Energy Storage

JURY

M. Rezak AYAD	PROFESSEUR DES UNIVERSITES	Président
M. Tarak BEN ZINEB	PROFESSEUR DES UNIVERSITES	Rapporteur
M. Olivier SICOT	MAITRE DE CONFERENCES - HDR	Rapporteur
Mme Xiao-Jing HU	PROFESSEURE DES UNIVERSITES	Examinatrice
M. Abdelatif MERABTINE	DOCTEUR	Examinateur
M. Yishi SU	ASSOCIATE PROFESSOR	Examinateur
M. Xiao-Lu GONG	PROFESSEUR DES UNIVERSITES	Directeur de thèse

Acknowledgements

The study and research in France are meaningful and precious for me. The China Scholarship Council (CSC) provides a scholarship to support my academic research. The University of Technology of Troyes (UTT) provides a good study and research environment for all students. I would like to express my deepest gratitude to them.

I would like to express my sincere appreciation to my supervisor, Prof. GONG Xiao-Lu, for his patient guidance and constant support during the past three years. With his guidance and help, I quickly understand my research field and gradually become an independent researcher. No matter what problems I encounter, he works with me until the problem is solved. Due to his broad knowledge, he can provide many constructive suggestions for my research. His positive attitude for work and life motivates me to move forward. I will remember this unforgettable time.

I specially thank the president of the committee, Prof. R. AYAD, for his organization of the defense. I am very grateful to Prof. T. BEN ZINEB and Dr. O. SICOT for their reviews on my thesis, despite their busy agenda. I would like to thank the members of the jury, Prof. X-J. HU, Prof. Y.S. SU, Dr. A. MERABTINE, for their attendance in my defense. Thanks to all for their selfless help.

I would like to thank all the administrative staff: Isabelle LECLERCQ, Pascale DENIS, Therese KAZARIAN, Celine DETURCHE, et al. I deeply appreciate their enthusiastic help during my PhD study. I want to thank Dr. ZHU Feng for his help in my scientific research. I thank my friends and colleagues at UTT, who are very genial and enthusiastic. I thank them for their help and encouragement.

I would like to sepecially thank Prof. FAN Shidong for his support to my study abroad. I am very grateful to my parents for their love and waiting for me. I thank my wife very much for her company. She brings pleasure and sweetness to my life.

HU Xusheng

Abstract

The aim of this Ph.D. thesis is to study the thermal performance of metal foam and phase change material (PCM) composite by using experimental and numerical methods, in which metal foam possesses a cubic cell structure and is fabricated by 3D printing technique. Firstly, the effects of contact and heat conditions on heat storage rate of PCM composite are investigated to provide theoretical guidance for the practical application of PCM composite in thermal energy storage (TES) system. Then the metal foam with a cubic cell structure is designed and fabricated by 3D printing. The experimental investigation is carried out to examine the melting evolution of PCM embedded in metal foam. Meanwhile, the pore-scale numerical method is also proposed and used to investigate heat transfer characteristics inside the PCM composite. It is found from the results that the embedding metal foam can short the total melting time of PCM. Considering the influence of morphology parameters of metal foam, the thermal behavior of metal foam with different porosities and pore densities is numerically studied. The last part of this thesis explores the application of metal foam in PCM based heat sink. The thermal response of heat sinks using PCM composite is obtained by experimental tests, including base temperature, temperature variation, operating time and enhancement ratio of operating time. Also, the effects of the porosity of metal foam and the power level of the heater on the thermal response of heat sink are investigated.

Keywords: Metal foams; Metallic composites; Three-dimensional printing; Thermal analysis; Heat storage; Simulation methods

Résumé

Le but de cette thèse est d'étudier les performances thermiques d'une mousse métallique ainsi que de ses composites avec un matériau à changement de phase (MCP) en utilisant des méthodes expérimentales et numériques. La mousse métallique étudiée possède une structure cellulaire cubique. Les effets des conditions de contact et de chaleur sur le taux de stockage de chaleur dans le composite MCP sont d'abord simulés numériquement. Ensuite, la mousse métallique avec une structure cellulaire cubique est conçue et fabriquée par impression 3D. L'étude expérimentale permet par la suite d'observer l'évolution de la fusion du MCP introduit dans la mousse métallique. Parallèlement, une méthode numérique à l'échelle des pores est utilisée pour simuler les caractéristiques de transfert thermique dans le composite MCP. Il ressort des résultats que la mousse métallique d'enrobage peut réduire le temps total de fusion du matériau MCP. Compte tenu de l'influence des paramètres de morphologie de la mousse métallique, nous avons étudié numériquement le comportement thermique de la mousse métallique en variant la porosité et la densité de pores. La dernière partie de cette thèse consiste à explorer une application de la mousse métallique dans les dissipateurs thermiques à base de MCP. Les essais expérimentaux sur composite MCP permettent d'obtenir la réponse thermique des dissipateurs thermiques. Les effets de la porosité de la mousse métallique et de la puissance du chauffage sur la réponse thermique du dissipateur thermique sont également mis en évidence.

Mots-clés : Mousse métallique; Composites à matrice métallique; Impression 3D; Analyse thermique; Chaleur -- Stockage; Simulation, Méthodes de

Table of contents

Glossaries

Symbols

A_m	mush constant
a	ligament thickness, m
B	correlation coefficient
C	inertial coefficient, 1/m
c	specific heat capacity, J/kg K
d_p	cell pore diameter, m
E	energy, J
e_r	enhancement ratio
Gr	Grashof number
g	gravitational acceleration, m/s^2
h	heat transfer coefficient, W/m^2 K
K	permeability, m^2
k	thermal conductivity, W/m K
L	latent heat of PCM, J/kg
l	ligament length, m
m	mass, kg
p	pressure, Pa
$\dot{q}$	heat generation rate, W/m^3
S	source term
T	temperature, K
T_{m1}	solidus temperature, K
T_{m2}	liquidus temperature, K
t	time, s
Nu	Nusselt number
u, v	velocity in x and y direction, m/s
V	volume, m^3

Greek symbols

β	liquid fraction in pore
δ	contact gap, m
ε	porosity of metal foam
γ	thermal expansion coefficient, 1/K
φ	liquid fraction of PCM composite
μ	dynamic viscosity, kg/m s
ρ	material density, kg/m^3
ω	pore density

Subscripts

ave	time-average
eff	effective value
f	paraffin
m	melting
i	initial
p	pore
s	metal foam
total	total melting
w	wall

Abbreviations

ppi	pore number per inch
PCM	phase change material
SLM	selective laser melting
TES	thermal energy storage
TM	thermal management
TCE	thermal conductivity enhancer

Introduction

Phase change material (PCM) is an ideal energy storage material. Due to the considerable heat of fusion, PCM can store a large amount of energy with small temperature variation during the phase change process. Therefore, their application is extensive in thermal energy storage (TES) and thermal management (TM) system. However, most of the available PCMs have lower thermal conductivities, which decreases the heat storage and release rates and limits their wide application in the engineering field. To overcome this disadvantage, many enhancement methods were proposed and studied. Embedding metal foam in PCM is proved to be an effective method for enhancing the thermal conductivity of PCM. Therefore, the investigation of thermal behavior of PCM composite using the metal foam with a stochastic topology structure has been extensively conducted in the past decade. However, the studies of PCM composite using the metal foam with periodic cell structure are relatively rare.

At present, the commercial metal foam with stochastic topology structure is manufactured by the conventional manufacturing methods, such as electro-deposition method, powder metallurgy method, investment casting method, infiltration casting method, etc. Whereas, morphology structure of metal foam is difficult to be controlled by these manufacturing methods. Additive manufacturing, as one of advanced manufacturing technology, provides a possibility to fabricate the metal foam quickly and precisely with periodic cell structure based on the customization or optimization model. The metal foam with periodic cell structure is a promising material, which can be used as a thermal conductivity enhancer (TCE) to heighten the thermal behavior of PCM. Hence, the study of the thermal characteristics of PCM embedded in the metal foam with periodic cell structure fabricated by 3D printing technique is very significant.

In the thesis, the effects of heat and contact conditions on heat storage rate of

PCM composite for thermal energy storage are firstly explored. Then, the design and manufacture of metal foam with cubic periodic cell structure are presented. The thermal characteristics of PCM composite using metal foam with cubic cell structure are experimentally and numerically investigated. The numerical studies of the effects of porosity and pore density of metal foam on the thermal behavior of PCM composite are also carried out. In general, the potential application of metal foam fabricated by 3D printing technique in TES and TM system is presented in the thesis.

Chapter 1 describes a bibliographic study of metal foam and PCM composite for the thermal engineering field. The manufacturing methods of metal foam and the enhancement methods of the thermal performance of PCM are introduced. Furthermore, the literature review summarizes the application of PCM composite in thermal energy storage and thermal management, such as solar energy, energy-efficient building, electronic devices, cold energy storage and transport, etc.

In chapter 2, the effects of heat and contact conditions on the thermal performance of PCM composite for thermal energy storage are considered. Nine different heat and contact conditions are established to study the melting evolvement and heat transfer mechanism of PCM composite. Based on the volume-averaged method, the equilibrium temperature energy model is used to investigate the thermal characteristics of composite PCM under different heating and contact conditions, in which the thermal characteristics include solid-liquid interface, liquid fraction, velocity, total melting time and average heat storage rate.

In chapter 3, metal foam with cubic periodic cell structure is designed and fabricated, in which additive manufacturing (AM) as an advanced manufacturing technology can achieve the fast and precise fabrication of metal foam with a controlled structure. A visualized experiment setup is built to explore the thermal performance of metal foam/PCM composite, including solid-liquid interface, temperature variation, and total melting time. To further study the heat transfer characteristics of PCM composite, a three-dimensional numerical model is developed based on the pore-scale

numerical simulation method.

In chapter 4, metal foam with cubic cell structure is used to enhance the thermal performance of PCM. The employed metal foam not only possesses high thermal conductivity, high porous structure and low relative density but also can be rapidly manufactured by additive manufacturing technology. Thus, it is an excellent candidate used as metal matrix of composites. The pore-scale numerical method is employed to simulate the melting evolution of PCM composite. The studies of the effects of geometrical parameters of metal foam (i.e., porosity and pore density) on the thermal behavior of PCM composite are undertaken.

In chapter 5, the metal foam with cubic cell structure used as thermal conductivity enhancer is designed and fabricated to improve the heat transfer performance of PCM based heat sink. 3D printing technology is adopted to enable the fast and precise fabrication of metal foam with periodic cell structure. The commercial paraffin wax is selected as PCM. A plate heater is used to mimic the heat generation of the electronic component. The thermal response of heat sink using metal foam with different porosities (80%, 85%, 90%, and 95%) is examined at three heating power levels (8 W, 10 W, and 12 W).

In the end, the conclusions of this thesis are summarized, and some perspectives are provided for future studies.

Chapter 1.

Bibliography

Chapter 1. Bibliography

1.1 Introduction

Metal foams are a new class of porous material and possess novel physical, mechanical, thermal, electrical, and acoustic properties. The study of metallic foams could date from the 1940s when Sosnick [1] applied for a patent on a production method concerning the vaporization of low melting point constituents of metallic alloys. Then the research on the production and performance of porous metals was developed [2, 3]. Metal foam has many advantages, such as low density, larger specific area, and high specific strength/stiffness. Thus, the characteristics of metal foam are a research topic attracting extensive attention [4, 5], and their various industrial applications are also being explored [6, 7] in current years. For instance, metal foams are widely applied in many engineering fields, including electromagnetic shielding [8], aerospace [9], heat exchanger [10], electrochemistry [11], and silencer [12].

Due to the greenhouse effect caused by fossil fuel depletion, energy crisis and environmental pollution are becoming more and more severe in recent years [13]. As a result, energy-saving and high-efficiency energy utilization technology attract intensive attention [14]. Phase change material (PCM) is a new energy storage material. Due to its large melting latent heat, PCM can store a large amount of storage with a small temperature variation during the phase change process [15, 16]. While most of the available PCMs have low thermal conductivities ranging from 0.1 to 1 W/m k, which hinders their wide application. To overcome this disadvantage, many enhancement methods were proposed and investigated [17, 18]. The embedding metal foam is proved to be an effective method for enhancing the thermal behavior of PCM.

In this section, the manufacturing methods of metal foam and applications of PCM composite are presented. Firstly, three manufacturing methods of metal foam are introduced. Then four different enhancement methods for the thermal performance of PCM are described. The third part describes the application of PCM composite in thermal energy storage system. Finally, the usage of PCM composite in thermal management system is reviewed.

1.2 Manufacturing methods of metal foam

According to the pore structure, metal foam can be mainly classified into two categories: closed-cell foam and open-cell foam, as shown in Fig. 1.1. With the development of manufacturing techniques, there are many methods proposed and used for the manufacturing of metal foam. In the following sections, the manufacturing methods of open-cell metal foam are introduced. For instance, selecting the removable particles as the preform, namely infiltration casting method, manufactures open-cell metal foam. Additive manufacturing (i.e., 3D printing) as one of the advantage manufacturing techniques can also be used to fabricate the open-cell metal foam.

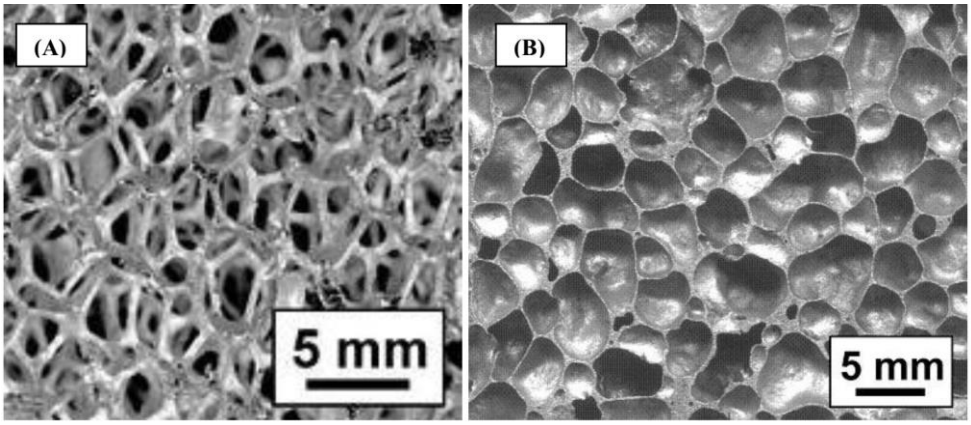

Fig. 1.1. (a) open-cell and (b) closed-cell metal foam [19]

1.2.1 Infiltration casting method

As a traditional manufacturing method, the infiltration casting technique is employed for the fabrication of metal foam. This method can be used to manufacture Al, Mg, Sn, Pb, and Zn metal foams [20]. The advantage of this method is the low price. The schematic diagram of infiltration casting method is presented in Fig. 1.2. Firstly, the inorganic particles, such as salt particles, are randomly stacked in the mold. Then the molten metal is injected into the mold. The molten metal penetrates the voids of preform. It is worth noting that the preform needs to be preheated to avoid premature solidification of metal. The negative pressure should be provided under the mold to make the molten metal quickly penetrate the voids of preform. The molten metal fast

fills the space between the salt particles under the action of negative pressure. After the solidification and cooling, the dissolvable particles need to be removed. For example, salt particles can be dissolved by using water. Finally, the open-cell metal foam with interconnected structures is successfully fabricated.

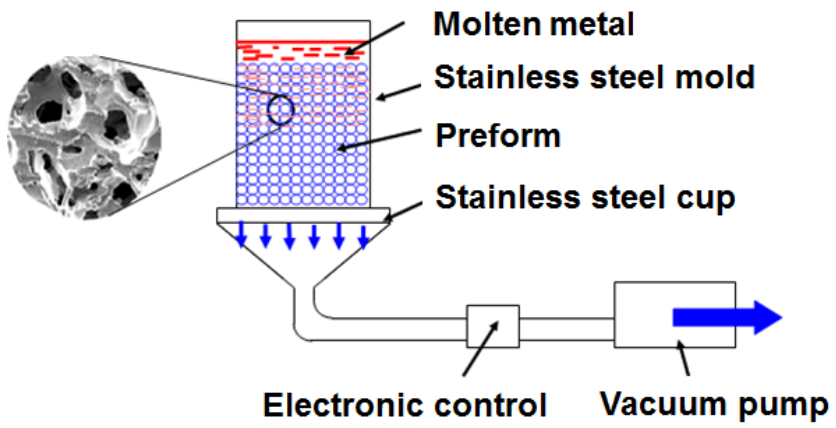

Fig. 1.2. Schematic diagram of infiltration casting method [21]

1.2.2 Improved infiltration casting method

According to the introduction in the above section, it is found that the morphology structure of metal foam fabricated by infiltrated casting mainly depends on the preform. The preform is made of salt particles in the form of a random stack. Therefore, metal foam manufactured by the infiltration cast method possesses a random pore structure. Also, the pore size of this metal foam is difficult to be controlled. In order to obtain metal foam with the controllable structure and size, the improved infiltration casting method is developed. The improved infiltration casting method is the combination of 3D printing technique and infiltration casting method.

Fig. 1.3 shows the manufacturing process of mold. Firstly, the mold with controllable structure is designed and modelled by CAD software. Then the 3D model of mold is set to STL format file. This format is available for the specific software used for 3D printing machine, which can cut into slices to get a new file containing each layer's information. The 3D model is transferred to the 3D printing machine for fabrication. The mold is made of plaster and produced layer by layer by binder jetting

on power bed. After the mold is fabricated, a fine cleaning is required to remove the plaster powder remained in the pore of mold, which is conducive to obtaining good open-cell metal foam. In order to obtain the preform with a large size, several molds need to be connected and fixed.

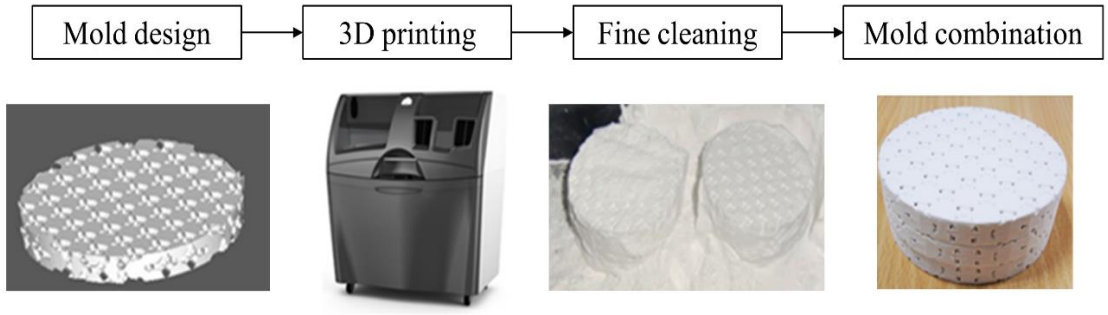

Fig. 1.3. Manufacturing process of mold using 3D printing [22]

The preparation of metal foam is similar to the above infiltration casting method. Firstly, plaster preform is placed in stainless steel mold. Before molten metal is poured, the preform and mold should be preheated to avoid the decline of the fluidity of liquid metal. The infiltration casting process should be under a negative pressure condition, which is conducive to filling molten metal in the voids of preform. After the metal solidifies and cools, the preform needs to be removed from the pore of metal foam. Some physical and chemical methods can be used to remove the preform, such as vibration, heating, and chemical material. Finally, this method can achieve the manufacturing of metal foam with a controlled structure, as shown in Fig. 1.4.

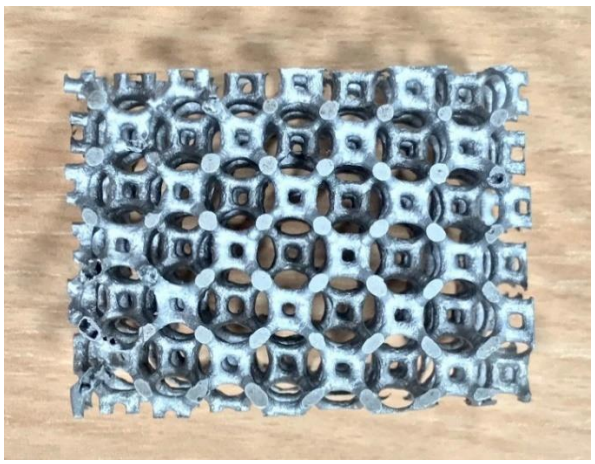

Fig. 1.4. Metal foam fabricated by the improved infiltration casting method

The advantage of this improved method is that the morphology structure of metal foam can be controlled by the preform. Furthermore, the pore shape and size within metal foam can be freely designed and optimized according to the requirement. Besides, if several plaster molds with different porosities or pore densities are connected, the metal foam with different porosities or pore densities can also be manufactured. Hence, it is immensely significant that graded metal foam can be fabricated using this improved infiltration casting method.

1.2.3 Additive manufacturing

The conventional methods for manufacturing open-cell metal foam mainly include infiltration and replication process, electro-deposition and vapor deposition. The shape and size of the pores could be adjusted by changing the related parameters of these manufacturing processes. But we only can achieve a random porous structure. Whereas additive manufacturing (AM) techniques can fabricate metal foams with a controllable porous structure. Among metal-based AM techniques, selective laser melting (SLM) and electron beam melting (EBM) can be used to manufacture the metal structure with complex configuration [23].

Fig. 1.5 shows a schematic diagram of SLM mechanism [24]. It mainly composes the build platform system, powder delivery system, laser system and scanner system. The main steps for fabricating a complicated porous metal from a digital CAD file to a real structure, as follows: (1) a 3D model of metal foam is built in CAD software to represent the actual structure, and CAD file of 3D model needs to be translated to the available file format (i.e., STL format) for AM machine. (2) the STL file, including geometrical information of metal foam, is sliced into multiple layers at a prescribed thickness and orientation in the particular software of AM machine. After the machine copies the manufacturing instructions, the powder is deposited on the plate, and the laser scanning begins work. (3) a new layer of powder is deposited on the top of the previous layer after scanning one layer. The manufacturing process continues until the last layer is completed. (4) After unloading the build plate from the machine, loose

powder and typical support structure are removed, and the 3D printed part is cleaned. Commonly a heat treatment is also performed to reduce internal stresses and improve the material properties.

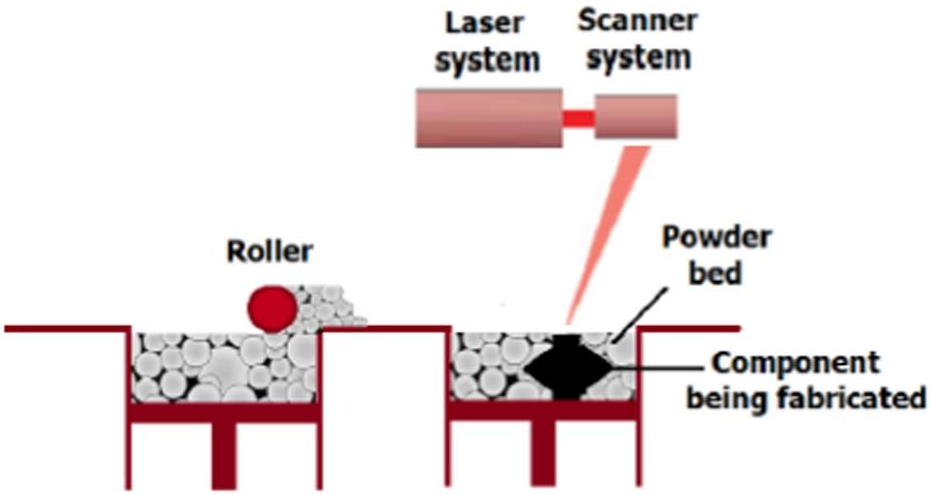

Fig. 1.5. Schematic diagram of SLM technology process [24]

The metal foams fabricated by SLM are shown in Fig. 1.6, as found in Ref. [25]. It is found that this method can directly and quickly manufacture the porous metal structure. The shape and size of the pores within metal foam can be freely designed and generated by 3D printing. The pore density and porosity of metal foam fabricated by 3D printing can also be more accurately controlled compared with that made by the traditional manufacturing method. The new manufacturing method is conducive to the wide application of metal foam in the industry and engineering fields. Besides, based on 3D printing technique, the optimization design of metal foam can be achieved.

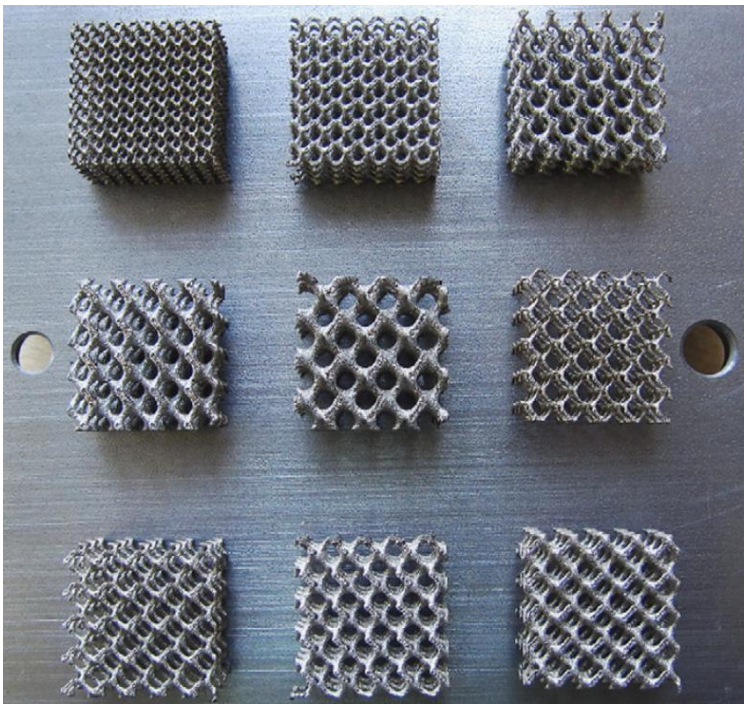

Fig. 1.6 Metal foam fabricated by the SLM technique [25]

1.3 Thermal performance enhancement of phase change material

Phase change materials (PCM) are widely utilized in thermal energy storage (TES) system [26] and thermal management (TM) system [27] owing to their large latent heat and capabilities of almost keeping constant temperature during the phase change process. The thermo-physical properties of six different phase change materials, including organic and inorganic PCMs, have been summarized in Table 1.1. It is found from thermal characteristics data that the organic and inorganic PCMs have low thermal conductivities. This disadvantage seriously hinders the heat transfer rate of PCMs in TES and TM systems [28]. Hence, a large number of investigations on heightening the thermal conductivities and heat transfer rate of PCMs are carried out using experimental and numerical methods [29, 30]. This section presents the recent progress of the studies on thermal performance enhancement of PCMs. Some enhancement methods can be used to improve the thermal behavior of PCMs, in which embedding metal foams have been proved to be a promising approach for heat transfer enhancement of PCMs.

Table 1.1 Thermal properties of various PCMs [28, 31]

Materials	Melting point, °C	Latent heat, kJ/kg	Density, kg/m^3	Specific Heat kJ/kg K		Thermal conductivity W/m K	
				Solid	liquid	Solid	Liquid
Formic acid	8	277	1227	1.00	1.17	0.30	0.27
Acetic acid	17	192	1214	1.33	2.04	0.26	0.19
Paraffin wax	0-90	150-250	880-950	3.00	2.00	0.20	-
water	0	333	920	3.30	4.18	1.60	0.61
Sodium acetate	58	265	1450	1.68	2.37	0.43	0.34
Magnesium nitrate	89	140	1640	2.50	3.10	0.65	0.50

1.3.1 Nanomaterial additive

Elgafy and lafdi [32] conducted the experimental and analytical investigation on the thermal performance of paraffin wax adding carbon nanofibers, including the measurement of transient temperature and the prediction of cooling rate. They found that the thermal conductivity of PCM nanocomposite was enhanced significantly. Moreover, an analytical model was proposed based on one-dimensional heat conduction method to predict the effective thermal conductivity for the new nanocomposite. Its findings showed good agreement with the experimental data. Ramakrishnan et al. [33], in an experimental study, further developed a novel paraffin/hydrophobic expanded perlite form-stable PCM composite for increasing heat transfer performance. In their research, various high conductive carbon-based additives, such as graphite (G), carbon nanotubes (CNT) and graphene nanoplatelets (GNP), were integrated into form-stable PCM composite. An ultrasonic bath was employed to disperse the carbon additive in acetone, and a homogenous suspension was obtained, as depicted in Fig. 1.7. The results show that three additives possess a good chemical compatibility, and can obviously improve thermal conductivity of PCM

composite, e.g., the usage of 0.5wt% G, CNT and GNP achieve thermal conductivity improvement of 45%, 30% and 49%, respectively.

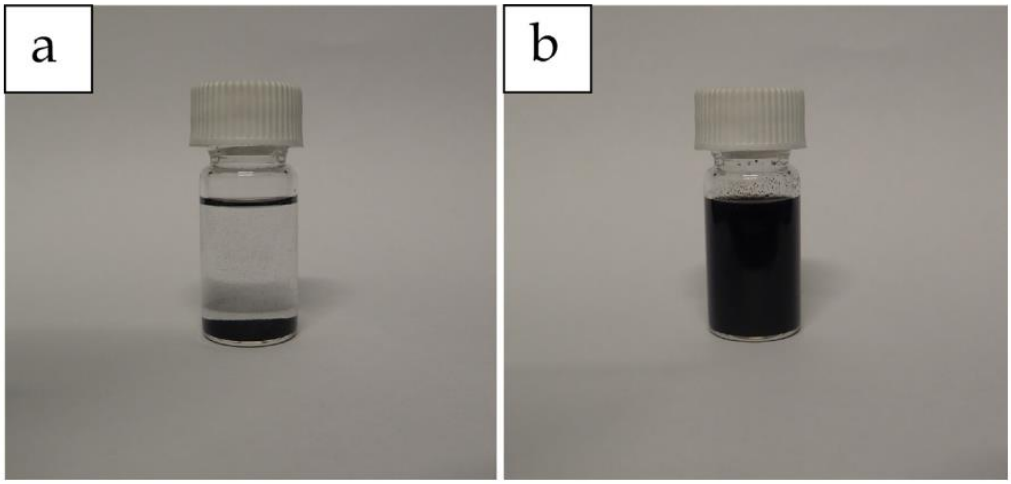

Fig. 1.7. Dispersion of CNT in acetone using an ultrasonic bath (a) before dispersion and (b) after dispersion [33]

In addition to carbon-based additives, the high thermal conductivity metallic nanoparticles can also be used as an additive to improve the thermal performance of phase change material. Ho and Gao [34] carried out the experimental tests for obtaining effective thermophysical properties of phase change material dispersed alumina nanoparticles, including latent heat of fusion, density, dynamic viscosity, and thermal conductivity. It is found that the use of alumina nanoparticles can achieve an increase in thermal conductivity of paraffin. It is noted that the rise in effective thermal conductivity of paraffin is nonlinear with the mass fraction of nanoparticles. Moreover, the dispersing Al_2O_3 nanoparticles in paraffin leads to increased dynamic viscosity compared to the pure paraffin. Venkitaraj and Suresh [35], in the experiment, investigated the influence of Al_2O_3, CuO and TiO_2 nanoparticles on the thermal characteristics of phase change material. They reported that the usage of nanoparticles causes a decrease in the supercooling during the discharge process. The thermal conductivities of PCM present the improvement of about 20.9%, 7%, and 14.1%, corresponding to 0.1 wt.% of Al_2O_3, TiO_2 and CuO nanoparticles.

1.3.2 Expanded graphite

Expanded graphite (EG) possesses high thermal conductivity and good chemical stability in both low temperature and high temperature region. EG could be employed for improving effective thermal conductivity not only for the low temperature organic PCMs (e.g. paraffin [36], glycol [37], stearic acid [38] and mannitol [39], but also for the high temperature salts PCMs (e.g., chloride [40] and nitrate [41]).

In low temperature field, Zhang and Fang [42] studied the paraffin/expanded graphite composite phase change thermal energy storage materials, in which PCM composite was prepared by impregnating the paraffin into expanded graphite. The SEM micrographs of the expanded graphite/paraffin PCM composite are shown in Fig. 1.8. They reported that the prepared paraffin/expanded graphite composite has a larger thermal conductivity and doesn't occur the liquid leakage during the solid-liquid phase change. Py et al. [43] explored the behavior of paraffin infiltrated in expanded graphite, and results represented the effective thermal conductivities of PCM composite can be improved up to 70 W/m K.

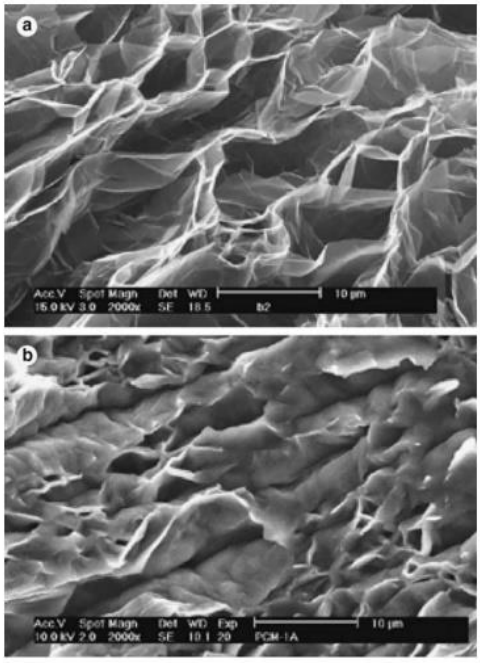

Fig. 1.8. SEM micrographs of: (a) expanded graphite and (b) paraffin/expanded graphite PCM composite [42]

In high temperature field, Pincemin et al. [44] experimentally investigated the thermal characteristics of PCM composite that is made of graphite and PCM ($NaNO_3/KNO_3$ eutectic). At both the laboratory and industrial scales, the thermal properties of PCM composites prepared using different elaboration routes and graphite are compared in terms of thermal conductivities, thermal capacity and stability. It was found that the dispersion of graphite can enhance the thermal performance of molten salt. At the same time, the thermal conductivity showed a decrease with the increase of the temperature. Xiao et al. [45] prepared expanded graphite/nitrate composite and examined the thermal properties of PCM composite with the different mass fraction EG. The experimental results indicated that adding EG can obviously heighten the thermal conductivities. For instance, the thermal conductivities of sodium nitrate using 20 wt.% EG were measured and improved up to 6.66-7.70 W/(m K) in the temperature range of 20-120 ℃, which was about seven times as much as those of pure sodium nitrate.

1.3.3 Metal fin

Metal fin has been proved to be an efficient approach for the thermal performance enhancement of PCM that is used for thermal energy storage and thermal management system [46, 47]. The materials for fins are some metals with high thermal conductivity, such as aluminum [48], copper [49], steel [50], nickel [51] etc. The thermal characteristics of four metal materials are listed in Table 1.2. The method using metal fin can achieve the enhancement in thermal performance by extending the heat transfer surface between metal fin and phase change material and increasing the effective thermal conductivity.

Table 1.2 Thermal-physical properties [50, 51]

Properties	Copper	Aluminum	Steel	Nickel
Density (kg/m^3)	8978	2719	3409	8900
Thermal conductivity (W/m K)	387.6	130	60.5	91.7
Specific heat capacity (J/kg K)	381	871	434	460.6

For thermal energy storage, Sathe and Dhoble [52] carried out a numerical study on the thermal behavior of finned PCM containers for solar thermal system, considering the effect of inclined angle. The results showed that the melting time for all cases increases with the decrease in inclination angles and the addition of a number of extended surfaces. Kamkari and Shokouhmand [53] experimentally investigated the melting characteristics of phase change material with and without metal fins. The temperature results revealed that the thermally stratified zone became smaller with the increase in the numbers of fins. It was found that the rise of fins reduces the melting time and increases the total heat transfer rate, while the surface-averaged Nusselt number reduces.

For thermal management system, Nayak et al. [54] conducted a numerical investigation of heat sink with phase change material and fin structure, and the thermal behavior of heat sinks with the different volume fraction of metal fins was also studied. The results revealed that convection plays a vital role in temperature uniformity during the phase change process. The thermal behavior can be improved by distributing the metal fins within PCM in the form of thinner fins. Baby and Balaji [55] implemented an experiment to study the performance of PCM based heat sinks with various types of fins (i.e., plate-pin and pin-fins). It found that the base temperature of heat sink using pin-fin is lower compared to that using plate-fin with the same volume fraction, which is owing to its availability of a larger surface area. Hosseininizadeh et al. [56] carried out experimental and numerical investigations on thermal behavior of PCM-based heat sinks with the different configurations of internal fins, in which the effects of the number of fins, fins height and fin thickness were studied. For instance, the PCM-based heat sink with the different number of fins is compared to that without fins, as shown in Fig. 1.9.

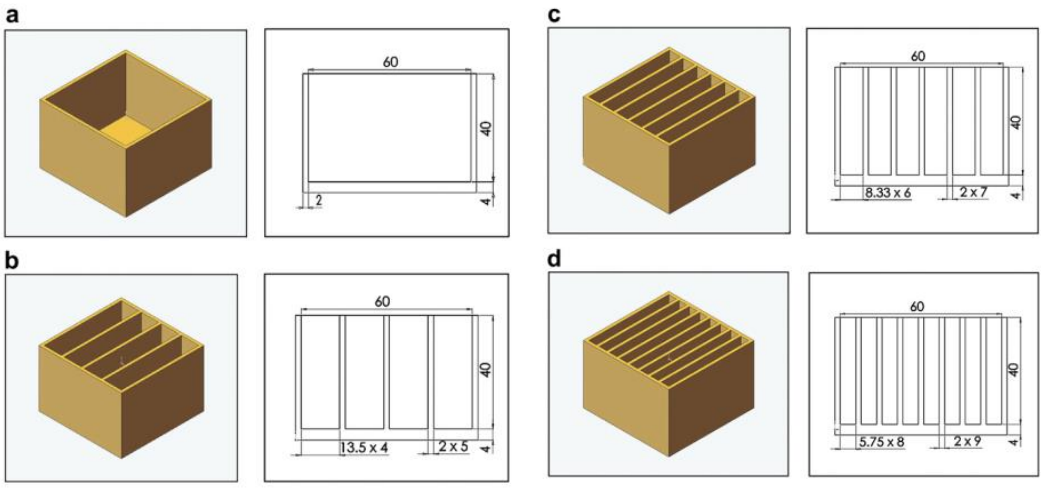

Fig. 1.9. Heat sinks with the different number of fins (a) without fin, (b) 3 fins, (c) 5 fins and (d) 9 fins [56]

1.3.4 Metal foam

Metal foam not only has high thermal conductivity but also possesses a lager specific surface [57, 58]. Hence, metal foam is a good heat transfer enhancer that can be used for the improvement of the thermal performance of PCM. Zhao et al. [59] carried out an experimental study on heat transfer enhancement of thermal energy storage using metal foam impregnated with PCM. They found that the addition of metal foam could increase the overall heat transfer rate by 3-10 times. Zhao and Wu [60] experimentally examined the enhancement in the thermal performance of PCM by using metal foams and expanded graphite. The results show that the heat transfer rate can be significantly improved by metal foam and expanded graphite. Furthermore, the overall performance of metal foams is superior to that of expanded graphite.

Lafdi et al. [61] conducted an experimental investigation on the heat transfer characteristic of phase change material embedded in metal foam. It is reported that the geometry parameters of metal foam have a noticeable influence on the heat transfer behavior of PCM. For instance, by the usage of higher porosity or bigger pore size aluminum foams, the steady-state temperature was reached faster in comparison with that using lower porosity or smaller pore size. Xiao et al. [62] prepared paraffin/metal foam composite and examined the thermal properties of PCM composite by the

experimental method. They found that the thermal conductivity of PCM can be distinctly improved, e.g., the thermal conductivities of composite with nickel foam was almost three times that of pure paraffin.

Yang et al. [63] experimentally investigated the solidification of water embedded in open-cell metallic foams with graded configuration and different materials, as shown in Fig. 1.10. The results indicated that the gradient of metal foam could affect the solidification rate and total solidification time. Moreover, they found that for the cooling boundary placing the high thermal conductivity foam (e.g., Cu) can achieve a further enhancement in thermal performance. Zhu et al. [64] designed the finned metal foams with a graded structure to heighten the energy storage efficiency of PCM. The numerical simulation was employed to investigate the effects of structural parameters on the energy storage of PCM. The results showed that finned metal foam could reduce the overall melting time. The highest average power of energy storage was obtained when the thickness of metal fin and the porosity gradient were 5 mm and 3%.

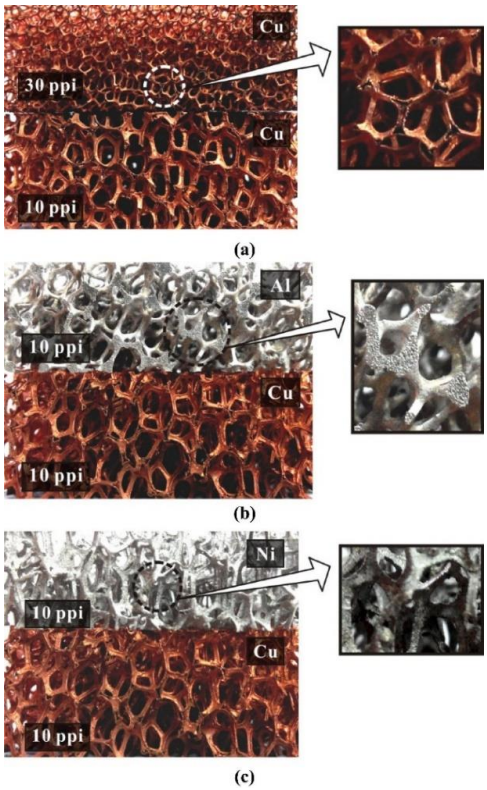

Fig. 1.10. Metal foams with graded pore morphologies: (a) copper foam with 10 and 30ppi, 10ppi copper foam with (b) aluminum foam and (c) nickel foam [63]

1.4 Application of PCM composite in thermal energy storage

With the deepening of the energy crisis and more serious environmental pollution, renewable energy resources and low-carbon eco-city development are being paid more and more attention in recent years. As a consequence, researchers pay extensive attention to the development of renewable energy resources, in which thermal energy storage plays a vital role in storing and release energy [26, 65]. Due to the high energy storage density and good thermal stability, PCM is widely used in the TES system, such as solar energy [66], energy-efficient building [67] and waste heat recovery [68].

1.4.1 Solar energy

Solar energy is a promising renewable energy source, considering its cleanliness and abundance in many parts of the world [69]. Due to the discontinuous nature of solar energy, the usage of thermal energy storage plays a vital role in the solar energy system to augment the operating hours of the energy storage system [66, 70]. Latent heat storage is a usual form of thermal energy storage, and latent heat energy storage for solar application attracts more attention due to its compactness, high energy storage density and steady operating temperature [71]. Hence, PCM, as a promising energy storage material, could be used for latent heat energy storage in the solar energy system, such as solar water-heating [72] and solar collector [73].

The solar water heater is the common equipment of solar energy collection because they are relatively cheap and straightforward to manufacture and maintain. Solar energy is stored within PCM in the form of latent heat, as reported in the literature [74, 75]. The working process of the solar water heater is as follows. For the solar water heater, the hot water is withdrawn and is substituted by cold water that absorbs energy from PCM. Due to the energy release, the PCM completes phase change from liquid to solid. Prakash et al. [76] studied the thermal performance of a new type of solar water heater that used a layer of PCM at the bottom. The PCM layer

is introduced to get hot water during off-sunshine hours.

The solar collector is a unique energy exchanger, which can convert solar irradiation energy either to thermal energy in the solar thermal application [77] or to electronic energy directly in photovoltaic application [78]. Fig. 1.11 shows two different types of solar collectors [79]. In the first type of collector, the traditional tank is replaced by PCM-integrated ones, as displayed in Fig. 1.11(a). A new solar thermal system was proposed, namely solar domestic hot water, which contains a PCM node in the heat transfer fluid primary solar loop, as shown in Fig. 1.11(b). The PCM node is between the collector and storage tank. This design can increase solar fraction by 8% in summer and 4% in winter compared to the traditional water-based solar thermal system.

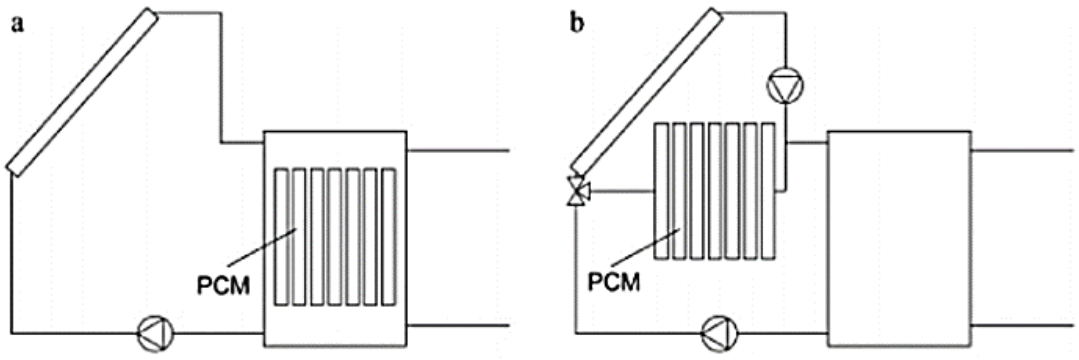

Fig. 1.11. Utilization of PCM in the solar thermal systems: (a) PCM integrated into the tank and (b) PCM node between the collector and the tank [79]

1.4.2 Building

PCMs have been employed for thermal storage in buildings filed before 1980 due to their high latent heat, stable chemical properties, incorporation and compatibility with building materials [80]. PCMs can be directly incorporated into the building structure, such as wallboards [81], ceiling boards [82] and floors [83] by microencapsulated and macroencapsulated methods. The aim of the usage of PCMs in the building is the storage or release of energy under different requirements. In the engineering application, the storage and release of energy are necessary to match

availability and demand concerning time and power.

Fig. 1.12 presents the basic concept for temperature control using PCM integrated into the building structure [84]. As it is seen, excess heat of the room can be stored in the PCM to maintain a lower room temperature during the high-temperature period throughout the day. Stored heat could be removed by active or passive heat exchange during the low-temperature period of the day, such as night or morning. Besides, it can be found that the microencapsulated PCM is usually incorporated for wallboards, while the macroencapsulated PCM is mainly employed for ceiling boards and floors.

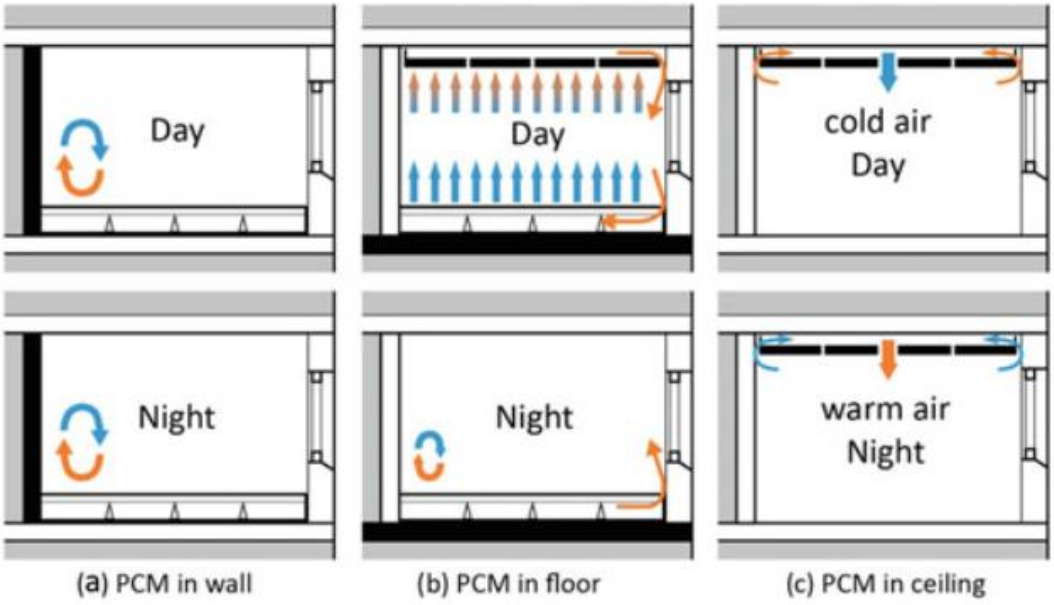

Fig. 1.12. PCM integrated into building structure [84]

Royon et al. [85] conducted experimental and numerical studies on the usage of PCM in building structures (i.e., floors). In order to increase the thermal inertia of the building structure, a new polymer PCM composite using paraffin is manufactured and integrated into the floor panel. The results depicted that the usage of PCM can decline the surface wall temperature amplitude and increase thermal energy storage. Ahmad et al. [86] investigated the thermal performance of a test-cell with a novel wallboard structure using PCMs, in which a comparison was also conducted with a test-cell without PCM. They proposed that a vacuum insulation panel is necessary to be associated with the PCM panel to improve the wallboard efficiency. They reported that

this new wallboard could achieve an increase in the apparent heat capacity of the building, and the thickness of the wallboard can be declined in comparison with that of convectional wallboards.

1.4.3 Off-peak electricity storage

The variation of electricity consumption during the day and night depends on industrial, commercial and residential activities. As it is known to all, various pricing system may be made according to the variation in electricity demand in peak and off-peak periods. The usage of electricity from the peak period to off-peak periods is conducive to improving economic benefit. The development of thermal energy storage system provides a possibility to achieve the storage of surplus energy until the energy is released when it is needed. Some methods have been investigated [87]. For instance, the typical domestic storage heater adopts ceramic bricks and structural cement, which is heated with electrical heating wires or hot fluids during the night. Then the heat is obtained from the heater by natural convection, radiation or forced convection during the day.

The application of PCM storage technology in off-peak electricity has been proposed and developed in some literature [80]. PCM could melt to store electrical energy in the form of the latent heat thermal energy, and also release heat when it is needed. So, if the latent heat thermal energy storage system is combined with the active system, it can reduce the peak load. This method can also reduce electricity generation costs. Agyenim and Hewitt [88] developed a finned PCM storage system to take advantage of off-peak electricity. They designed an experimental system concluding a longitudinally finned phase change material in a horizontal cylinder to explore the heat transfer characteristics. Besides, the latent heat method of heat storage will help in a significant weight reduction in the storage heaters.

Farid and Husian [89] proposed a new design of storage heaters via replacing ceramic bricks with paraffin wax encapsulated in the multi-units arranged to supply the heat to the air flowing between them during the heat discharge cycle. During the

heat charging period, the heat was provided to the units at a low heat flux, and paraffin wax stored a larger amount of heat as the latent heat of fusion. Then heat can be continuously discharged during the other periods. Bruno et al. [90] performed simulations using the effectiveness-number of transfer units representation of a PCM system to evaluate the instantaneous heat transfer when coupled to an inverter chiller cooling system. The domestic cooling system was comprised of a chiller, PCM thermal storage unit and fan coil units, as shown in Fig. 1.13. Results showed that 85% of energy consumption for cooling could be shifted to the off-peak period with an ice-based system, while the energy demand increased by 7.6%. Also, the studies indicated that using a PCM with a melting point of 4 ℃ could achieve an energy saving for cooling. A saving of about 13.5% can be obtained using a PCM with a melting point of 10 ℃.

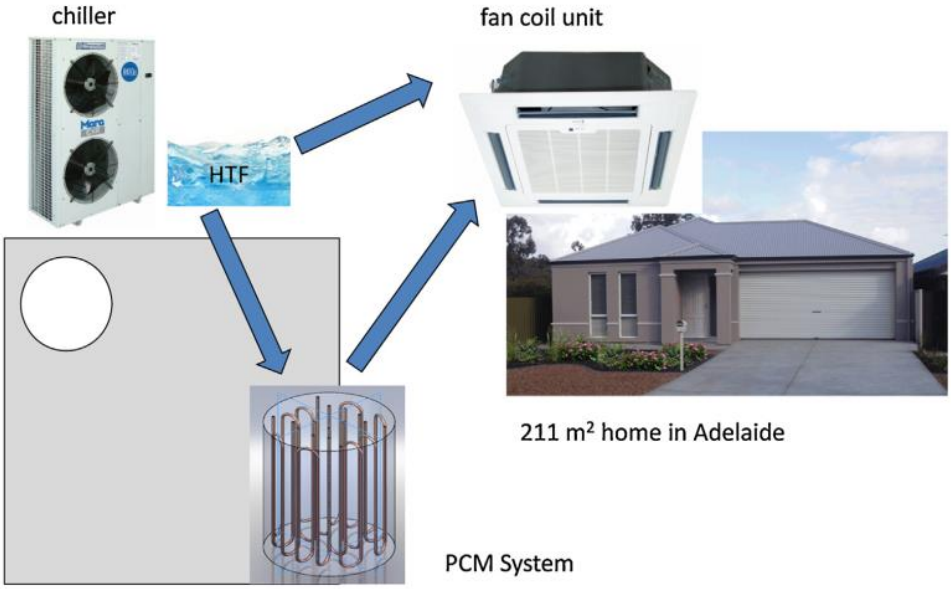

Fig. 1.13. Schematic diagram of the domestic cooling system with PCM [90]

1.5 Application of PCM composite in thermal management system

With the improvement of the performance of electronics, a large amount of heat is generated from electronic devices [91, 92]. For example, Battery is the core component of the electric vehicle, whose performance directly affects the endurance,

service life, and electric vehicle [93]. Thermal management is a significant issue for the utilization of battery [94]. Therefore, the development of new energy story materials is essential for thermal management. Due to the considerable energy storage density of the phase change materials, phase change materials are widely utilized in thermal energy storage, therefore attracting intensive attention from researchers.

1.5.1 Electronic devices

With the development of technology, the functions of electronic chip are gradually increasing, but also their sizes are becoming smaller, which results in the chips are subjected to high heat flux. Dissipating heat from the electronic device and suppressing temperature rise during the operating process has become a vital challenge in electronic fields [95]. As a consequence, the thermal management system must be designed for the cooling of electronic components. The active cooling using microchannel and finned metal foam has been developed and applied in the cooling of electronic devices [96, 97]. However, active cooling consumes too much power and adds the complexity of thermal management system [61]. Hence, passive cooling is proposed and studied to achieve effective thermal management for new generation electronic components.

Several studies have been conducted to explore the potential application of PCM in the cooling application of high-power electronics. Tan and Tso [98] conducted an experimental study on the cooling performance of mobile electronic devices (such as personal digital assistants and wearable computers), where a heat storage unit including PCM was used inside the device. Fig. 1.14 shows that the schematic diagram of the heat storage unit, in which the heaters were used in an experimental setup for mimicking the electronic packages inside personal digital assistants. Besides, the effect of the orientation heat storage unit on the heat dissipation of chips was also investigated by them. Hodes et al. [99] implemented an experimental investigation on the feasibility of transient thermal management of handset using the PCM, in which the base temperature of the handset was obtained by an infrared camera. Moreover,

they explored the effects of PCM material, power of heat resource and handset orientation on the thermal response of electronic devices.

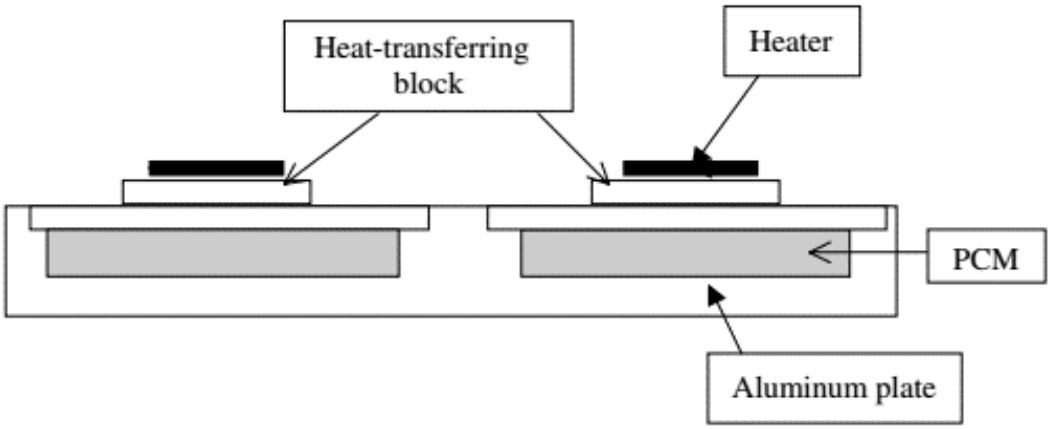

Fig. 1.14. Heat storage unit including PCM [98]

The low thermal conductivity of PCM may result in a decrease in the cooling rate of the heat sink using PCMs. Hence, some enhancement methods have been proposed and developed. The metal foam/PCM composite is an available approach to improve the cooling performance of heat sink. For instance, Rehman and Ali [100] experimentally investigated the thermal behavior of heat sink using metal foam/PCM composite for electronic components cooling. They found that the heat sink using 95% porosity showed better cooling performance compared with the heat sink with 97%. Zhu et al. [101], in their experiment, investigated the transient performance of PCM based heat sink using metal foam, in which the effects of pore size of metal foam and filling ratio of metal foam in heat sink were considered. It was found that the thermal performance of heat sink is enhanced with the increase of filling height ratio. The effect of pore size can be ignored under lower heating power, while larger pore size can achieve a better performance when the heat sink is subjected to high power density.

1.5.2 Electric vehicles

Electric vehicle (EV) has attracted tremendous attention from the past decade since it is one of the promising greenhouse gasses solution [102]. Power battery is a core component of the electric vehicle. Many researchers have carried out some

studies on prolonging the cycle life, increasing the power density and ensuring the safety and stability of power battery [103]. Both excessive high and low operating temperatures will affect the performance of the battery, especially the cycle life [104]. Therefore, thermal management for power battery must be considered to improve thermal behavior and ensure its safe use.

In recent years, the battery thermal management system using PCM has gained more and more attention [105, 106]. Hallaj and Selman [107] proposed a new battery thermal management system using PCM and studied its application in electric vehicle. Fig. 1.15 represents the schematic of the battery module using PCM. The results revealed that the thermal management system using PCM was effective in thermally sensitive batteries such as Li-ion and most Li-polymer batteries. The temperature variation of the battery cell integrated into the module design containing PCM was significantly smoother than that without PCM. Javani et al. [108] numerically investigated heat transfer performance of phase change material in battery thermal management for the electric vehicle. They reported that the maximum temperature and temperature excursion for the battery cell using PCM were reduced.

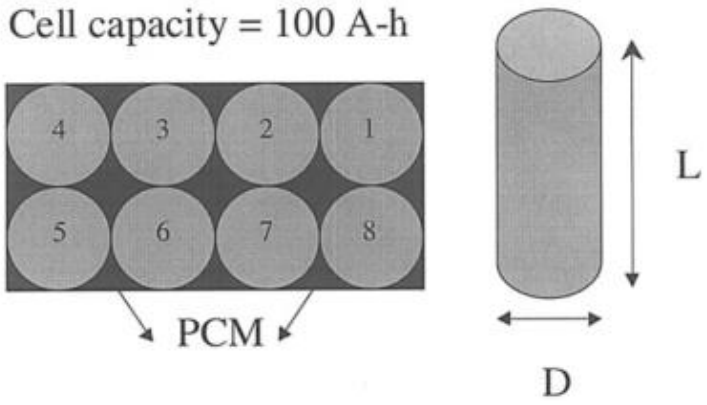

Fig 1.15. A schematic of the proposed battery module [107]

The effect of the graphene and multi-walled carbon nanotubes (MWCNT) as additives on enhancing the thermal performance of lithium-ion power battery thermal management system was studied by Zou et al. [109]. They found that PCM composite

using the MWCNT/graphene at a mass ratio of 3/7 could exhibit the best enhancement role by comparing the experimental results. The MWCNT/graphene composite possessed the highest increase/decrement rate of temperature, which could be shortened by 63.3% and 50.0% compared to pure PCM. Finally, the PCM composite using graphene and MWCNT as additives showed a significant influence on the lithium-ion power battery thermal management. It can be found from the above literature that all the PCMs employed in the thermal management system are paraffin owing to their low cost and steady melting temperature. Whereas the low thermal conductivity can lead to a decrease in the cooling performance of the thermal management unit using PCM. To improve the heat transfer performance of paraffin in the thermal management unit, various materials with high thermal conductivity, such as carbon nanotubes [109], expanded graphite [110, 111], metal fiber [112, 113] and metal foam [114-116], are added in paraffin to form PCM composite. It is proved that the battery thermal management system using PCM composite shows a better thermal characteristic compared to that using single PCM [117-119].

1.5.3 Cold energy storage and transport

The transport and storage of low temperature-sensitive products are a worldwide issue considering the requirement of maintaining the quality and prolonging the shelf-life [120]. In recent years, about 4 million refrigerated vehicles are used within the globe, and the usage of refrigerated transport presents continuous growth. Refrigeration approximately consumes 40% of the total energy during product transportation, which promotes the related studies on reducing energy consumption for the refrigerated transport system. Cold energy storage could be an appropriate way to address the gap between the demand and consumption of the cold chain.

Cold energy storage using phase change material (PCM) is an advanced energy technology. Many researchers have investigated saving energy and energy efficiency improvement by the use of PCM in domestic refrigeration [121], freezers [122], and refrigeration plants [123]. Gin et al. [124] carried out an experiment on the application

of PCM in a domestic freeze. They investigated the effects of the door opening, defrost cycle and loss of electric power on the freezer with and without PCMs. Cheralathan et al. [125] conducted an experimental study of the cooling performance of an industrial refrigeration system using encapsulated PCM. In the experiment, the effects of inlet temperature on the cooling system were explored. They reported that optimal evaporator temperature and charging system at lower condensing could enhance the thermal behavior of cold storage system.

Transport of temperature-sensitive products is a critical line in the food industry. Many researchers put the effort in order to study the industrial application of PCM in refrigerated transport [74, 126]. Tan et al. [127] performed an experimental study of the cold storage system selecting water as PCM for cold energy recovery of LNG refrigerated vehicle, as illustrated in Fig. 1. 16. Michel et al. [128] conducted the experimental and numerical investigation on the insulation walls using PU-PCM composite for the refrigerated vehicle. It was concluded that the composite material was recommended to be placed close to the external walls of the vehicle to obtain a better cooling performance.

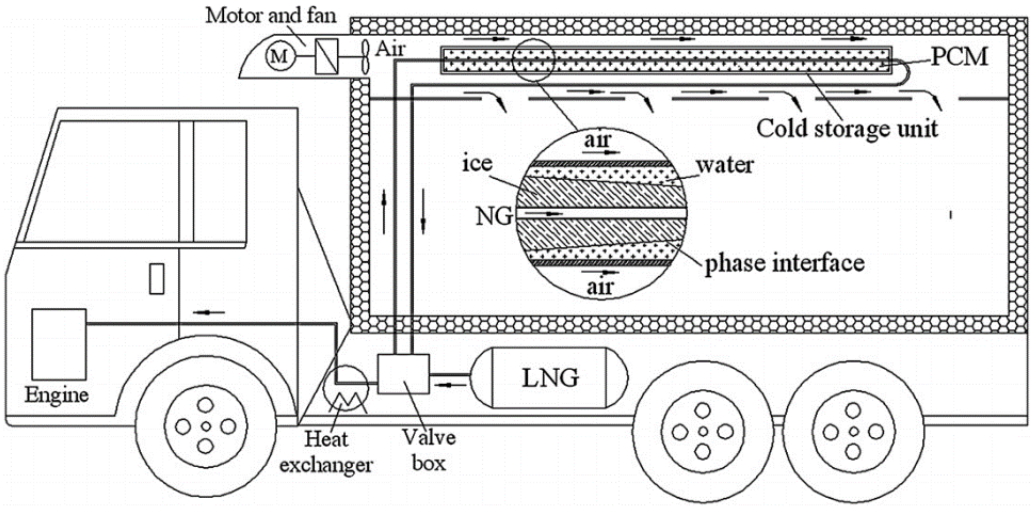

Fig. 1.16. Schematic illustration of refrigeration using PCM [127]

1.6 Conclusion

Phase change material (PCM) is a promising candidate to be applied for thermal energy storage. However, low thermal conductivity hinders its wide application. Many methods have been studied to enhance the thermal performance of PCM, such as encapsulated PCMs, adding high thermal conductivity additive, inserting metal fin and embedding metal foam. Among the above methods, embedding metal foam is proved to be an efficient approach to heighten the thermal behavior of PCM due to its lightweight, larger specific surface and high thermal conductivity.

In this section, the review of studies of PCM composite is performed, including the manufacturing methods, the thermal performance enhancement, and the application in the thermal energy storage and thermal management system. It is found that the metal foam as the thermal enhancer plays an important role in the thermal performance enhancement of PCM. In the previous literature, metal foam with a stochastic structure has been extensively investigated by many researchers. In comparison, the metal foam with a periodic cell structure is still relatively rare. The structure characteristics of metal foam could affect the thermal performance of PCM composite. Therefore, the main aim of the present work is to study the heat transfer characteristics of PCM embedded in metal foam with periodic cell structure fabricated by 3D printing technique. The experimental and numerical methods are used to examine and simulate the thermal performance of PCM composite for the thermal energy storage and thermal management system.

Chapter 2.

Effects of heat and contact conditions

Chapter 2. Effects of heat and contact conditions

2.1 Introduction

As reported in the above chapter, PCMs can be applied in many fields of TES systems, such as solar thermal storage [73] and thermal management of electronic devices [27]. For the different applications, the heating position of the thermal energy storage unit is different, which can affect their thermal performance. Furthermore, for the same TES unit, the investigation of the heating position is also very necessary and significant [129]. For instance, the heating position may affect the thermal charging performance of thermal battery that can be employed to store heat by taking advantage of off-peak electricity. However, the mechanism of the effect of heating condition on heat transfer of PCM composite is not sufficiently studied.

In practical application, PCM composite is necessary to be encapsulated in containers [130]. The junction types between PCM composite and container wall could lead to the difference of contact condition. For example, we should select the natural contact or bonding metal foam to the wall by sintering or brazing, which is still an open question. Therefore, the effect of contact condition on thermal behavior of PCM composite used in TES needs to be studied, which conduces to evaluating which kind of junction should be selected.

In this section, the effects of heating and contact conditions on the thermal charging performance of PCM composite are explored. Based on the volume-average method, the numerical simulation is employed to investigate the thermal performance of PCM composite during the phase change process in terms of solid-liquid interface, velocity vector, liquid fraction, melting time and average heat storage rate. Nine different cases are designed to study the heat transfer performance and mechanism for composite subjected to the various heating and contact conditions.

2.2 Numerical model

2.2.1 Problem description

Fig. 2.1 shows the contact status of PCM composite utilized in TES. For ease of assembly, there may be a clearance fit between metal foam and container wall. A small contact gap appears between metal foam and container wall. The gap can be filled with PCM taking into account of the flow of PCM with liquid phase. The additional thermal resistance caused by the gap may significantly affect the heat transfer performance of composite PCM. Considering different processing and assembly processes, the gap may yield in each pair of contact surfaces. Besides, the effect of heating conditions on the energy storage properties of PCM composite is also investigated.

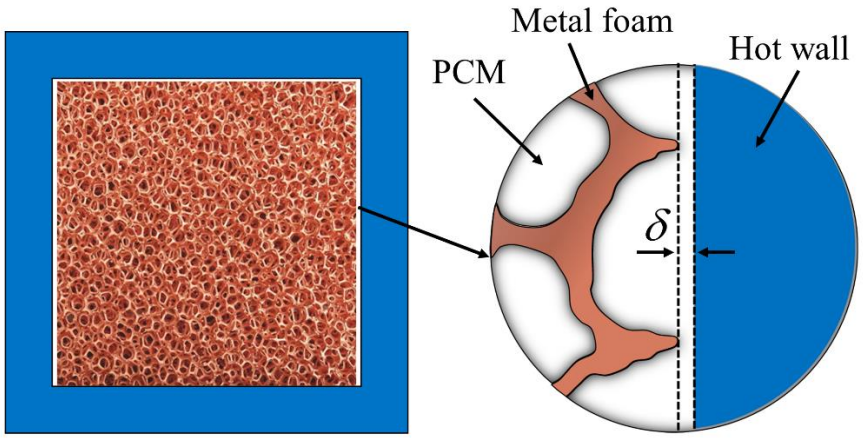

Fig. 2.1. Schematic diagram of contact condition of PCM composite for TES [131]

For investigating the combined effects of the heating and contact conditions on the thermal behavior of PCM composites, nine different heating and contact condition cases are developed, as depicted in Fig. 2.2. For example, Conds. 1, 4 and 7 are used for investigating the effect of heat position (the blue wall is heated at a constant temperature, and other walls are adiabatic) and Conds. 4-6 are employed to study the effect of contact condition (i.e., different gap size) on thermal performance when the heating condition is the same. The dimension of metal foam is the same and 50×50 mm^2 for these nine cases. The contact gaps δ with the size of 0, 0.4 and 0.8mm are set.

Since copper foam possesses not only high thermal conductivity but also a large specific area, copper foam with a porosity of 95% and pore density of 5ppi is selected as the metal matrix. Paraffin can store a large amount of heat by latent heat and is widely applied in TES, so it is used as PCM in this study.

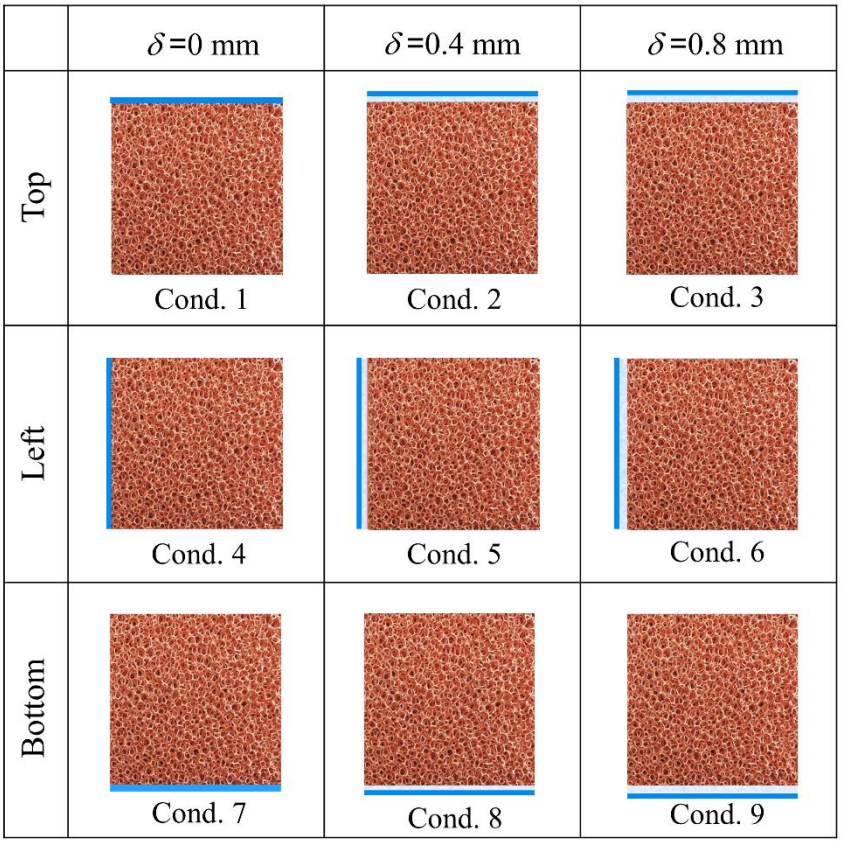

Fig. 2.2. Different heating and contact conditions

2.2.2 Assumption condition

Some assumptions should be made in mathematical method for the present physical model, as follows: (1) metal foam is homogenous and isotropic; (2) the flow of liquid paraffin in the pore of metal foam is impressible and Newtonian; (3) the thermo-physical properties of paraffin is constant and same at solid and liquid phase, except density that is subjected to the Boussinesq approximation. The thermophysical properties of the phase change material and metal foam are presented in Table 2.1.

Table 2.1 Thermal characteristics of paraffin and copper foam

Property	Material	
	Paraffin	Copper foam
Specific heat, c (J/kg K)	2300	386
Density, ρ (kg/m^3)	900	8900
Thermal conductivity, k (W/m K)	0.3	380
Viscosity, μ (kg/m s)	0.00324	
Thermal expansion coefficient, γ (1/K)	0.0005	
Latent heat, L (J/kg)	148800	
Solidus temperature, T_{m1} (K)	323	
Liquidus temperature, T_{m2} (K)	331	

2.2.3 Mathematical method

The volume-averaged method is employed to imitate phase change heat transfer within PCM composite. Based on the assumption of local thermal equilibrium, one-temperature energy model is adopted to describe heat transfer between PCM and metal skeleton. Darcy-Brinkman-Forchheimer model is used to consider the effect of metal foam on the flow of liquid PCM. Based on the above assumptions and method, the volume-averaged continuous, momentum and energy equations can be given as follows:

Continuous equation:

$$\frac{\partial \rho_f}{\partial t} + \nabla \cdot (\rho_f \vec{U}) = 0 \tag{2-1}$$

Momentum equations:

$$\frac{\rho_f}{\varphi}\frac{\partial u}{\partial t} + \frac{\rho_f}{\varphi^2}(\vec{U}\cdot\nabla)u = -\frac{\partial p}{\partial x} + \frac{\mu}{\varphi}\nabla^2 u - \left(\frac{\mu}{K} + \frac{C\rho_f|\vec{U}|}{\sqrt{K}}\right)u + S(u) \tag{2-2}$$

$$\frac{\rho_f}{\varphi}\frac{\partial v}{\partial t} + \frac{\rho_f}{\varphi^2}(\vec{U}\cdot\nabla)v = -\frac{\partial p}{\partial y} + \frac{\mu}{\varphi}\nabla^2 v - \left(\frac{\mu}{K} + \frac{C\rho_f|\vec{U}|}{\sqrt{K}}\right)v + \rho g\gamma(T - T_m) + S(v) \tag{2-3}$$

where ρ_f and μ are the density and viscosity of PCM, u and v are the velocity in x and

y direction.

The terms $S(u)$ and $S(v)$ in Eqs. (2-2) and (2-3) are the source term of damping force and defined as the following equations:

$$S(u) = -\frac{(1-\beta)^2}{\beta^3 + \lambda} A_m u \tag{2-4}$$

$$S(v) = -\frac{(1-\beta)^2}{\beta^3 + \lambda} A_m v \tag{2-5}$$

where A_m is a mushy zone constant and set as 10^5, and λ is a smaller constant and set as 10^{-3}. β is the liquid fraction within the pore and defined by:

$$\beta = \begin{cases} 0 & T_f < T_{m1} \\ \left(T_f - T_{m1}\right)/\left(T_{m2} - T_{m1}\right) & T_{m1} < T_f < T_{m2} \\ 1 & T_f > T_{m2} \end{cases} \tag{2-6}$$

The relationship between β and φ can be written as:

$$\varphi = \varepsilon \cdot \beta \tag{2-7}$$

where φ is the liquid fraction of PCM composite.

Energy equation for PCM and metal foam:

$$\frac{\partial T}{\partial t}\left[\varepsilon\rho_f c_f + (1-\varepsilon)\rho_s c_s\right] + \varepsilon\rho_f c_f \left(\vec{U}\cdot\nabla\right)T = k_{eff}\nabla^2 T - \varepsilon\rho_f L\frac{\partial \beta}{\partial t} \tag{2-8}$$

The pore size d_p of metal foam can be determined by:

$$d_p = \frac{22.4\times10^{-3}}{\omega} \tag{2-9}$$

The permeability K and inertial coefficient C are required for the calculation of the liquid flow within porous medium, which are complex parameters and difficult to be obtained by the experimental test. K and C are finally determined by using the model proposed in Ref. [132] and written by the following equations:

$$\frac{K}{d_p} = 0.00073(1-\varepsilon)^{-0.224}\left[1.18\sqrt{\frac{1-\varepsilon}{3\pi}}\left(\frac{1}{1-e^{-((1-\varepsilon)/0.04)}}\right)\right]^{-1.11} \tag{2-10}$$

$$C = 0.00212(1-\varepsilon)^{-0.224}\left[1.18\sqrt{\frac{1-\varepsilon}{3\pi}}\left(\frac{1}{1-e^{-((1-\varepsilon)/0.04)}}\right)\right]^{-1.63} \tag{2-11}$$

For the one-temperature model, the effective thermal conductivity of PCM composite is an indispensable parameter to simulate the phase change heat transfer numerically. Many models are employed to determine the effective thermal conductivities, which are proposed in previous literature. The theoretical model developed by Bhattacharya et al. [133] is very close to the actual structure of metal foam. Thus, Bhattacharya's model is used in this study. The effective thermal conductivity is calculated as:

$$k_{eff} = 0.35(\varepsilon k_f + (1-\varepsilon)k_s) + \frac{0.65}{(\frac{\varepsilon}{k_f} + \frac{1-\varepsilon}{k_s})} \tag{2-12}$$

2.3 Numerical simulation

2.3.1 Physical model

The PCM composite is simplified to a two-dimensional model employed for the volume-averaged simulation. Fig. 2.3 presents the schematic diagram of the physical model for the left heating condition. A square computational domain with size of 50×50 mm^2 is used to represent the PCM composite, in which PCM is saturated in metal foam. The worse contact condition is considered (i.e. there is a gap with the width of δ between hot wall and PCM composite) to investigate the effect of contact condition. We assume that the gap is filled with pure paraffin. The hot wall is heated with a constant temperature T_w = 350 K. The other walls are set to be adiabatic. The initial temperature of the model is T_i = 298 K.

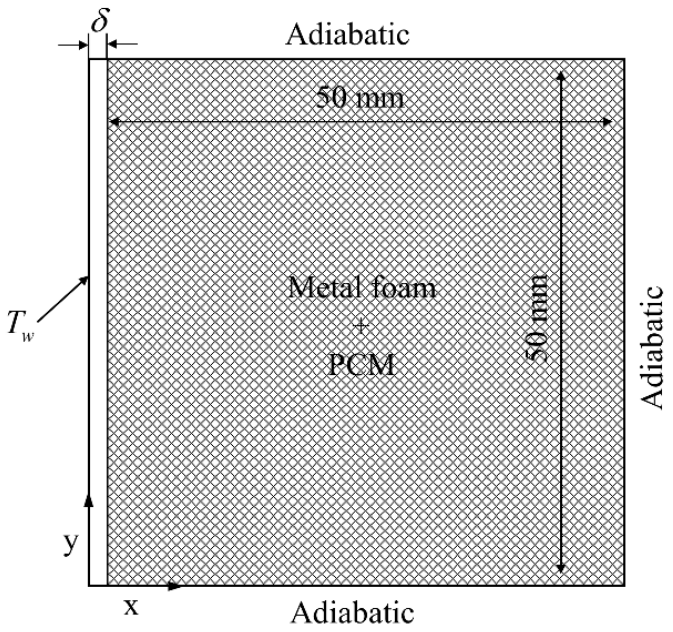

Fig. 2.3. Physical model of PCM composite

2.3.2 Initial and boundary conditions

The initial temperature of model is at a constant temperature of 298K, and the initial velocity for PCM is zero. The initial condition can be given by:

$$0 \leqslant x \leqslant 50\,,\ 0 \leqslant y \leqslant 50,\ \ u = v = 0,\ T_i = 298\text{K} \tag{2-13}$$

The boundary conditions required for the governing equations can also be found in Fig. 2.3 and defined by the following equations:

$$x = 0,\ 0 \leqslant y \leqslant 50,\ \ u = v = 0,\ T_w = 350\text{K} \tag{2-14}$$

$$x = 50,\ 0 \leqslant y \leqslant 50,\ \ u = v = 0,\ \frac{\partial T}{\partial x} = 0 \tag{2-15}$$

$$y = 0,\ 0 \leqslant x \leqslant 50,\ \ u = v = 0,\ \frac{\partial T}{\partial y} = 0 \tag{2-16}$$

$$y = 50,\ 0 \leqslant x \leqslant 50,\ \ u = v = 0,\ \frac{\partial T}{\partial y} = 0 \tag{2-17}$$

2.3.3 Numerical procedure

Based on finite volume method, commercial software FLUENT 18.0 was adopted to solve the governing equations along with the initial and boundary conditions. The second order upwind differencing scheme was used to discretize the governing equation for momentum and energy. PRESTO was applied to compute the pressure equation, which is recommended to calculate the liquid flow within the porous medium. PISO algorithm was employed to couple the velocity-pressure field. The convergence of solution was checked at every time step for the unsteady state numerical simulation. The convergence criteria of scaled residual are set to 10^{-6} to monitor the calculation stability of energy and momentum equations.

2.3.4 Independence analysis and validation

Structure grids were generated in the computational domain of two-dimension model. The grid sensitivity analysis was performed to guarantee the grid independence of numerical simulation using three different numbers of grids (43k, 63k and 77k cells). The liquid fraction of PCM composite was tested using the above different grids under Cond.1. The comparison result is presented in Fig. 2.4. It is observed that the results of the three grids exhibit good agreement and the relative error is within 2%. In order to ensure the calculation accuracy and reduce the computation time, the medial grid 64k cells and time step 1 s are enough for numerical simulation.

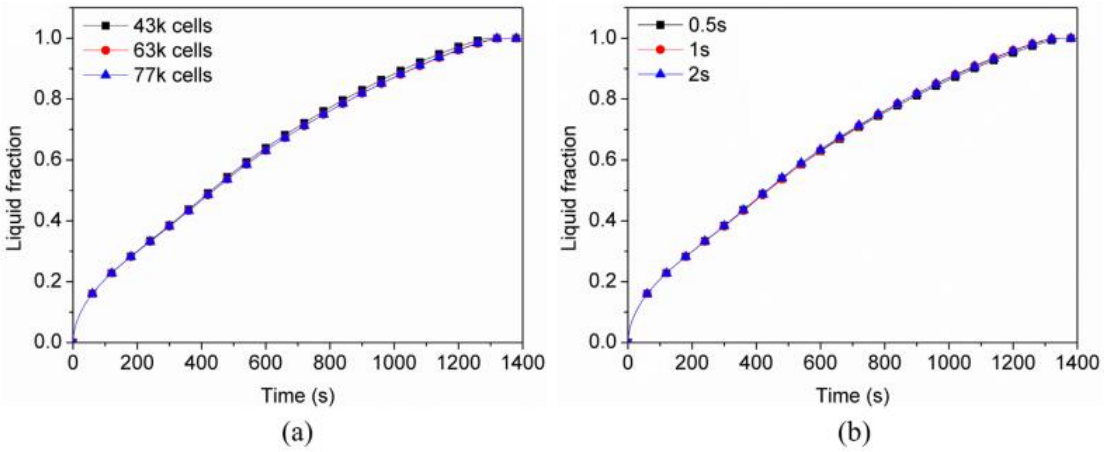

Fig. 2.4. Independence tests of (a) grids and (b) time step

The numerical model in this study was validated with the experimental results found in the literature [134]. The same copper foam and paraffin are used in numerical simulation, and the same initial and boundary conditions also are adopted. The evolvement comparison of solid-liquid interface is presented in Fig. 2.5. Blue represents the solid phase for PCM composite. It can be found that the numerical results are good in agreement with the experimental photos. Therefore, the numerical model can be used to numerically simulate the phase change heat transfer of copper foam impregnated with paraffin.

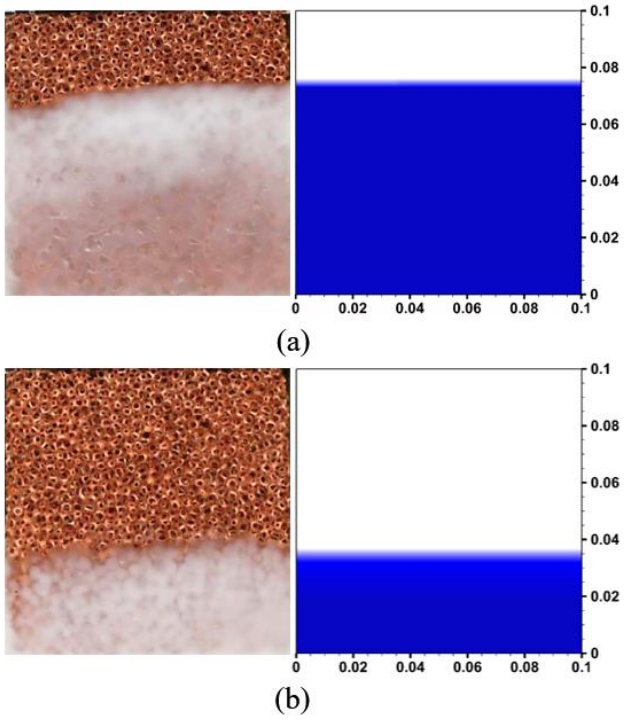

Fig. 2.5. Comparison of numerical results and experimental data [134]
(a) at t = 3 h, (b) at t = 4.5 h

2.4 Thermal behavior of PCM composite

2.4.1 Evolvement of phase change

Fig. 2.6 shows the evolvement of phase change of PCM composite under Conds. 1-3 (see Fig.2.2) as a function of time. The solid-liquid interface photos for every condition are extracted at 20%, 40% and 80% liquid fraction, respectively. The solid-liquid interfaces are greatly flat and parallel with the top face under these three heating

conditions, which indicates that the natural convection is suppressed. It is found that the velocity in the PCM composite is very small (order of magnitude 10^{-6}) and can be almost ignored during the melting process, which is also demonstrated that the natural convection of liquid PCM can be neglected, and the heat conduction dominates the heat transfer within PCM composite in the whole phase change process. The melting time of the PCM composite is almost the same at the same liquid fraction.

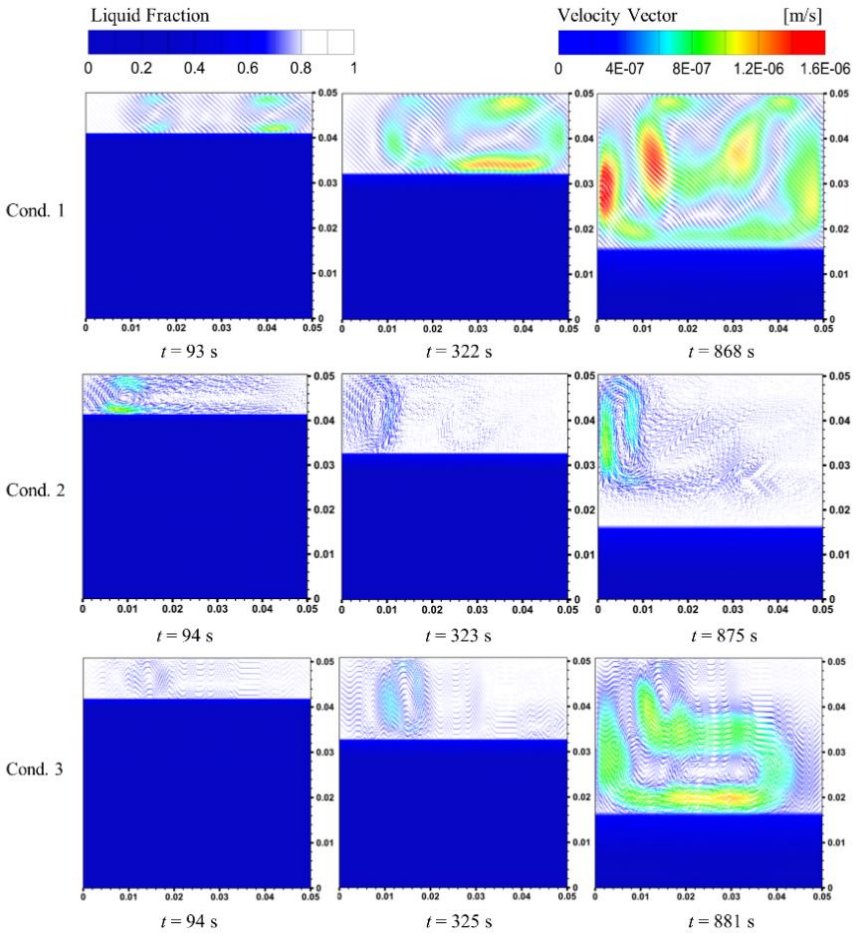

Fig. 2.6. Evolvement of phase change for composites with top heating at 20%, 40% and 80% liquid fraction, as a function of time

Fig. 2.7 presents the evolution of phase change of PCM composite under Conds. 4-6 as a function of time. The solid-liquid interface is mildly inclined at the early stage of melting, which is due to the effect of natural convection. As the melting progresses, the liquid paraffin flows upward and collides with the solid paraffin at the interface location. It is noted from the vector diagrams that the velocity value is greater in the vicinity of the hot face and interface during the melting process. It can be found that

the melting of PCM composite in the top zone is faster than that of the bottom zone, and the solid-liquid interface is inclined, which results from the natural convection. It is demonstrated that natural convection plays a dominant role in the phase change process. It is seen that the velocity decreases with the increase of the contact gap at the same liquid fraction. This phenomenon indicates that the natural convection can be restrained as the contact conditions are worse and worse (i.e. the gap size increases). As a result, the melting time is longer for the larger contact gap when the liquid fraction is the same, e.g., the melting time of Cond. 6 is 1387s and almost prolonged about 2.8 times as much as that of Cond. 4 at the 80% liquid fraction.

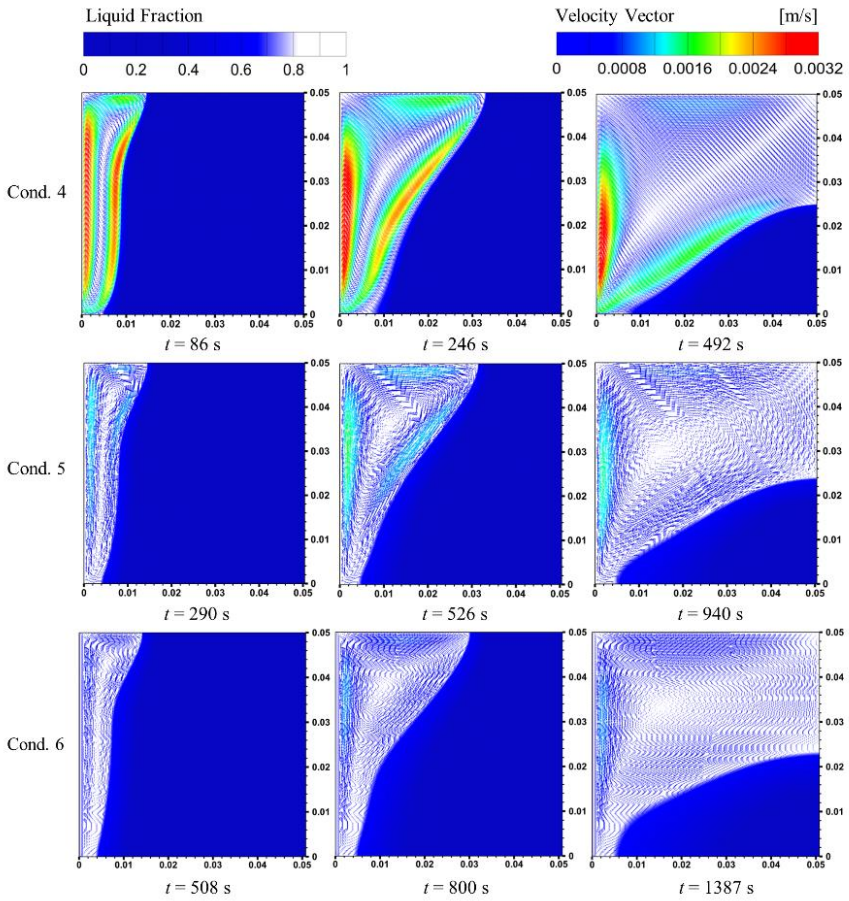

Fig. 2.7. Evolvement of phase change for composites with left heating at 20%, 40% and 80% liquid fraction

Fig. 2.8 illustrates the evolution of phase change of PCM composite under Conds. 7-9. We can find that the solid-liquid interface is flat and parallel to the bottom at the beginning of the melting process. Also, velocity is extremely weak in the liquid phase

domain. It indicates that heat conduction dominates the heat transfer in the initial stage of the thermal charging process. As time progresses, the melting interface is wavy, which is attributed to the effect of natural convection. It can be found from the experimental results of Yang et al. [129] that a similar phenomenon was showed in melting evolution of PCM composite with bottom heating (i.e., there is a wavy melting interface). It is demonstrated that heat conduction and natural convection have comprehensive influences on the phase change process. It is also noted that the melting of PCM composite in the middle domain is faster than other domains, and the velocity increases as the melting progresses, which confirms that the natural convection is strengthened and gradually dominates the thermal charging process of PCM composite in the late stage of melting. We can find from the velocity vector diagrams that the contact conditions have a significant effect on natural convection. Then, the melting time of PCM composite is lengthened due to poor contact conditions at the same liquid fraction.

To investigate the effect of heating conditions, the numerical results of Conds. 1, 4 and 7 are compared and analyzed. It can be found that heat transfer mechanism is significantly different under different heating conditions, e.g., heat conduction dominates the thermal charging process under top heating conditions, whereas natural convection plays a dominant role in heat transfer under the left heating condition. It is seen that the melting time of PCM composite under three heating conditions is different when the liquid fraction is the same. For instance, the melting time of composite with left heating is the shortest and reduced by about 43% than that of composite with top heating, which indicates that the natural convection conduces to the enhancement of thermal charging performance of PCM composite. It is concluded that the heating condition has an apparent influence on thermal charging performance by affecting heat transfer mode.

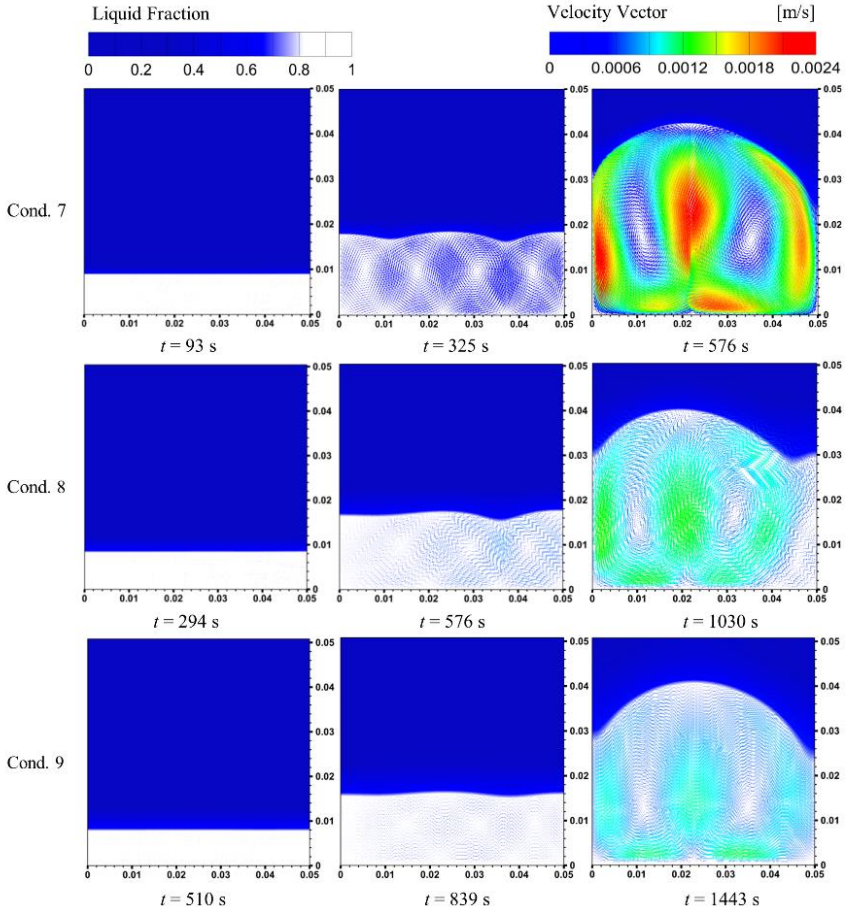

Fig. 2.8. Evolvement of phase change for composites with bottom heating at 20%, 40% and 80% liquid fraction

2.4.2 Liquid fraction and melting time

The variation of liquid fraction with 0 mm gap under three heating conditions is investigated, as shown in Fig. 2.9. It is observed from liquid fraction curves that the melting rate of composite with left heating is the fastest and almost remains the value until the end of the phase change process. Also, it is found that the melting rate of composite under the top and heating conditions is almost the same during the initial period of phase change. The melting rate for top heating is nearly invariable in the whole melting process since the natural convection is suppressed, and heat conduction dominates the heat transfer, as mentioned before. Whereas the melting rate for bottom heating is visibly heightened, which is attributed to the occurrence of natural convection in the mid stage of the melting process.

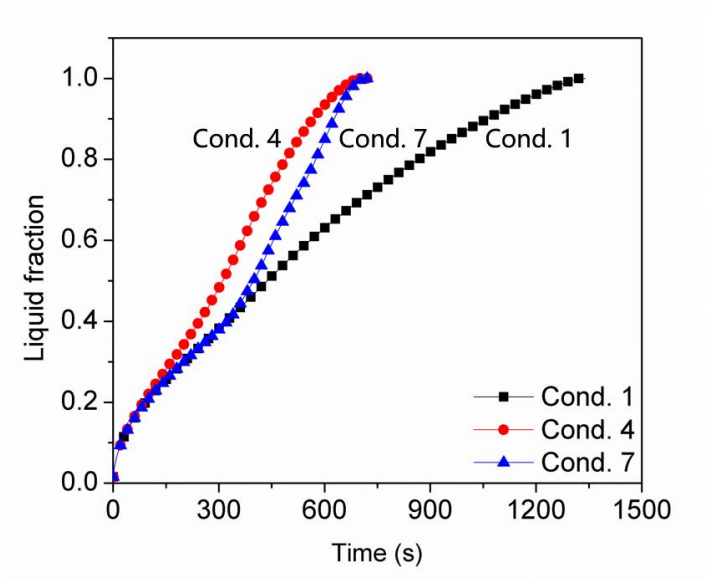

Fig. 2.9. Variation of liquid fraction under three different heating conditions

The variation of liquid fraction for left heating under three heating conditions is displayed in Fig. 2.10. We can see that the liquid fraction curves for different contact conditions show a similar variation tendency but different slope (i.e., melting rate). For example, the melting rate of PCM composite with ideal contact condition (0 mm contact gap) is the fastest and 2.6 times of that with 0.8mm contact gap. It is also observed that the melting rate of PCM composite decreases as the contact condition worsens, which is due to the additional thermal resistance caused by the contact gap between the PCM composite and the hot wall.

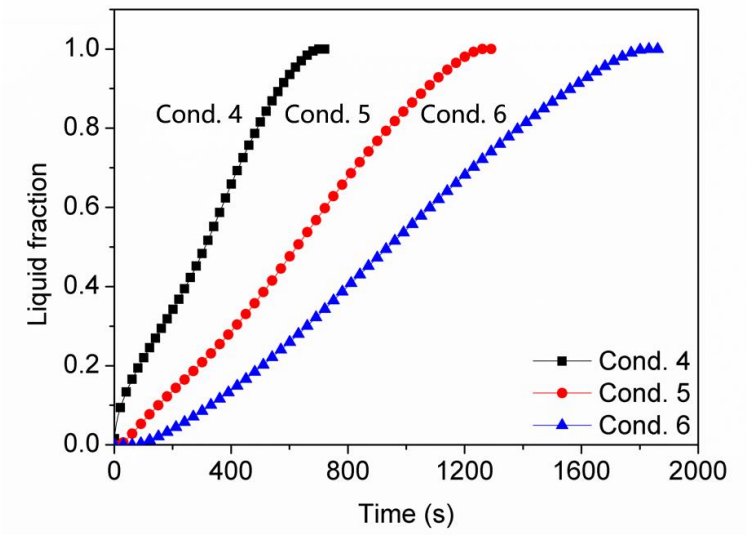

Fig. 2.10 Variation of liquid fraction under three different contact conditions

The total melting time of PCM composite with nine different conditions is presented in Fig. 2.11. The total melting time for left and bottom heating shows a linear increase with the contact gap. Whereas the total melting time of composite for top heating has not a visible change with the contact gap. This phenomenon is because contact resistance increases with the contact gap between composite and wall, but the contact resistance can be ignored compared to the thermal material resistance of PCM composite. Hence, the poor contact condition has a minimal effect on thermal behavior of composite in which the heat transfer is dominated by heat conduction. For the ideal contact condition (i.e., $\delta = 0$ mm), the total time is almost the same for left and bottom heating conditions, which is nearly cut in half compared with the top heating condition. This phenomenon is attributed to different heat transfer modes induced by the heating condition. For instance, natural convection dominates the heat transfer process of composite under the left heating condition, which is conducive to the improvement of thermal behavior, whereas natural convection is restrained for top heating in the whole melting process, as analyzed in Section 2.4.1.

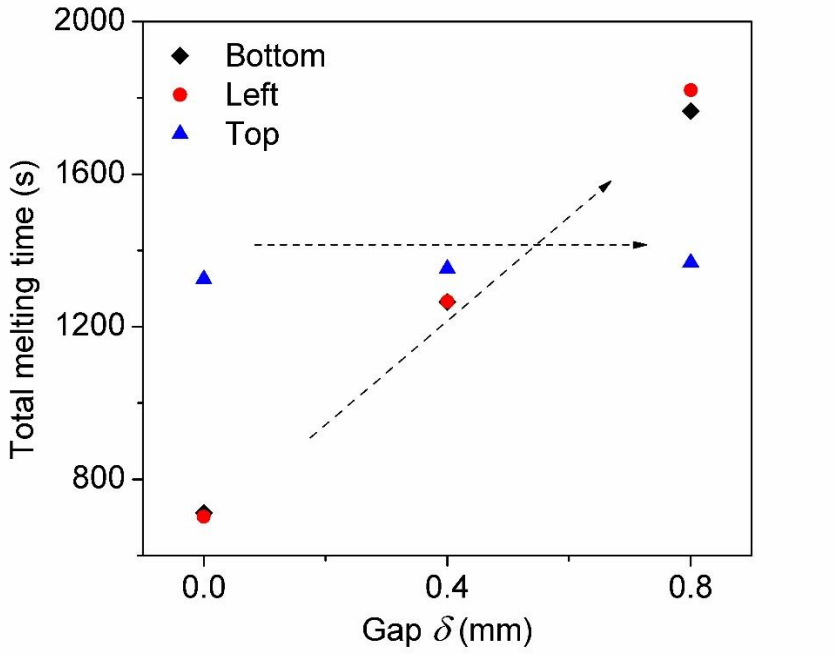

Fig. 2.11. Total melting time of PCM composite in all cases

2.4.3 Heat storage rate

The heat storage rate is a vital criterion for estimating the thermal charging performance of PCM composite. Hence, we perform the investigation of average heat storage rate (i.e., per unit time per mass of PCM composite stores energy in the whole melting process). The average heat storage rate of PCM composite under nine different conditions is shown in Fig. 2.12. The finding can be summarized as follows:

(1) the heat storage rate with the left heating (in red) and the bottom heating (in green) decreases with the increase of the contact gap δ. The contact gap has an obvious impact on thermal performance, which is due to the role of natural convection.

(2) the heat storage rate with the top heating (in blue) remains almost unchanged (approximately 120 W/kg) when the contact gap is ranging from 0 mm and 0.8 mm. It indicates that the contact condition has a slight effect on the thermal behavior of the composite, in which the heat transfer is dominated by heat conduction.

It is noted from the above results that the influence of the heating and contact conditions on the heat storage rate is not negligible. The heat storage rate is largest when the contact is under an ideal condition (i.e., $\delta = 0$ mm).

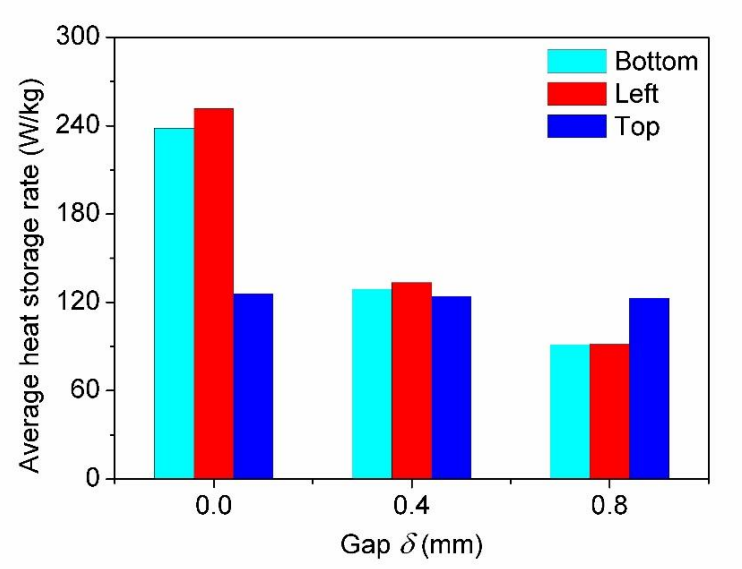

Fig. 2.12. Comparison of average heat storage rate

2.5 Conclusion

In this chapter, the numerical investigation is carried out to examine the effect of heating and contact conditions on the thermal performance of PCM composite. A two-dimensional model based on volume-averaged method is built to study the heat transfer mechanism of PCM composite during the phase change process. Nine different cases are designed to compare the effect of heating and contact conditions on thermal behavior. The conclusions can be obtained as follows:

(1) The effect of heating conditions can be investigated under the same contact condition. It is found from numerical results that natural convection is suppressed in the whole thermal process for top heating. In contrast, natural convection plays a dominant role in heat transfer for left and bottom heating. It is demonstrated that the heat transfer mechanism is different under different heating conditions, which results in a distinct impact on the thermal performance of PCM composite. For instance, the melting time of the left and bottom heating is almost the same and nearly shorten by 50% compared to the top heating when the contact gap δ is 0 mm.

(2) The contact condition has a significant impact on the thermal performance of PCM composite under left and bottom heating conditions, e.g., the total melting time for left and bottom heating presents a linear increase versus the contact gap δ. It is concluded that the contact condition has a distinct effect on the thermal characteristic of TES, where the heat transfer is dominated by natural convection. Conversely, the influence of contact conditions is very small, e.g., the total melting time for top heating is almost the same under three contact conditions (i.e., contact gap δ is 0, 0.4 and 0.8mm), which indicates that the influence of contact condition on the thermal behavior of TES dominated by heat conduction can be neglected and it is not necessary for metal foam to be bonded to the container wall via brazing, sintering, etc.

(3) The numerical results show that the heating and contact condition has a synthetical effect on the thermal performance of PCM composite. The heat storage rate of left and bottom heating is almost the same and higher than that of top heating

when the contact condition is ideal (i.e., gap is 0 mm). Therefore, left and bottom heating conditions are recommended in the practical application of TES owing to the high heat storage rate. The heat storage rate of the three heating conditions is almost the same under middle contact condition (i.e., gap is 0.4 mm). While the heat storage rate of top heating is higher than that of the other two heating conditions as the contact condition worsens (i.e., gap is 0.8 mm).

Chapter 3.

Thermal performance of PCM embedded in metal foam

Chapter 3. Thermal performance of PCM embedded in metal foam

3.1 Introduction

Additive manufacturing (i.e., 3D printing) can fabricate intricate three-dimensional (3D) structure by successive printing thin layers of materials according to 3D model data [135]. This method provides a possibility to manufacture metal foam quickly and precisely with periodic cell structure based on the customization or optimization model [23, 135]. Merabtine et al. [136] carried out the experimental and numerical study on thermal behavior for PCM saturated in metal foam with a periodic cell structure that was designed by topological optimization and fabricated via 3D printing technique. They reported that the pore size and porosities of porous metal had a significant influence on heat transfer within PCM composite. Metal foam is a particularly promising candidate as a thermal enhancer in PCM composite due to its controllable geometrical structure by introducing 3D printing.

The literature indicates that embedding metal foam with a periodic cell structure can heighten the thermal behavior of PCM. The structured porous media was used as the thermal conductivity enhancer, and heat transfer enhancement of PCM embedding porous structure with different configurations was numerically investigated by Gopalan et al. [137]. The results indicated that the impregnation of metal foam with periodic cell structure into PCM could strengthen the thermal performance of PCM. Righetti et al. [138] conducted a study on thermal performance of PCM embedded in metal foam with periodic cell structures. They reported that the usage of metal foam with periodic structure could enhance the thermal performance of PCM, and PCM infiltrated in periodic metal foam with 10 mm pore size exhibits the best thermal behavior. It can be understood from the above literature that the investigation of the thermal performance of PCM embedding metal foam with periodic cell structure is still rare. Besides, the metal foam with periodic cell structure is difficult to be manufactured by traditional fabrication techniques due to its special and complicated configuration, which also results in the lack of related experimental investigation.

In this chapter, the metal foam with the cubic cell structure was fabricated by

selective laser melting (SLM) as one of the 3D printing techniques. The heat transfer characteristics of PCM with and without metal foam are experimentally and numerically studied, including solid-liquid interface evolvement, liquid fraction, temperature field, velocity field and enhancement ratio, etc. Furthermore, the effect of materials of metal foam on the thermal behavior of PCM composite is explored based on pore-scale numerical simulation, which provides a reference for the choice of materials of metal foam used as a heat transfer enhancer. Thus, the study of thermal performance of PCM infiltrated in metal foam is of great significance.

3.2 Metal foam with cubic cell structure

3.2.1 Design of metal foam

As shown in Fig. 3.1, porous metal foam with cubic cell structure is designed as enhancement material in the present study. It is seen that porous aluminum material possesses a periodic cubic cell structure. The reason to choose a cubic periodic cell structure is that this structure can be produced easily by the new manufacturing technology, such as electron beam melting (EBM) and selective laser melting (SLM). The cubic cell is the simple structure that encompasses the specificity of foams and geometrically convenient. The basic unit of metal foam is ideal cube-shaped, in which matrix struts are connected with 90 angles at nodes and come into being a large number of communicating pores. A three-dimensional model of metal foam is modeled as the cubic array of members of ligament length l and square cross-section of side thickness a. With l and a, the porosity ε of metal foam can be written as:

$$\varepsilon = \frac{l^3 - 12a^2 l + 16a^3}{l^3} \tag{3-1}$$

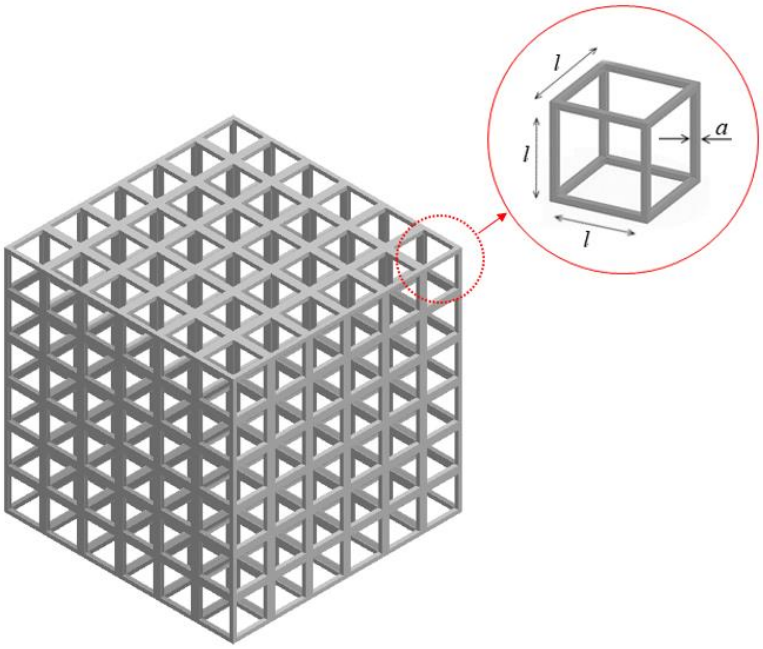

Fig. 3.1. Scheme diagram of metal foam with periodic cell structure

3.2.2 Manufacture of metal foam

The superiority of porous material fabricated by 3D printing is the controllability of shape and size. Moreover, with the development of additive manufacturing material, 3D printing exhibits excellent potential for the fabrication of metal foam using various materials, such as aluminum alloy, copper alloy, titanium alloy, stainless steel, etc. In the present study, the metal foam was made of high thermal conductivity aluminum alloy using selective laser melting (SLM), as shown in Fig. 3.2. The length and thickness of metal ligament within metal foam are l and a, respectively. According to the theoretical design using Eq. (3-1), the metal foam with 90% porosity is manufactured.

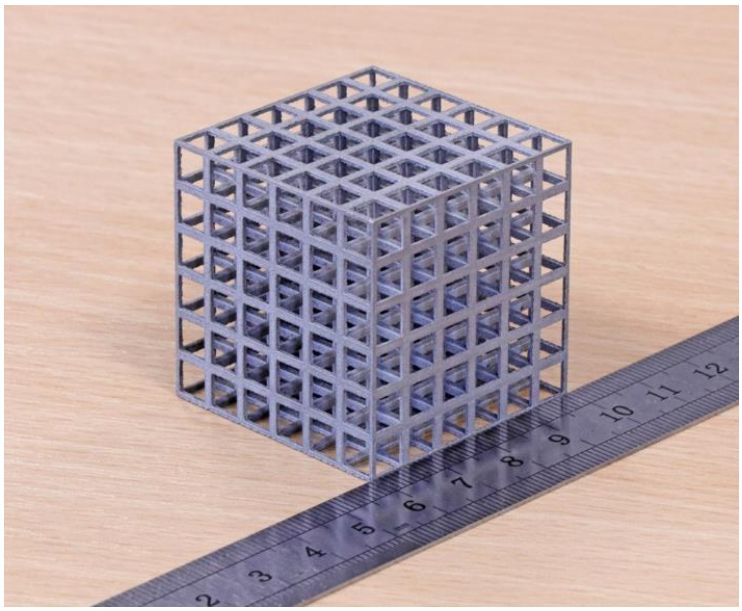

Fig. 3.2. Metal foam fabricated by 3D printing

3.3 Experimental investigation

3.3.1 Experimental apparatus and samples

As depicted in Fig. 3.3, the experimental setup is built to examine the thermal performance of PCM with and without porous metal foam in terms of solid-liquid interface evolvement, temperature variation and total melting time. The apparatus consists mainly of a test box, heating system, data measurement and collection system, and snapshot image system. The test box is composed of a rectangular enclosure container, test sample and insulation material. The HD camera is employed to capture snapshots of melting interface through transparent plexiglass at a specific time interval. An electric copper heater with size of $40\ \text{mm} \times 40\ \text{mm} \times 1\ \text{mm}$ is employed. The heater is mainly made of copper, which is conducive to providing uniform heat flux during the experiment process. The constant power is supplied to the heater by DC power for the heating system, where the power can be determined by recording the electric voltage and current. For current experiments, eleven pre-calibrated K-type micro-thermocouples with a wire diameter of 0.127 mm are utilized along the vertical mid-plane of container. Two typical locations (the center of heater and PCM composite) are selected to obtain the temperature variation of the heated wall and metal structure,

in which thermocouples are attached to the copper heater and metal skeleton using thermal adhesive. In order to determine heat loss from the sidewall, eight thermocouples are attached to the inner surface of insulation material using thermal tape. The last thermocouple is employed to obtain ambient temperature.

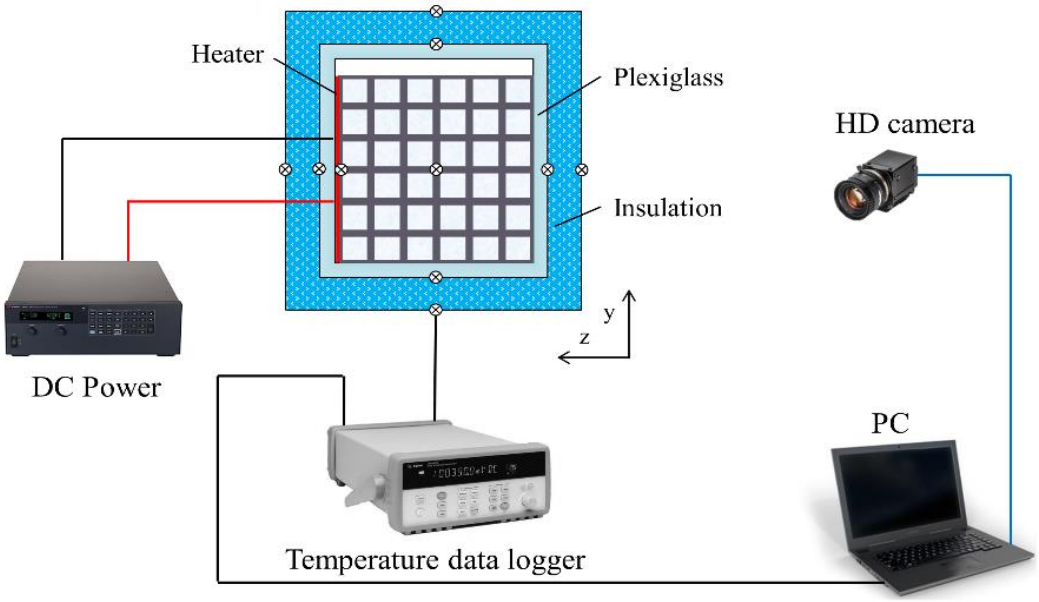

Fig. 3.3. Schematic illustration of experiment setup

In practical utilization, we will face how to select appropriate 3D printing metal materials. In the present study, we choose four representative metal materials (i.e., aluminum alloy, copper alloy, titanium alloy and stainless steel) to investigate the effect of materials of metal foam on the thermal behavior of PCM composite. The commercially available paraffin RT42 (RUBITHERM, Germany) is selected as PCM. The employed PCM possesses considerable latent heat, stable thermal performance, and low phase transition temperature, which is conducive to reducing the heat loss in the experiment process. The thermal-physical properties of paraffin and metal materials are listed in Table 3.1.

Table 3.1 Thermo-physical properties [139]

Property	RT42 paraffin	Aluminum alloy	Copper alloy	Stainless steel	Titanium alloy
Specific heat, c (J/kg K)	2000	940	370	500	560
Density, ρ (kg/m^3)	880/760	2670	8910	8000	4430
Thermal conductivity, k (W/m K)	0.2	183	340	15	7.1
Viscosity, μ (kg/m s)	0.0235				
Thermal expansion coefficient, β (1/K)	0.0001				
Latent heat, L (kJ/kg)	165				
Solidus temperature, T_{m1} (K)	311				
Liquidus temperature, T_{m2} (K)	315				

3.3.2 Experimental procedure

The schematic diagram of test box is displayed in Fig. 3.4. The aluminum structure/paraffin (PCM) composite with size of $40\ \text{mm} \times 40\ \text{mm} \times 40\ \text{mm}$ is used as test sample, which is prepared by impregnating aluminum foam with paraffin. The detailed preparation can be seen in [62]. The cubic pure paraffin with the same size is also employed as test sample for comparative tests. The insulation material (polyurethane foam with 0.02 W/m K) is used for wrapping plexiglass container for minimizing heat loss, in which the inside dimension of insulation cavity is based on the external size of the plexiglass container. We found that the material of enclosure container has a significant effect on the melting evolvement of PCM by doing some tests. The relative lower thermal conductivity plexiglass (0.2 W/m K) is recommended compared to quartz glass. Thus, the rectangular enclosure container is made of plexiglass with a thickness of 3 mm. The about 5 mm gap between the top face of PCM and the inner surface of plexiglass is given for considering the volume expansion of paraffin during the phase change process. Four small round holes are drilled through the top wall of plexiglass, which is used for releasing the pressure within the enclosure container as well as conducive to the fixation of wires of thermocouples and heater. The front face of insulation cavity is removed for about 20 s for tracing snapshot of

melting interface at the selected time interval. The temperature data at different locations are traced at every 1 s via the data logger and then stored in PC for further investigation.

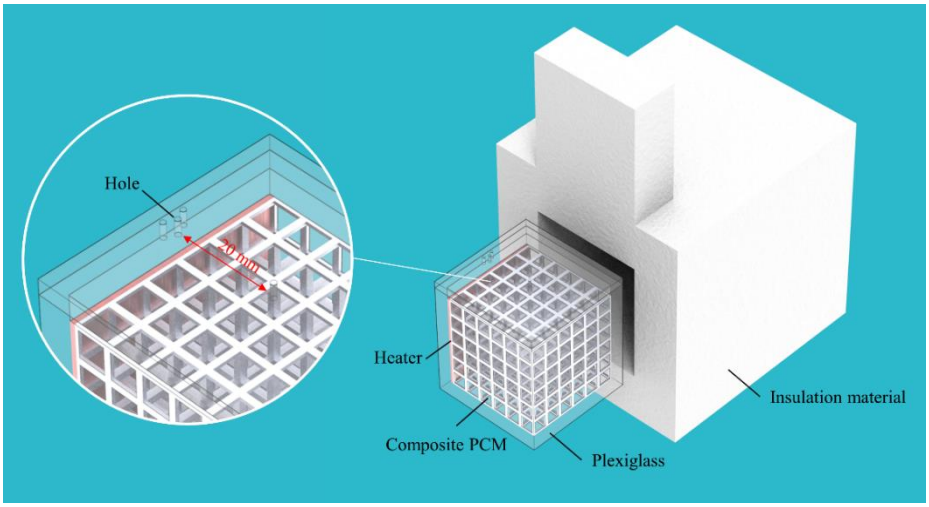

Fig. 3.4. Schematic illustration of the test box

3.3.3 Uncertainty analysis

The experimental uncertainty is determined in this section. The uncertainties of experiment are mainly caused by the errors of employed instruments, including the DC power, electric heater, thermocouples. The uncertainties of DC power (U_{power}) and electric heater (U_{heater}) are 1% and 5%, which are offered by manufacturers. The deviation of thermocouple (ΔT) connected with the data collection system is ±0.5 °C. In addition, heat dissipation through insulation material should be considered for experimental uncertainty. Based on the one-dimensional Fourier's law, the heat loss (Q_{loss}) can be evaluated according to temperature data of thermocouples attached to the insulation cavity. The power input (Q_{input}) supplied by DC power is 6.4 W. The overall uncertainty of experiment can be determined at 6.8% by the following equation:

$$U=\sqrt{U_{\text{power}}^2+U_{\text{heater}}^2+\left(\frac{\Delta T}{T_{\text{ave}}}\right)^2+\left(\frac{Q_{\text{loss}}}{Q_{\text{input}}}\right)^2}\times 100\% \tag{3-2}$$

where T_{ave} is the time-averaged surface temperature.

3.3.4 Heat transfer enhancement of PCM

Fig. 3.5 displays experimental results of melting interface of pure paraffin at 15 min, 25 min and 35 min. It is observed that melting interface is slightly crooked at 15 min, which reveals that natural convection and heat conduction have a comprehensive effect on melting heat transfer. As the melting progresses, the incline of melting interface of paraffin is more pronounced, which indicates the natural convection develops and gradually dominates melting phase change heat transfer. In the later stage of melting, the curvature of melting interface is larger, and melting of pure paraffin at the right bottom domain is slow until paraffin becomes completely liquid phase after about 68 min.

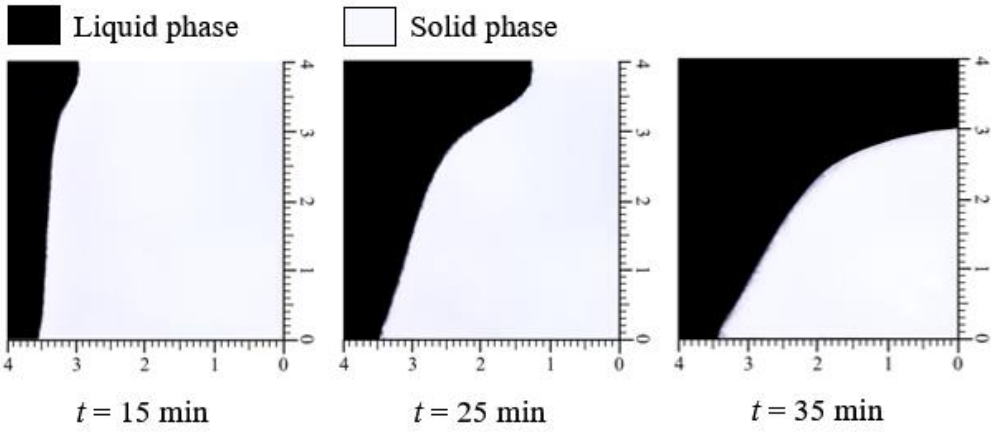

Fig. 3.5. Evolvement of solid-liquid interface of pure paraffin

The evolution of melting interface of PCM with metal foam is shown in Fig. 3.6. In the early stage of melting, melting interface of PCM composite is parallel to the heated wall, which is attributed to that heat conduction plays a significant role in melting heat transfer. As the melting continues, solid-liquid interface remains nearly straight at 25 min, which is different from the melting of pure paraffin. This phenomenon reveals that melting heat transfer within PCM composite is still dominated by heat conduction. The melting interface slightly slopes at the later stage of melting evolution, which represents the natural convection within PCM composite is strengthened and also has an effect on melting evolvement of PCM composite until paraffin completely melts after about 42 min.

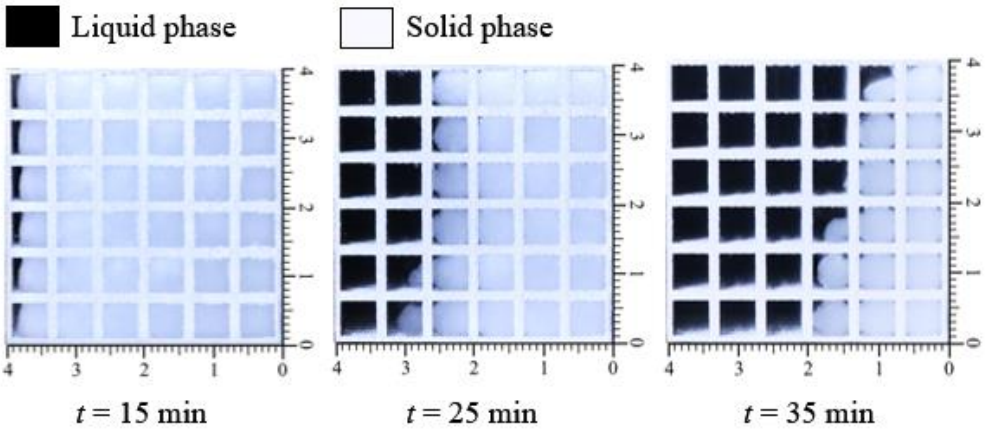

Fig. 3.6. Evolvement of solid-liquid interface of PCM composite

3.4 Numerical study

3.4.1 Numerical method

The pore-scale numerical simulation is employed to investigate the heat transfer mechanism in the current study. Fig. 3.7 presents the schematic diagram of the computational domain of PCM infiltrated in metal foam in which numerical models of PCM with and without metal foam are reconstructed according to the actual test sample. In order to accurately simulate the physical problem of experiment, the numerical model considers the configuration of plexiglass container with 3 mm thickness and copper heater with 1 mm thickness. Thus, the computational domain with the overall size $46\ \text{mm} \times 46\ \text{mm} \times 47\ \text{mm}$ is established. Meanwhile, the following assumptions are adopted in the present numerical simulation: (1) The flow of liquid paraffin in metal foam is laminar flow and subjected to the Boussinesq approximation; (2) The thermo-physical properties of metal structure and paraffin are constant, and the volume variation of PCM is neglected; (3) The heat transfer coefficient is assumed to be constant for simulation of heat loss, where heat loss is mainly caused by convective heat transfer between the insulation material and ambient.

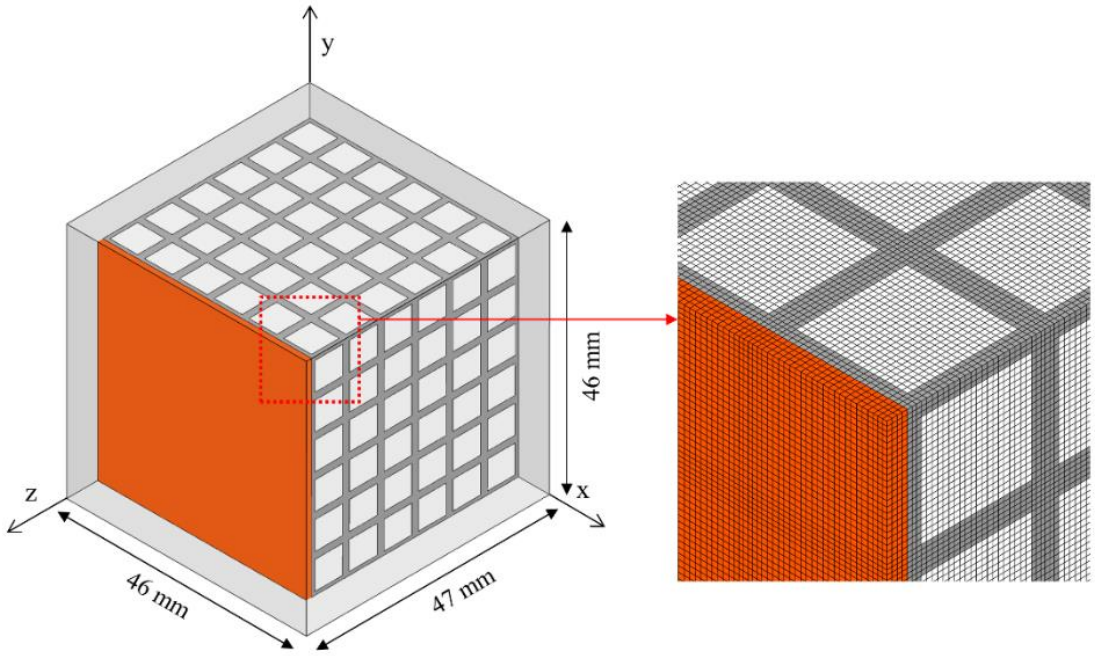

Fig. 3.7. Computational domain and representative mesh of PCM composite with plexiglass enclosure

According to the above assumptions, the governing equations of the numerical model can be written as follows:

Continuity Equation:

$$\nabla \cdot \vec{U} = 0 \tag{3-3}$$

Heat transfer in PCM composite is complex and mainly consists of conduction, phase change and heat convection. The conduction heat transfer in the whole computational region can be defined by:

$$\rho c \frac{\partial T}{\partial t} = \nabla \cdot \left(k \nabla T \right) + \dot{q} \tag{3-4}$$

where $\dot{q}$ is heat generation rate of heat source (i.e., copper heater).

Momentum equation:

$$\rho_f \frac{\partial \vec{U}}{\partial t} + \rho_f \left(\vec{U} \cdot \nabla \right) \vec{U} = -\nabla p + \mu_f \nabla^2 \vec{U} + \rho_f g \gamma \left(T_f - T_m \right) + S\vec{U} \tag{3-5}$$

where $\vec{U}$ is the velocity vector of liquid phase PCM.

The momentum term $S\vec{U}$ in Eq. (3-4) is used to damp velocity in the solid-phase domain, where S is given by:

$$S = -\frac{(1-\beta)^2}{\lambda+\beta^3} A_{\mathrm{m}} \tag{3-6}$$

where A_{m} is a mush zone constant between 10^4 and 10^7 that is recommended in [140], λ is a small constant and set as 0.001 to avoid zero in denominator [141]. β is the liquid fraction between 0 and 1, which can be determined by:

$$\beta = \begin{cases} 0 & T_f < T_{m1} \\ (T_f - T_{m1})/(T_{m2} - T_{m1}) & T_{m1} < T_f < T_{m2} \\ 1 & T_f > T_{m2} \end{cases} \tag{3-7}$$

Heat transfer in solid and liquid regions of PCM can be governed by [142]:

$$\rho_f c_f \frac{\partial T_f}{\partial t} + \rho_f c_f \vec{U} \cdot \nabla T_f = \nabla \cdot (k_f \nabla T_f) - \rho_f L \frac{\partial \beta}{\partial t} \tag{3-8}$$

Heat transfer in metal structure is described as [143]:

$$\rho_s c_s \frac{\partial T_s}{\partial t} = \nabla \cdot (k_s \nabla T_s) \tag{3-9}$$

Temperature and heat flux continuity is defined at the interface between PCM and metal structure, as the following equations:

$$T_f = T_s \tag{3-10}$$

$$k_f \frac{\partial T_f}{\partial n} = k_s \frac{\partial T_s}{\partial n} \tag{3-11}$$

3.4.2 Initial and boundary conditions

The initial temperature of PCM with and without metal foam is measured by

thermocouples inserted in sample. It is found that the initial temperature is equal to ambient temperature $T_0 = 20$ ℃. The initial conditions can be expressed as follows:

$$T_f = T_s = T_0,\ 0 \leqslant x \leqslant 46, 0 \leqslant y \leqslant 46, 0 \leqslant z \leqslant 47 \tag{3-12}$$

Although the outer surfaces of enclosure container are wrapped by insulation material, the heat loss should be considered in numerical simulation. Hence, the outer surfaces of model are set as convective boundary conditions. The boundary conditions for the governing equations are represented by the following equations:

$$-k\frac{\partial T}{\partial x} = h_w(T_w - T_0),\ \ x = \{0, 46\},\ \ 0 \leqslant y \leqslant 46, 0 \leqslant z \leqslant 47 \tag{3-13}$$

$$-k\frac{\partial T}{\partial y} = h_w(T_w - T_0),\ \ 0 \leqslant x \leqslant 46,\ \ y = \{0, 46\},\ \ 0 \leqslant z \leqslant 47 \tag{3-14}$$

$$-k\frac{\partial T}{\partial z} = h_w(T_w - T_0),\ \ 0 \leqslant x \leqslant 46, 0 \leqslant y \leqslant 46,\ \ z = \{0, 47\} \tag{3-15}$$

where T_w is wall temperature. Convective heat transfer occurs between insulation material and ambient air, in which the heat transfer coefficient can be estimated using the empirical correlations [144]:

$$h_1 = \frac{0.62k_{air}}{D}(GrPr)^{1/5} \tag{3-16}$$

$$h_2 = \frac{0.59k_{air}}{D}(GrPr)^{1/4} \tag{3-17}$$

where Gr is Grashof number, Pr is Prandtl number.

3.4.3 Numerical procedure and mesh test

The CFD software Fluent 18.0 is used to perform pore-scale numerical calculation. The momentum and energy equations are discretized using second order upwind schemes. PISO algorithm is employed for coupling velocity and pressure field. The PRESTO method is adopted to calculate pressure term. ICEM CFD 18.0 is used to divide computational domain of model. The grids of computational domain are

generated using a structured hexahedron element. Structured grids can reduce computation time and improve computation accuracy. Mesh details of metal structure and paraffin are presented in Fig. 3.8, where the mesh of plexiglass domain is omitted for clarity. The mesh independence test is performed to validate the accuracy of numerical calculation. Two different numbers of grids (coarse grid with 3156k cells and fine grids with 6735k cells) are tested. The liquid fraction of PCM composite with different grids is compared, as shown in Fig. 3.8. It is observed that the numerical results of the two grids are almost the same, and the deviation of results is less than 1%. In order to ensure the accuracy of calculation and reduce computational time, the grid of 3156k cells is selected. Besides, the power density of copper heater is set as 4×10^6 W/m^3 in the numerical calculation according to the power input of experiment.

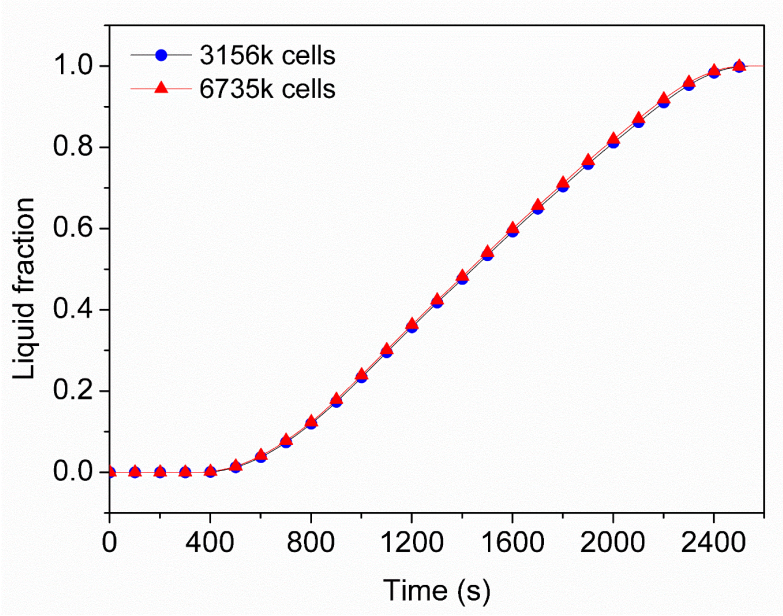

Fig. 3.8. Mesh independence test

3.4.4 Thermal characteristics of PCM composite

Fig. 3.9 illustrates the comparison of numerical results and experimental data of temperature variation for PCM composite at two measurement points TC#1 (y = 23 mm, z = 43 mm) and TC#2 (y = 23 mm, z = 23 mm). The melting process within PCM composite can be divided into three stages: pre-melting stage, melting stage and post-melting stage. It can be found that numerical results of temperature are consistent with

experimental data in the phase change process, especially the melting stage and post-melting stage. In the pre-melting stage, the temperature is below the melting point of paraffin, and the increasing rate of temperature is larger. In the melting stage, the considerable heat is stored in paraffin by the latent heat, and the temperature rises with a relatively lower rate. When the melting of paraffin is completed (i.e., post-melting stage), the increasing rate of temperature becomes large again. Moreover, it can be found that the rate of temperature rise at two monitor points is almost the same, which is due to the heat is stored by sensible heat at that time. The numerical results exhibit good agreement with experimental data, which can demonstrate the validity of numerical method.

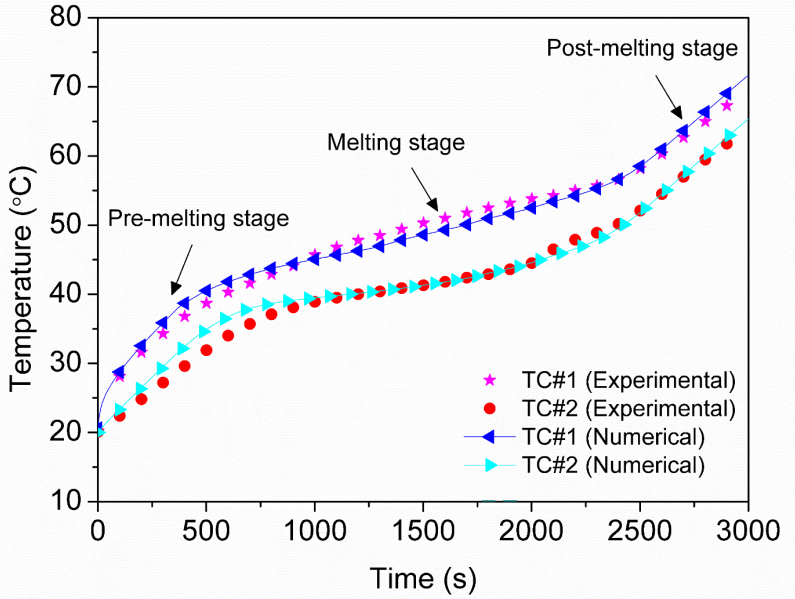

Fig. 3.9. Comparison of numerical results and experimental data of temperature

To further study the thermal performance enhancement of PCM, the numerical predicted results of liquid fraction of PCM with and without metal foam are shown in Fig. 3.10. At the beginning of melting process, the temperature of pure paraffin close to heated wall quickly reaches melting point, and pure paraffin starts to melt. This is because low thermal conductivity results in heat accumulation at the domain near heated wall. Conversely, the PCM composite starts to melt after about 500 s, which is attributed to that the heat can be fast transferred within PCM composite through the high thermal conductivity metal foam. Therefore, it is noticed that the liquid fraction

of PCM composite is smaller than that of pure paraffin before about 1000 s. However, it is noted that the melting rate of PCM composite is larger than that of pure paraffin in phase change process. Though the melting of pure paraffin is earlier than that of PCM composite, the total melting time of PCM composite is shorter and decreased by 38% compared with paraffin without metal foam. The deviation of total melting time obtained by numerical simulation and experimental measurement is within 2%, e.g., for PCM composite, the numerical result of total melting time is 2555 s, and the experimental date of total melting time is 42 min (i.e., 2520 s).

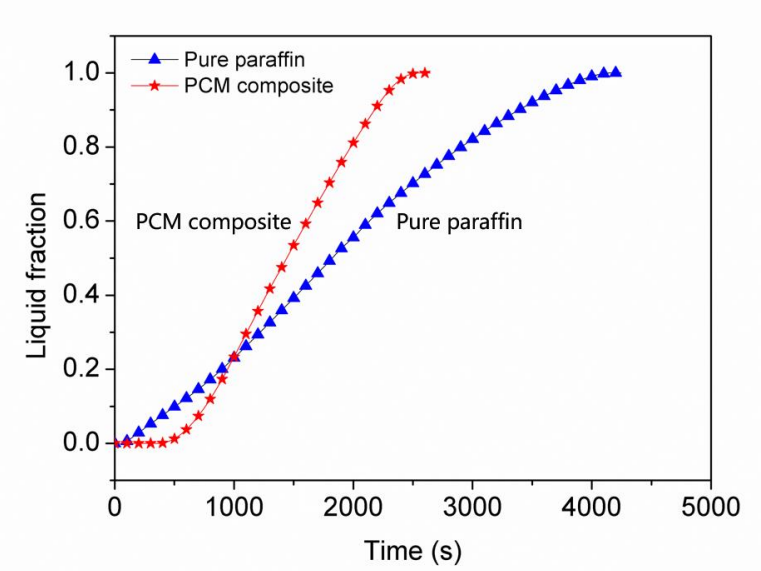

Fig. 3.10. Comparison of liquid fraction

To better understand the thermal performance enhancement of PCM, a comparison of temperature field of PCM with and without metal foam is shown in Fig. 3.11. It is clearly found from Fig. 3.11(a) that the temperature of liquid paraffin close to the heated face keeps high value, while the temperature of solid paraffin at the right bottom part remains at approximately initial temperature 293K in the whole melting process. This phenomenon exhibits the temperature non-uniform within pure paraffin. Conversely, the temperature field of PCM composite is uniform compared to pure paraffin at the same time, as depicted in Fig. 3.11(b). This is because heat can be quickly transferred from the hot wall to the whole domain of PCM composite through high thermal conductivity metal structure. The numerical precited result indicates the maximum temperature difference of PCM embedded in metal foam is decreased by

about 81% compared with pure paraffin in the phase change process.

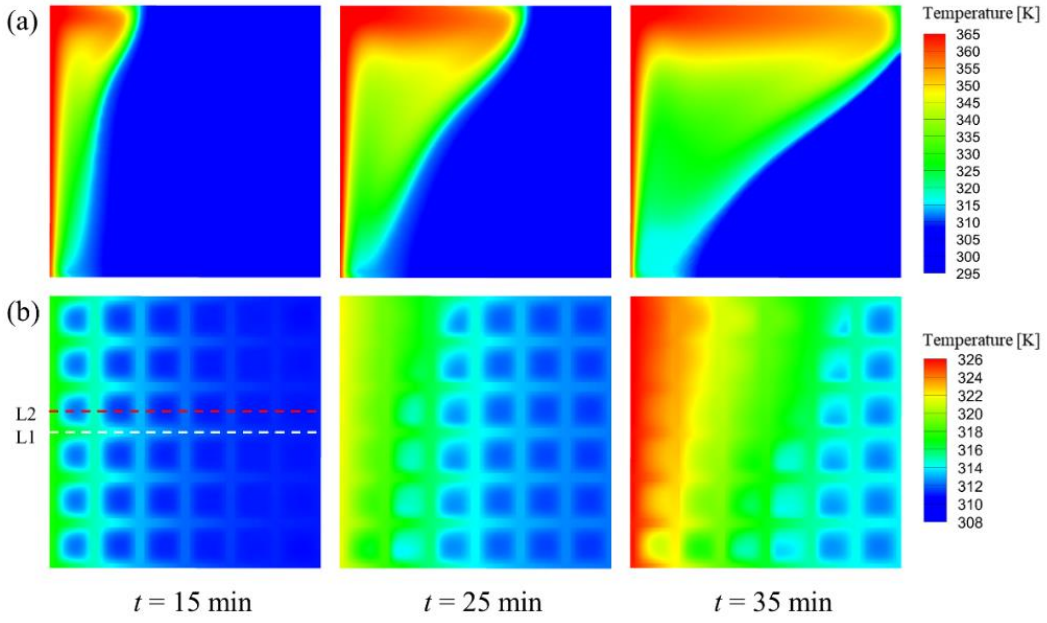

Fig. 3.11. Temperature field of (a) pure paraffin and (b) PCM composite

It can be observed that there is local thermal non-equilibrium between metal structure and paraffin, as presented in Fig. 3.11(b). To visibly illustrate heat transfer characteristic of PCM composite, Fig. 3.12 shows temperature variation along two horizontal lines (L1 of y = 23 mm, and L2 of y = 26.3 mm) drawn in Fig. 3.11(b). It is found that the temperature of PCM composite along L1 drops gradually from hot wall to cold wall, which is owing to L1 is located in high thermal conductivity metal ligament, and heat is transferred by heat conduction. Whereas it can be noticed that the temperature variation of PCM composite along L2 exhibits periodic fluctuation, which is caused by the difference of thermal conductivity between PCM and metal foam. Furthermore, we can find that the local temperature difference ΔT between metal structure and paraffin is obvious. The local temperature difference close to heated wall is larger than that away from heated wall.

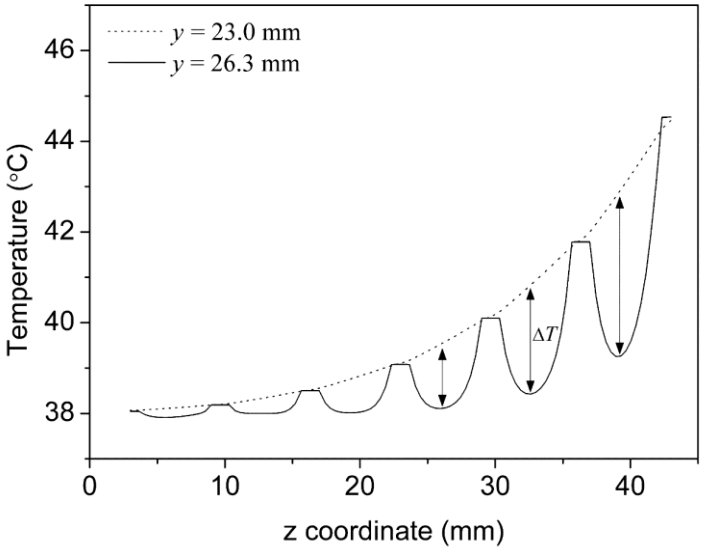

Fig. 3.12. Temperature variation along two horizontal lines

To study heat transfer mechanism, the velocity field of pure paraffin and PCM composite is displayed in Fig. 3.13. Fig. 3.13(a) depicts the velocity field of pure paraffin on the plane of x = 23 mm. Due to buoyancy force, liquid paraffin near heated wall flows upward, and ascends to the top part. Then liquid paraffin flows downward along melting interface, which yields circulating current in the liquid region of paraffin. This reveals the natural convection plays a vital role in melting heat transfer for pure paraffin. It is found that the flow of liquid paraffin is most distinct at 25 min. It is observed that the velocity of liquid paraffin adjacent to the heated wall and melting interface is larger than that of other domains during the melting process. Moreover, it is seen that the maximum velocity within pure paraffin is larger than that within PCM composite, which is due to the larger flow resistance resulted from embedding metal foam.

The velocity fields of paraffin with metal foam on the plane of x = 26.3 mm and x = 23 mm are illustrated in Fig. 3.13(b) and Fig. 3.13(c), respectively. It is found that the velocity of liquid paraffin on plane x = 23 mm is very small during the whole melting process. This is due to the liquid paraffin on this plane is divided into some small region by metal structure, which leads to the larger flow resistance. The liquid paraffin just forms a very faint flow within a cell structure. While the velocity of liquid

paraffin (the plane of x = 26.3 mm) is more obvious compared to the liquid paraffin (the plane of x = 23 mm). It is found that the velocity of molten paraffin is almost 0 m/s at the initial stage, which demonstrates heat transfer in PCM with metal foam is dominated by heat conduction during this period. As the melting continues, the flow of liquid paraffin driven by buoyancy gradually develops, and the velocity is becoming larger, which reveals that natural convection starts to occur. It can be found that the flow of liquid paraffin can also form a circulating current at post-melting stage, which implies that the natural convection is strengthened. Furthermore, we can find some small circulating current around the metal struts (seen by the circle), which can heighten the heat exchange between the metal structure and paraffin. According to the above analysis, it is proved that there is some difference in heat transfer mechanics between pure paraffin and PCM composite.

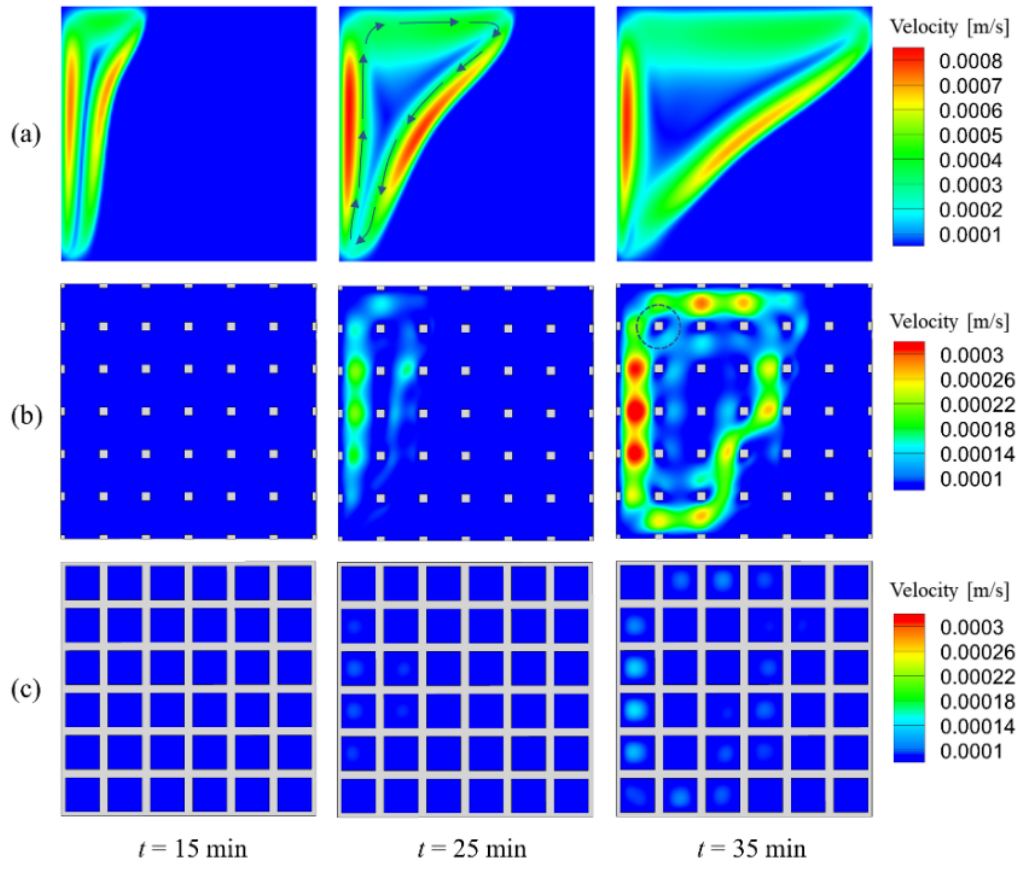

Fig. 3.13. Velocity field of (a) pure paraffin, (b) PCM composite (x = 26.3 mm) and (c) PCM composite (x = 23 mm)

To estimate the thermal storage performance of PCM with and without metal foam, we perform the analysis of energy storage rate (i.e., per unit time per mass of PCM stores energy). The energy (E) stored from the beginning of heating to the completion of melting can be calculated by the following equation [64]:

$$E_f(t) = \begin{cases} m_f c_f (T_f(t) - T_0) & T_f < T_m \\ m_f c_f (T_f(t) - T_m) + m_f L + m_f c_f (T_m - T_0) & T_f > T_m \end{cases} \quad (3\text{-}18)$$

where E_f is the energy stored in paraffin, t is the total melting time, and T_f is the average temperature of paraffin.

Based on the numerical simulation and above theoretical calculation, a comparison of energy storage is shown in Table 3.2. It is found that energy stored in PCM with metal foam is smaller than that of PCM without metal foam, which can be attributed to the fact that embedding metal foam results in a reduction in the mass of paraffin. However, it is seen from the results that the energy storage rate of paraffin without metal foam is 74.7 J/kg s, and the energy storage rate of paraffin with metal foam is 90.3 J/kg s. The energy storage rate thus improves 1.2 times by embedding metal foam.

Table 3.2 Comparison of energy storage

	Melting time, t (s)	Energy, E (J)	Energy storage rate (J/Kg s)
PCM with metal foam	2555	11692	90.3
PCM without metal foam	4153	17464	74.7

3.4.5 Effect of the metal material

Fig. 3.14 shows the comparison of liquid fraction of PCM embedded in metal foam with four different materials. It can be found that the variation tendency of liquid fraction for PCM composite with different materials is similar, i.e., the liquid fraction of composite is zero in the pre-melting stage, and liquid fraction gradually increases

until the melting completes. While the melting rate of PCM composite is different, where the melting rate of PCM with copper foam is most lager among embedding these four materials. It is demonstrated that the high thermal conductivity material is better conducive to enhancing the heat transfer performance of PCM, e.g., the total melting time of PCM embedding copper foam can be reduced by 42% compared to embedding titanium alloy structure.

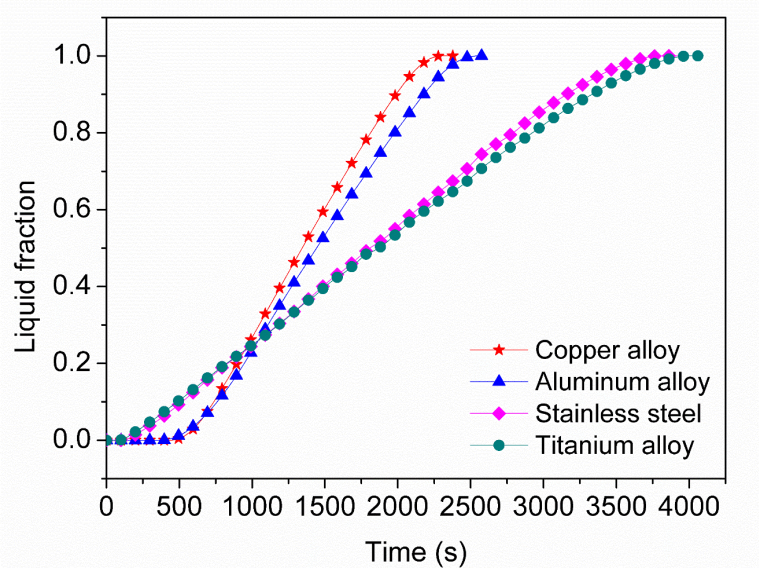

Fig. 3.14. Comparison of liquid fraction of PCM embedded in metal foam with four materials

The liquid fraction of pure paraffin is selected as a benchmark, and the enhancement ratio of PCM embedded in four metal materials can be defined by:

$$e_r = \left[\frac{\beta(\text{composite})}{\beta(\text{paraffin})} - 1 \right] \times 100\% \tag{3-19}$$

To facilitate quantitative comparison of thermal performance enhancement of PCM, the enhancement ratio e_r in the whole melting evolution is depicted in Fig. 3.15. At the beginning of melting, the e_r is a negative value for four metal foam, which means the melting rate of PCM infiltrated in metal foam is smaller than that of pure paraffin. This is because heat is fast transferred from the heated wall to the whole domain of composite through the metal ligament, and temperature of paraffin near heated wall doesn't reach to melting point. As time continues, the e_r rises quickly and

becomes a positive value, which indicates that the melting rate of PCM composite is larger than that of pure paraffin. It is noticed that the effect of embedding aluminum foam and copper foam on the thermal performance enhancement of PCM is significant, in which maximum e_r for PCM with copper foam can reach 63%. Furthermore, it is found that the e_r for PCM composite with stainless steel and titanium alloy is very small, which reveals the role of embedding low conductivity metal foam in the thermal performance enhancement of PCM is negligible.

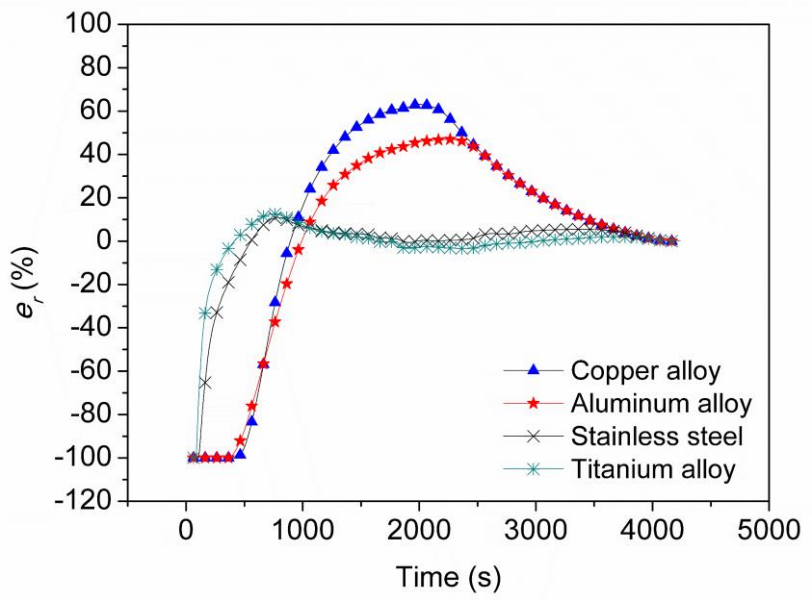

Fig. 3.15. Comparison of the enhancement ratio e_r of PCM embedded in metal foam with different materials

3.5 Conclusion

In this chapter, the thermal performance enhancement of PCM has been experimentally and numerically investigated. PCM composite is fabricated by embedding porous aluminum structure in paraffin. The visible experiment has been conducted to study the enhancement in the thermal performance of PCM, in which metal foam fabricated by 3D printing is used as a heat transfer enhancer. Based on the pore-scale numerical method, the 3D model is developed to investigate further heat transfer characteristics of PCM with and without metal foam.

It is demonstrated from experimental and numerical results that embedding metal

foam with cubic cell structure can improve the thermal behavior of PCM, e.g., the total melting time of paraffin with metal foam is shortened by 38% compared to pure paraffin. Also, the temperature field of paraffin with metal foam is more uniform, e.g., the maximum temperature difference of PCM with metal foam can be decreased by about 81% compared to pure paraffin. In addition, it is found that the energy storage rate of PCM with metal foam is improved by 21% that of pure paraffin. The numerically predicted results are in good agreement with experimental data.

The heat transfer mechanics of paraffin with metal foam is different from pure paraffin by analyzing the solid-liquid interface and velocity field, e.g., the heat conduction plays an important role in the melting process of PCM composite. Whereas the melting heat transfer of pure paraffin is dominated by natural convection during the melting process. In addition, it can be found that there is a temperature difference between metal structure and paraffin, and local thermal non-equilibrium near the hot wall is more evident than that away from the hot wall.

Metal foam with different materials has a different effect on the thermal performance of PCM composite. It is found that the use of high thermal conductivity metal foam can dramatically strengthen the thermal behavior of PCM, e.g., the maximum enhancement ratio of PCM with porous copper structure can reach 63%. However, embedding low thermal conductivity metal foam has a small effect on the thermal performance enhancement of PCM. The study of the effects of metal material is significant for the material choose when metal foam is used as thermal enhancer in thermal energy storage and thermal management system.

Chapter 4.

Effects of structure parameters of metal foam

Chapter 4. Effects of structure parameters of metal foam

4.1 Introduction

The studies on the thermal performance of PCM embedded in metal foam have been carried out by some researchers. For instance, Xiao et al. [145] examined the thermal characterization of phase change material infiltrated in metal foam. They found that the thermal conductivity of PCM composite was drastically improved compared to the pure paraffin by the experimental measure and theoretical calculation, e.g., the thermal conductivity of the PCM composite using metal foam with 96.95% porosity and 25ppi is about thirteen times as much as that of pure paraffin. We performed the experimental and numerical investigation on the thermal behavior of PCM composite using metal structure in previous study [139]. According to the results shown in Chapter 3, it is demonstrated that embedding metal foam with cubic periodic cell can effectively enhance the thermal behavior of PCM.

Several studies reveal that the structure parameters of metal foam have an influence on the thermal performance of PCM composite. For example, Lafdi et al. [61], in the experiment, investigated the effect of metal foam porosity and pore size on the melting process and temperature variation of phase change material infiltrated in the high thermal conductivity metal foam. They reported that the system parameters of metal foam had a drastic influence on the heat transfer behavior of PCM composite. Li et al. [146] also performed an investigation of the effects of foam morphology parameters, including porosity and pore density, on the wall temperature and temperature uniform within PCM composite.

In this chapter, the effects of morphology parameters of metal foam on thermal performance of the PCM composites are investigated, in which metal foam with idealized cube cell possesses high thermal conductivity, highly-porous structure and low relative density and is an excellent candidate used as the metal matrix of composites. The low melting temperature paraffin wax R56 is selected as phase change material. The pore-scale numerical method is used to calculate the temperature variation and trace the melting evolution of both pure paraffin and the PCM composite.

We perform the study on the effects of morphology parameters in order to further investigate the heat transfer characteristics of PCM composite using metal foams with various morphology parameters, which is of great significance for the application of metal foam in the TES and TM system.

4.2 Modeling of metal foam with cubic cell structure

4.2.1 Geometrical model

Fig. 4.1 presents schematic diagram of metal foam that is composed of a cubic cell structure. The metal foam with cubic cell structure not only can be fabricated easily by additive manufacturing technology but also has all characteristics of metal foam. The unit cell of metal foam is ideal cube-shaped, in which metal struts are connected with 90^{o} angle at each vertex. A three-dimensional model of metal foam with periodic structure is modeled as the cubic array of members of ligament length l and square cross-section of side thickness a. With l and a, the porosity ε of metal foam can be determined by Eq. (3-1).

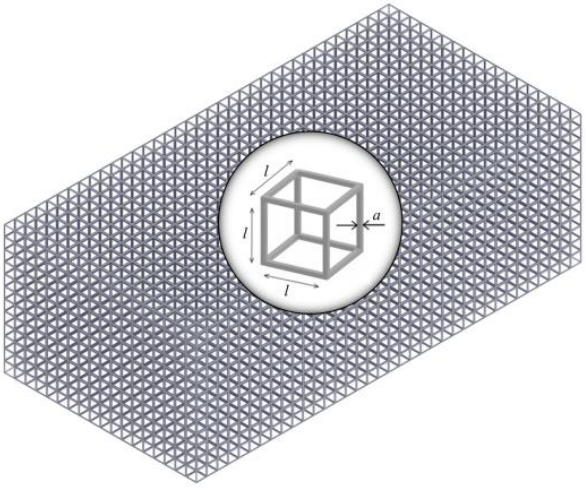

Fig. 4.1. Schematic diagram of metal foam with cubic periodic cell [147]

In this study, paraffin wax R56-58 (produced by Merck Millipore Malaysia) is utilized as PCM and impregnated in the pore space of metal foam for preparing PCM composite. As we all know that the metal materials used for manufacturing metal foam have many kinds. The high conductivity aluminum is chosen as metal matrix to

research the thermal behavior of PCM composite. The thermal properties of paraffin wax and aluminum AS7G are summarized in Table 4.1.

Table 4.1 Thermal properties of paraffin and aluminum [147]

Property	Material	
	Paraffin	AS7G
Specific heat, c (J/kg K)	2100	963
Density, ρ (kg/m^3)	840	2680
Thermal conductivity, k (W/m K)	0.2	160
Viscosity, μ (kg/ m s)	0.003	
Thermal expansion coefficient, γ (1/K)	0.0004	
Latent heat, L (kJ/kg)	120.7	
Solidus temperature, T_{m1} (K)	323.75	
Liquidus temperature, T_{m2} (K)	339.65	

4.2.2 Numerical model

To save computing time, a cubic aluminum foam with sizes of 15 mm ×15 mm ×15 mm is selected as the computational domain, as depicted in Fig. 4.2. The thermal behavior of aluminum foam/paraffin PCM composite with different morphology parameters is investigated under steady and unsteady state. Moreover, the thermal behavior of PCM composite is compared to that of pure paraffin. In steady state, the effective thermal conductivity of PCM composite can be calculated based on Fourier's equation to investigate the effects of porosity and pore density on the effective thermal conductivity. The temperatures of the left/right walls are 290K/310K, respectively. The other walls are insulated. The heat flux can be obtained in steady state, in which there is only the heat conduction between the paraffin and aluminum matrix, since the paraffin is solid phase between 290K and 310K.

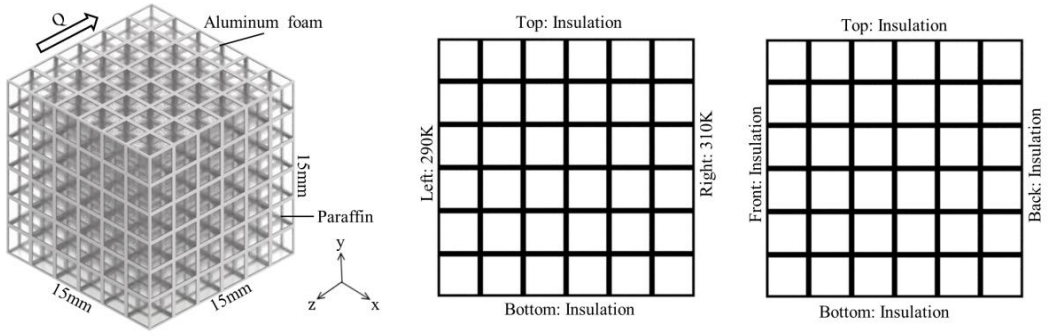

Fig. 4.2. Numerical model of aluminum foam/paraffin PCM composite in steady state

To study the melting evolution and heat transfer characteristics of PCM composite during the melting processes, the numerical simulation is conducted in the unsteady state. It is very important to take the combined influence of heat conduction and heat transfer convection between paraffin and aluminum foam into account. The paraffin wax with an initial temperature of 293.15 K is heated by the left hot wall that is at a constant temperature of 350 K. The other walls are insulated. In order to obtain the temperature variations within PCM composite during the phase change process, nine temperature monitoring points (T1, T2, T3… etc.) are inserted into the composites, as shown in Fig. 4.3.

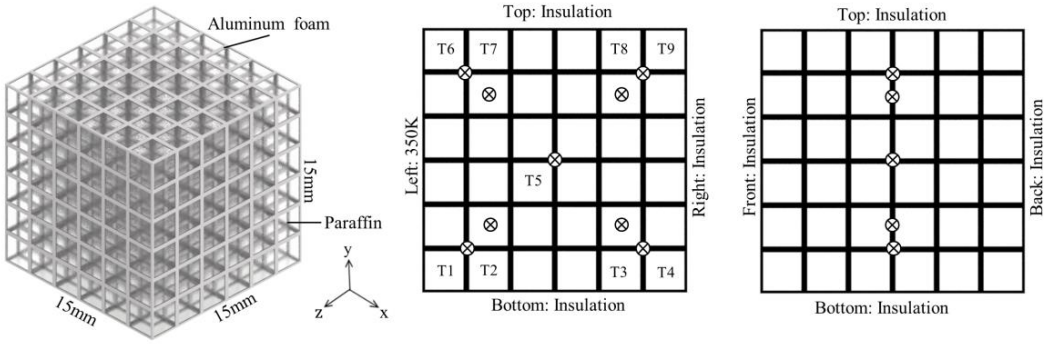

Fig. 4.3. Numerical model of aluminum foam/paraffin PCM composite in unsteady state

4.2.3 Numerical method

The heat transfer of PCM composite is very complicated during the phase change process, including convective heat transfer between the metal foam and liquid PCM, heat conduction between the metal foam and solid PCM, natural convection of the liquid PCM, etc. In the numerical simulations, several assumptions should be adopted:

(1) the paraffin of liquid phase is considered as incompressible, and the flow is laminar inside the enclosed space; (2) the natural convection caused by Buoyancy is subject to the Boussinesq assumption; (3) the thermal radiation inside the composite could be neglected; (4) the thermal properties of the paraffin and aluminum foam are constant and considered as homogeneous and isotropic, except the density of PCM in liquid phase. Based on the above assumptions, the pore-scale numerical method is used for simulating thermal performance of pure paraffin and PCM composite. The governing equations can be written as follows:

(1) Equations of fluid dynamics:

Continuity equation:

$$\nabla \cdot \vec{U} = 0 \tag{4-1}$$

Momentum equation:

$$\rho_f \frac{\partial \vec{U}}{\partial t} + \rho_f \left(\vec{U} \cdot \nabla\right)\vec{U} = -\nabla p + \mu \nabla^2 \vec{U} + \rho_f g \gamma \left(T_f - T_m\right) + S\vec{U} \tag{4-2}$$

where ρ_f and μ are the density and viscosity of phase change material, respectively.

The term $S\vec{U}$ in Eq. (4-2) is an additional source term of damping velocity in solid phase region of PCM:

$$S = -\frac{A_m \left(1-\beta\right)^2}{\lambda + \beta^3} \tag{4-3}$$

where A_m and λ are the simulation coefficients which are proposed to be 1×10^5 and 1×10^{-3} respectively; β is the liquid fraction ranging from 0 to 1, which is variable according to the temperature of PCM:

$$\beta = \begin{cases} 0 & T_f < T_{m1} \\ \left(T_f - T_{m1}\right)/\left(T_{m2} - T_{m1}\right) & T_{m1} < T_f < T_{m2} \\ 1 & T_f > T_{m2} \end{cases} \tag{4-4}$$

(2) Energy equation of heat transfer:

Energy equation for heat transfer of solid and liquid regions within PCM:

$$\rho_f c_f \frac{\partial T_f}{\partial t} + \rho_f c_f \vec{U} \cdot \nabla T_f = \nabla \cdot \left(k_f \nabla T_f \right) - \rho_f L \frac{\partial f_l}{\partial t} \tag{4-5}$$

Energy equation for heat transfer of metal foam:

$$\rho_s c_s \frac{\partial T_s}{\partial t} = \nabla \cdot \left(k_s \nabla T_s \right) \tag{4-6}$$

Eqs. (4-7) and (4-8) show the temperature and heat of contact surface between PCM and metal foam, respectively:

$$T_f = T_s \tag{4-7}$$

$$k_f \frac{\partial T_f}{\partial n} = k_s \frac{\partial T_s}{\partial n} \tag{4-8}$$

4.2.4 Computational details

The CFD package ANSYS Fluent 18.0 is used for pore-scale numerical simulation. With pore-scale numerical simulation, the assumption of local thermal equilibrium (or non-equilibrium) for heat transfer between metal foam and PCM is no longer needed. The governing equations for energy transport in the metal foam and momentum/energy transport in paraffin within pores are discretized using second order upwind schemes. PISO algorithm is employed for velocity-pressure coupling, and PRESTO method is applied as the pressure equation discretization, and then the finite volume approach is used to numerically solve. With the rapid development of computer technology, a high-performance computer and parallel process is recommended considering a large amount of 3D grids in this model.

The time step has real physical meaning for numerical simulation in unsteady state. If the time step cannot be reasonably chosen, it will lead to computation non-

convergence. Therefore, the time step is a vital influence factor for the numerical simulation in unsteady state. The time independence analysis is conducted using three different time-steps (0.1 s, 0.5 s, 1 s). In comparison with the three results of liquid fraction, it can be found that the three time-steps have almost the same prediction results, as shown in Fig. 4.4. Hence time step 1 s is selected, which can ensure time-step independence and accuracy of results.

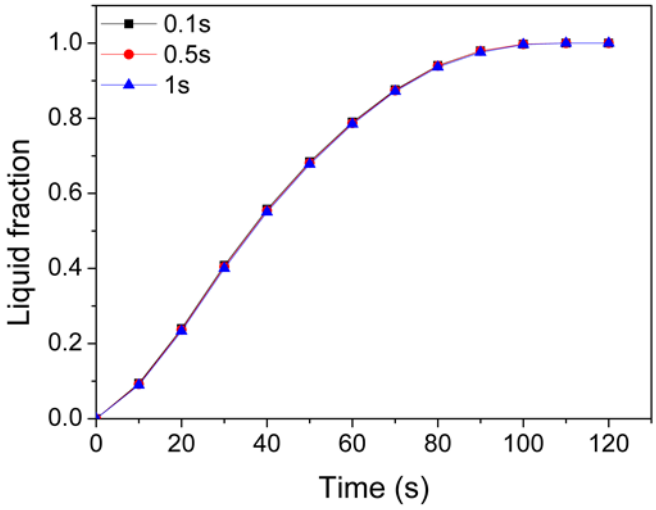

Fig. 4.4. Time independence analysis

Software ICEM CFD 18.0 can be used to generate grids in the computational domain. The structured element is adopted to discretize the solid and fluid domains of PCM composite. The mesh independence analysis is conducted adopting three different number meshes, i.e., the coarse mesh with 90k cells, medial mesh with 580k cells, and fine mesh with 2200k cells. The results are displayed in Fig. 4.5. By comparing with the results of three meshes, it can be seen that the differences of liquid fraction for meshes with 580k and 2200k cells are less than 2%, and the three meshes have almost the same prediction results. Considering the accuracy and time of the numerical calculation, the mesh with 580k cells is selected, which can ensure the mesh independence.

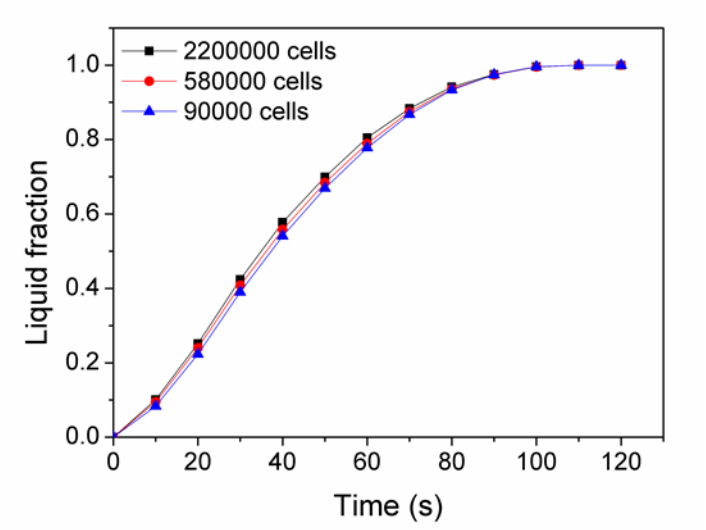

Fig. 4.5. Mesh independence analysis

4.3 Thermal behavior of PCM composite

4.3.1 Melting evolution

To distinctly show the melting process, the phase distribution diagrams of PCM composite (ε=95%, 10ppi) in three plane sections, as presented in Fig. 4.6. The red region is the liquid phase. It is noted that the solid-liquid interface almost parallels the hot wall at 50 s initial stage of melting. This phenomenon indicates that heat conduction is the primary way in the heat transfer of PCM composite, which is owing to the high thermal conductivity of aluminum foam. The melting of PCM composite in the top domain is a little faster than that of the bottom zone at 90 s. This phenomenon is owing to the natural convection strengthen in liquid paraffin. As the melting progresses, the melting of composite in the top domain is much faster than that of the bottom zone, and the solid-liquid interface does not parallel the hot wall anymore. It is demonstrated that heat convection dominates the heat transfer inside PCM composite. Moreover, we can find that paraffin wax always melts from outside to inside within each cubic unit cell, which results from the temperature difference between paraffin wax and aluminum matrix in the melting process. This phenomenon not only conduces to the increase of melting rate but also improves the uniformity of melting for PCM composite.

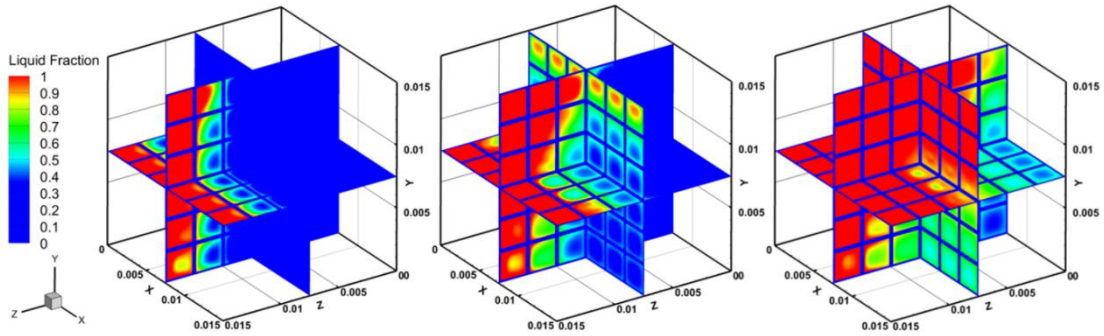

t=50s *t*=90s *t*=152s

Fig. 4.6. Phase distribution diagrams of PCM composite at 30%, 50% and 80% liquid fraction in the melting process

4.3.2 Heat transfer characteristic

To understand the heat transfer performance of PCM composite in the melting process, the temperature of aluminum foam (ε=90%, 10ppi) at five various locations (T1, T4, T5, T6 and T9) and paraffin at four various locations (T2, T3, T7 and T8) are extracted in terms of temperature-time history, as shown in Fig. 4.7. The temperature increase of aluminum struts is fast at the solid state for paraffin shown in Fig 4.7(a). This is due to the high thermal conductivity of aluminum foam that is conducive to heat transfer from the hot wall to the whole aluminum skeleton. The temperature of locations (T1/T4 and T6/T9) in parallel with the hot wall is almost the same. It reveals that the heat is transferred by heat conduction and transmitted along the direction perpendicular to the hot wall. The temperature of aluminum skeleton increases slowly for paraffin at the mush state, which results from the energy extensively stored in the paraffin by latent heat. Besides, the temperature of the location near the hot wall and at the top region is high such as T6. As time progresses, the temperature of five different locations is almost the same when the paraffin is liquid phase. The temperature increase of the paraffin is fast, and the temperature of locations (T2/T7 and T3/T8) in parallel with the hot wall is almost the same at the solid state for paraffin, as shown in Fig. 4.7(b). It is demonstrated that the heat can be rapidly transferred from aluminum skeleton to paraffin by heat conduction. The temperature increase of paraffin is slow at the mush state for paraffin, which indicates a larger amount of the

energy stored by paraffin in the form of phase change latent heat. The temperature of four different locations is almost the same at the liquid state for paraffin.

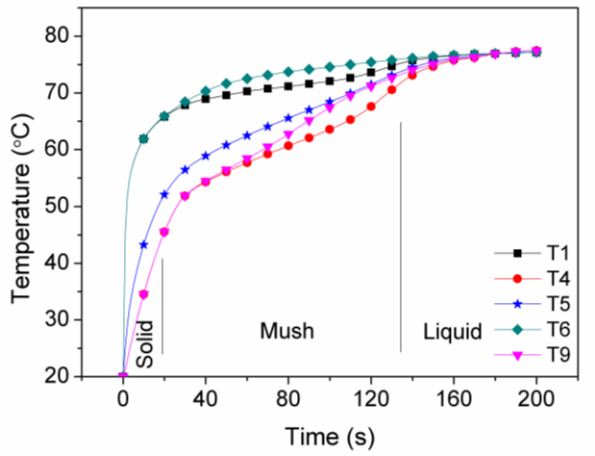

(a) Aluminum foam

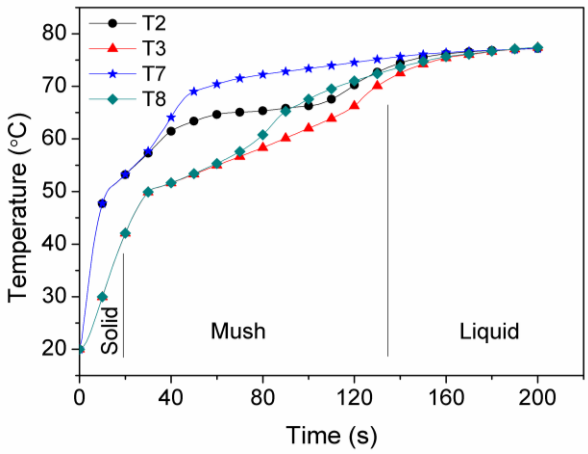

(b) Paraffin

Fig. 4.7. Temperature variation of aluminum foam and paraffin at different locations during the melting process

To investigate the local thermal equilibrium and thermal non-equilibrium phenomenon within PCM composite, the temperature difference at four different locations is presented in Fig. 4.8. It is observed that the temperature differences at different locations increase at the beginning of melting and then decrease. It is demonstrated that there is local thermal non-equilibrium within PCM composite during the melting process. The temperature difference increases quickly, and the temperature difference of the location near the hot wall (T1/T2 and T6/T7) is greater

than that of the location away from the hot wall (T3/T4 and T8/T9) at the beginning of the melting, which is owing to that the heat can be rapidly transferred through high thermal conductivity aluminum skeleton and the temperature increase of aluminum skeleton is very quick. While the temperature increase of paraffin is relatively slow due to low thermal conductivity. The temperature difference decreases after the PCM composite is heated for a few seconds, which results from the heat conduction between aluminum foam and paraffin. As time continues, the temperature differences are relatively stable, which owes to the natural convection of liquid paraffin and convection heat transfer between aluminum skeleton and paraffin. Due to the natural convection enhancement at the liquid state for paraffin, the temperature difference finally decreases to 0 ℃, and it is local thermal equilibrium state between aluminum skeleton with paraffin.

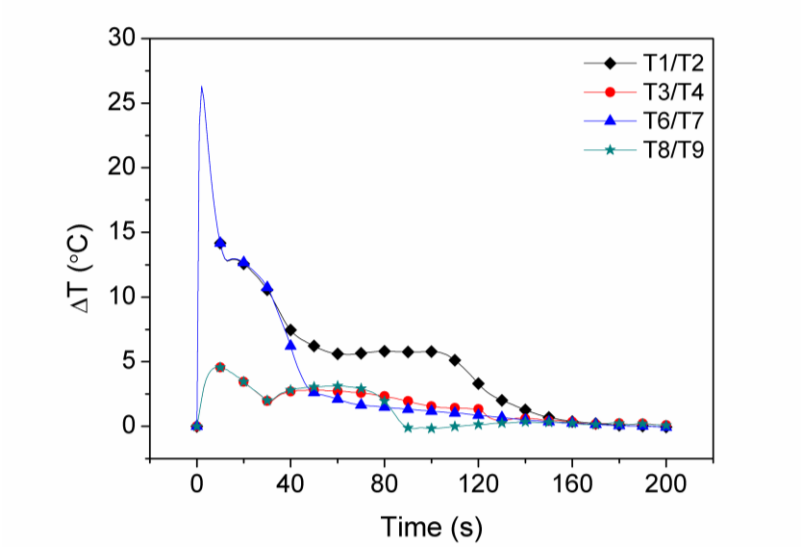

Fig. 4.8. Temperature difference between aluminum skeleton and paraffin at different locations

4.3.3 Velocity field

To exhibit the natural convection within PCM composite during the melting evolution, the velocity contours of paraffin wax inside PCM composite (ε=95% and 10ppi) in three plane sections are depicted in Fig. 4.9. It is noted that the range of velocity distribution gradually increases as the melting progresses. It reveals that the

natural convection within composite is strengthened. It is also seen that the velocity for the local region in the vicinity of the hot wall and solid-liquid interface is much greater than the other regions. The natural convection is very distinct at the left top domain of PCM composite.

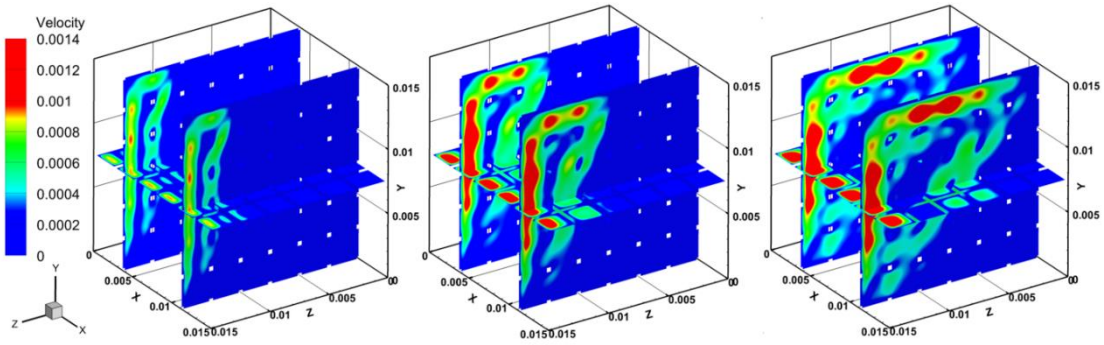

t = 50 s t = 90 s t = 152 s

Fig. 4.9. Velocity contours of paraffin within PCM composite at 30%, 50% and 80% during the melting process

Fig. 4.10 presents the velocity diagram of paraffin within PCM composite in section x = 0.00375 m at 90 s. We can see that the flow circulation of the liquid paraffin is quite distinct, which can be attributed to the natural convection of liquid paraffin. The liquid paraffin close to the hot wall flows upward. The liquid paraffin near the solid-liquid interface flows down. This phenomenon is attributed to the buoyancy effect caused by the temperature difference. Also, it is observed that the local flow takes place around the aluminum struts. It is proved that the convection heat transfer occurs between aluminum skeleton and paraffin, which augments the heat exchange within PCM composite during the phase change process.

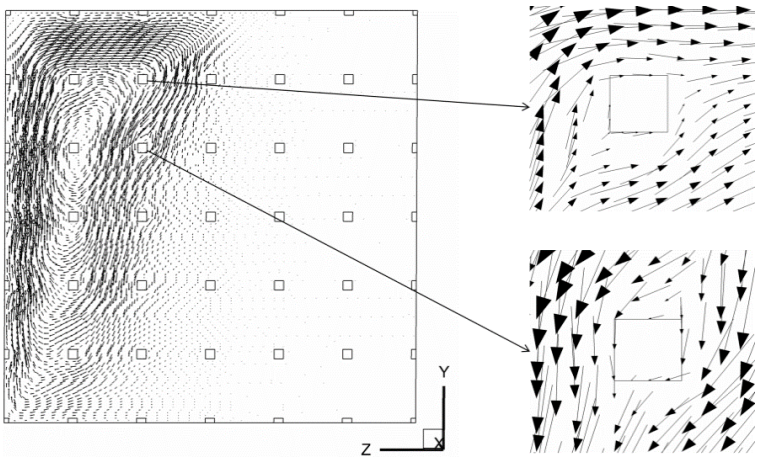

Fig. 4.10. Velocity diagram of paraffin within PCM composite at t = 90 s

4.4 Effects of morphology parameters

4.4.1 Thermal performance enhancement

Fig. 4.11 shows the temperature comparison of both pure paraffin and paraffin wax inside PCM composite (ε=95%, 10ppi). It can be observed that the temperature buildup of paraffin is evident in the vicinity of the hot wall at t = 50 s. The temperature of both pure paraffin and paraffin wax gradually reduces from left to right, which is owing to heat flux transferred from the hot wall to the cold wall. Fig. 4.11(a) presents that the temperature distribution of paraffin wax inside composite is uniform and parallels the hot wall. This phenomenon is attributed to the high thermal conductivity of aluminum foam, which is conducive to transfer heat quickly, thereby homogenizing the temperature of the whole composite. Whereas the temperature field of pure paraffin shows a distinct gradient distribution, and the temperature at the left top is higher than that of the right bottom, as displayed in Fig. 4.11(b). This phenomenon results from the low thermal conductivity of pure paraffin, which results in the accumulation of temperature at the top region. Totally, the temperature field of paraffin wax inside PCM composite is more uniform, and its melting time is shorter as compared to pure paraffin.

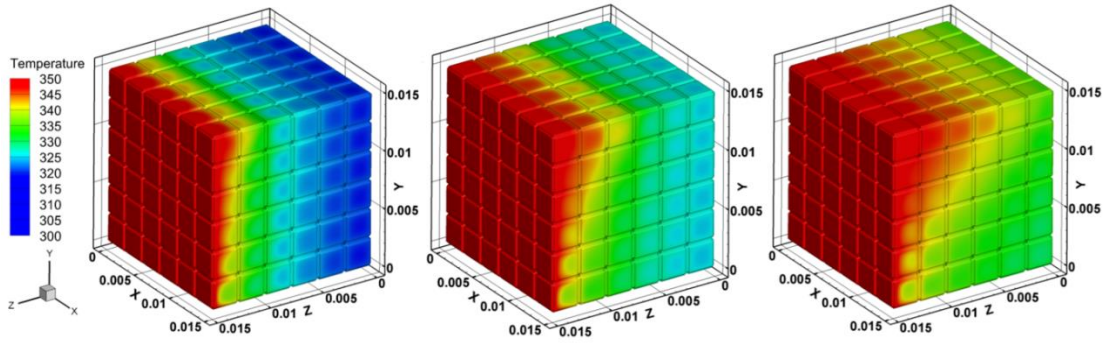

t = 50 s t = 90 s t = 152 s

(a) Temperature distribution diagrams of paraffin wax inside PCM composite

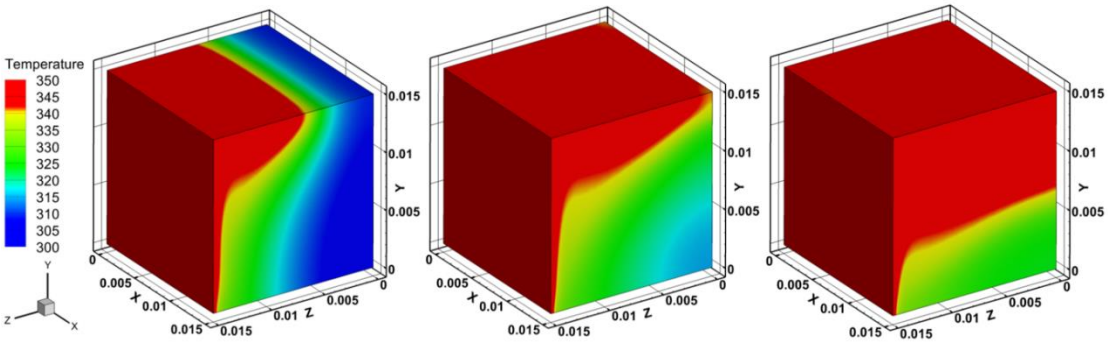

t = 380 s t = 592 s t = 880 s

(b) Temperature distribution diagrams of pure paraffin

Fig. 4.11. Temperature comparison of both pure paraffin and paraffin wax inside PCM composite at 30%, 50% and 80% liquid fraction

4.4.2 Effective thermal conductivity

The effective thermal conductivities for PCM composite with different porosities and pore densities are numerically calculated in the present investigation. The numerical results are compared to the prediction models developed by Xu et al. [148] and Bhattacharya et al. [133] to verify the validity of numerical calculation. The classical models used to calculate the effective thermal conductivity are the parallel model and series model, respectively. These two limit values of effective thermal conductivity of PCM composite are calculated by the following equations:

Parallel $k_{\parallel} = \dfrac{k_f k_s}{\varepsilon k_s + (1-\varepsilon) k_f}$ (4-9)

Series $k_{\perp}=\varepsilon k_f+(1-\varepsilon)k_s$ (4-10)

Based on the above equations, Bhattacharya et al. developed an empirical correlation. The effective thermal conductivity is given by:

$$k_1=Bk_{\parallel}+(1-B)k_{\perp} \tag{4-11}$$

According to fitting some dates, B=0.35 is recommended.

Xu et al. developed a phase distribution model for PCM composite, which is comprised of the cubic cell and cavity caused by the solidification shrinkage of PCMs. The effective thermal conductivity is given by:

$$k_2=k_f\left((1-\xi)^2 x_s+\frac{2\xi(1-\xi)x_s}{1-\xi+x_s}+\frac{\xi^2\left(\xi^2-\zeta_s{}^2\right)}{\xi^2-\zeta_s^2+\zeta_s^3}\right) \tag{4-12}$$

where ξ is the length ratio $(l-2a)/l$, ζ_s is the length ratio c/l, c is the length of cavity, and x_s represents the thermal conductivity ratio k_s/k_f.

In the present numerical calculation, some assumptions should be adopted: (1) the heat transfer is primarily one-dimension heat conduction; (2) The heat flux of any cross-section is equal along heat conduction direction. The thermal conductivity λ can be calculated according to Fourier's equation:

$$Q=-Ak\frac{\mathrm{d}T}{\mathrm{d}x} \tag{4-13}$$

Fig. 4.12 presents a comparison of effective thermal conductivities of PCM composite. For the porosities 70% and 95% PCM composite with pore density 10ppi, effective thermal conductivities are 24.6 W/(m K) and 3.3 W/(m K), which are about 123 and 17 times as much as that of paraffin wax. It is found that the effective thermal conductivity of PCM embedded in metal foam is significantly improved. Moreover, the effective thermal conductivities of PCM composite reduce as the increase of porosities, whereas the effective thermal conductivities of 5ppi and 10ppi composites with the same porosity are almost the same, which indicates that there is no the

significant effect of pore density on the effective thermal conductivity. It can be found that numerical results of the paraffin/aluminum foam PCM composite with the porosities 90% and 95% agree well with the theoretical prediction from models proposed by Xu et al. and Bhattacharya et al., while numerical results of the paraffin/aluminum foam PCM composite with the relatively low porosities are greater than the theoretical prediction results. This may be because these prediction models are recommended to theoretically calculate the effective thermal conductivities for composites with the porosity range higher than 90%, resulting in the deviation of numerical simulation from theoretical prediction with porosity range lower than 90%.

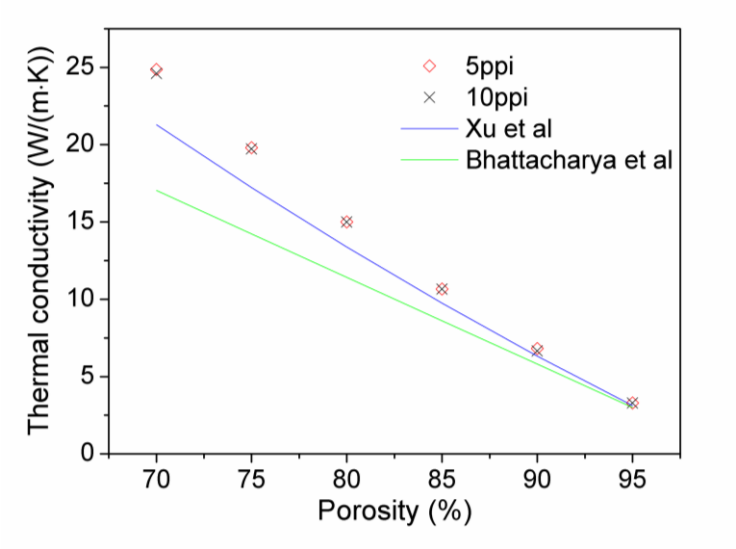

Fig. 4.12. Comparison of numerical results and theoretical prediction

4.4.3 Thermal optimization of PCM composite

The liquid fraction variations of PCM composite with different geometrical parameters are displayed in Fig. 4.13 during the melting process. It is noted that there is a similar variation tendency for liquid fraction variations of these PCM composites. However, melting rates of PCM composite with different structure parameters are different. It can be seen from the results the melting rate for composite (ε=70%, 10ppi) is the fastest, and the melting rate for composite (ε=95%, 5ppi) is the lowest. The melting rates of composites with low porosity are larger than that of composite with high porosity, which is due to a larger volume fraction (i.e., low porosity) of metal

enhancer material can achieve a more obvious enhancement in thermal performance of PCM. In addition, it is noted that the melting rates of PCM composite with 10ppi are larger than that of PCM composite with 5ppi. Meanwhile, it is demonstrated that embedding metal foam is conducive to improve the melting rate of PCM composite.

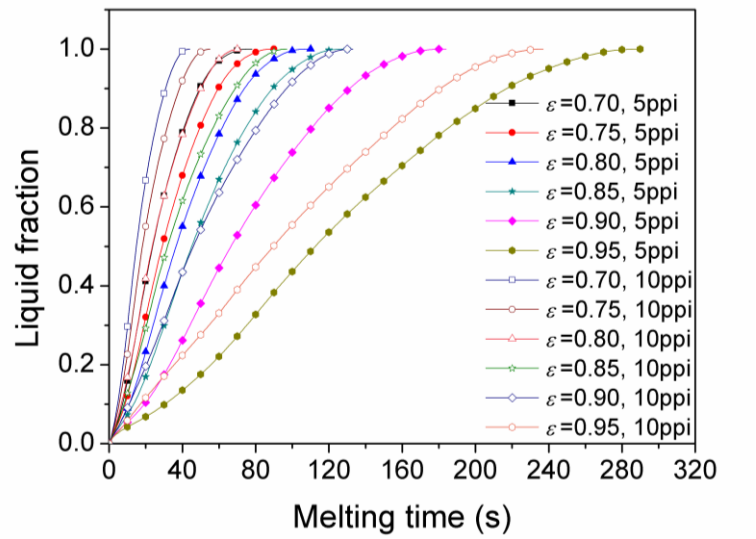

Fig. 4.13. Liquid fraction of PCM composites with melting time

The total melting times for PCM composites with different geometrical parameters are plotted in Fig. 4.14. It is found that the melting time of PCM composite with the same pore density increases as the porosity increases. Also, the total melting time for PCM composite with 10ppi is smaller than that of PCM composite with 5ppi when the porosity of PCM composite is the same. The total melting time of pure paraffin without the aluminum foam is 1216s. The melting time for composites with 5ppi and 10ppi aluminum foam can be shortened to 6.6-24.1% and 3.7-19.7% of that of pure paraffin, respectively. It demonstrates that the pore density and porosity have a comprehensive influence on the melting time of PCM composite. Hence it is necessary to take into account of the combined effects of both pore density and porosity when metal foam is used in the thermal energy storage or thermal management system. In all cases, the PCM composite with 70% porosity and 10ppi exhibits the best thermal performance. This study is of great significance for the optimization of the thermal performance of PCM composite.

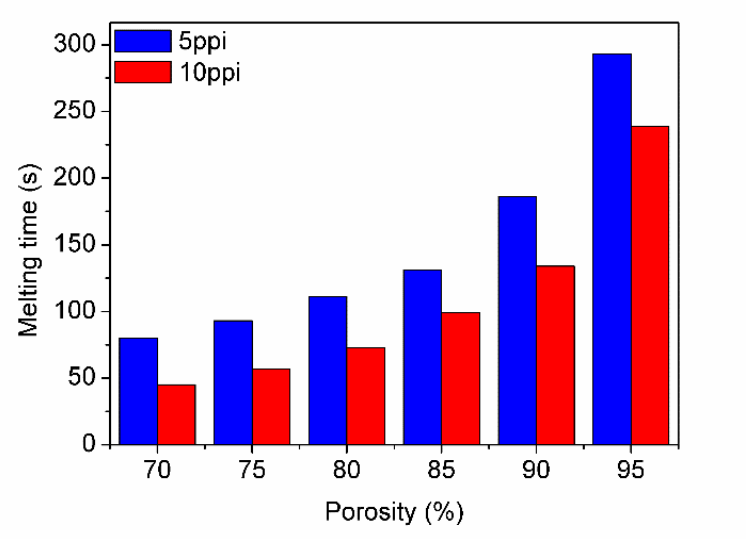

Fig. 4.14. Comparison of melting time for PCM composites with different geometrical parameters

4.5 Conclusion

In this chapter, the effects of structure parameters on the thermal performance of PCM composites are investigated by using pore-scale numerical method. Aluminum foam with cubic cell structure is selected as the porous material, and the low melting temperature paraffin wax R56 is used as the PCM. Compared to pure paraffin, the melting time of paraffin embedded in aluminum foam has a significant reduction, and temperature distribution is more uniform. The effect of embedding metal foam on the thermal performance of PCM composites is very distinct, e.g., the effective thermal conductivity of PCM composites can be enhanced about 123 and 17 times as much as that of pure paraffin. The numerical results of effective thermal conductivity agree well with the theoretical predictions from the models of Xu et al. and Bhattacharya et al.

It is found from the results that the geometrical parameters of metal foam have a significant effect on the thermal performance of PCM composites. The melting time for PCM composites by using the high porosity or low pore density aluminum foam is longer as compared to the PCM composite with the low porosity or high pore density aluminum foam. That is attributed to the integrated effect of porosity and pore density

on the heat conduction and convection heat transfer between metal foam with paraffin. The effective thermal conductivity increases with the decrease of the metal foam porosity for PCM composites when the pore density is the same. However, the pore density has no evident influence on the effective thermal conductivity for the PCM composites with the same porosity.

Using the pore-scale numerical simulation, we can obtain the direct visualization for the melting evolution, temperature and velocity within PCM composites during the melting process. It is noted that there is the local thermal non-equilibrium between the aluminum matrix and paraffin during the melting process, and the thermal non-equilibrium phenomenon gradually weakens with the decrease of the temperature difference between paraffin and metal foam. It is proved that natural convection happens in the liquid phase domain of paraffin during the melting process by observing the velocity contour.

Chapter 5.

Application of 3D printed metal foam in heat sink

Chapter 5. Application of 3D printed metal foam in heat sink

5.1 Introduction

With the development of high-performance electronic chips, a large amount of heat is generated in electronic devices. This can lead to the decline in work performance and reduction of operating life of electronic devices [92]. Thermal management plays an important role in the utilization of electronic devices subjected to high heat generation density [149]. In the past few years, some studies on the use of phase change material in the thermal management of electronics were performed. It is found that the thermal management system using PCM requires a lower weight and fewer volume of equipment in comparison to the conventional thermal management system. Therefore, PCM based heat sink as a novel cooling method is great promising to be applied for the thermal management of electronic devices.

However, the low thermal conductivity of PCM diminishes heat transfer rate of heat sink, which can cause the increase of base temperature of heat sink once PCM melts close to the heat sink base [150]. To overcome this disadvantage, the enhancement method of inserting some materials with high thermal conductivity, known as thermal conductivity enhancer (TCE), into heat sink was proposed. TCE was utilized in different forms including fin [151], pin-fin [152], metal foam [153], and honeycomb structure [154]. For instance, Gopalan et al. [137] numerically investigated the role of structured porous metal in the thermal enhancement of PCM based heat sink, where the employed porous metal has different structures, including square, diamond, octahedral lattice frame, and hexagonal honeycomb structure.

The literature has presented that porous metal as TCE can strengthen thermal behavior of heat sink. Therefore, the investigation on the usage of metal foam in the thermal management unit is of great significance. In this chapter, the experimental investigation is performed to study the role of metal foam on the enhancement in the thermal performance of heat sink, in which the metal foam with cubic cell structure is fabricated by 3D printing. Meanwhile, the effects of porosity of metal foam and power level of heat source on the thermal performance of heat sink are also investigated.

5.2 Experimental investigation

5.2.1 Test sample

When phase change material is selected, some characteristics need to be considered, including chemical stability, latent heat, supercooling and melting point. For the present study, the commercial paraffin RT 62HC is chosen as PCM. The thermophysical properties are provided by the manufacturer (Rubitherm, Germany) [155], as listed in Table 5.1. RT 62HC has an appropriate phase change temperature and considerable latent heat, which is a benefit for heightening the thermal behavior of heat sink. It is known from the literature that a significant volume change of PCM during phase change has a negative influence on the encapsulation of PCM and needs to be considering for the design of the encapsulated containers. Therefore, the small volume expansion (2%) of RT 62HC is another critical reason for the selection of PCM. Besides, RT 62HC has a relatively low cost (about US$ 7.5/kg). Commercial paraffin RT 62HC is employed based on the above reasons.

Table 5.1 Properties of employed materials [156]

Materials	Thermal conductivity (W/m k)	Density (kg/m^3)	Specific heat (J/kg K)	Latent heat (kJ/kg)	Melting point (°C)
RT 62HC	0.2	850/840	2000	230	62-63
Aluminum	183	2670	940	-	-

A metal foam with a cubic cell structure is developed to be used as thermal enhancer material, where the metal ligament of metal foam is connected at an angle of 90°. The length and thickness of metal ligament are l and a, respectively. According to the theoretical equation, the porosity ε could be calculated depending on the value of l and a. According to the designed metal foam, the test sample with dimensions $40 \times 40 \times 40$ mm^3 is fabricated by selective laser melting (SLM) technique, as shown

in Fig. 5.1. Metal foam is made of aluminum alloy in the present study. Aluminum alloy is selected as the thermal enhancer material due to its high thermal conductivity, low density, corrosion resistance, and extensive utilization in the electronic industry field. Due to the controllability of structure and material, the effects of 3D printed metal foam on the thermal performance of heat sinks will be studied.

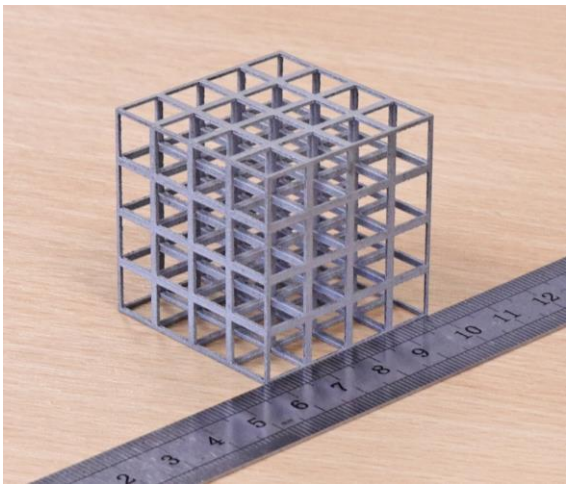

Fig. 5.1. 3D printed metal foam with cubic cell structure

5.2.2 Experimental apparatus and procedure

Fig. 5.2 shows the schematic diagram of experimental setup. The experimental apparatus contains a heating system, test section, data measurement and collection system. DC power can provide steady input power to the heater in the heating system. According to the various operating status of electronic devices, three different input powers (i.e., 8 W, 10 W and 12 W) is provided for imitating the heat generation from the electronic component. In the data measurement and collection system, the data logger is used to trace temperature data at a time interval of 1 s. Then temperature data is transferred to the computer. The test section mainly consisted of heat sink, PCM, and insulation block. The detailed structure parameters of heat sink and metal foam for different types of PCM based heat sinks are given in Table 5.2.

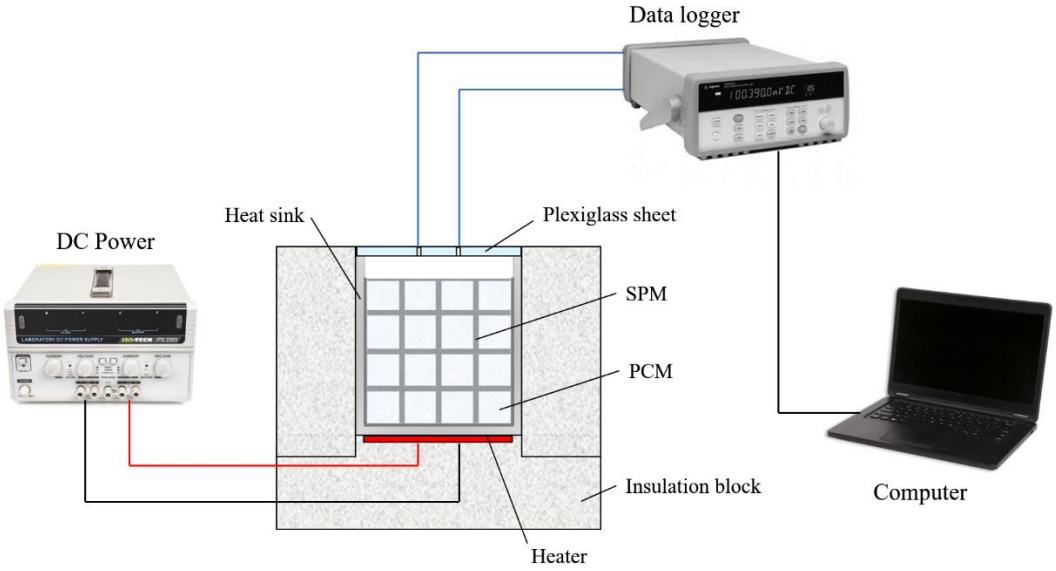

Fig. 5.2. Schematic diagram of experimental setup

Table 5.2 Structure parameters of heat sink and metal foam

Heat sinks Type	Dimensions of heat sink (mm)	Porosity ε (%)	Ligament length l (mm)	Thickness a (mm)
ε = 95%	44 × 44 × 52	95	10	0.68
ε = 90%	44 × 44 × 52	90	10	0.98
ε = 85%	44 × 44 × 52	85	10	1.22
ε = 80%	44 × 44 × 52	80	10	1.43

The cross-section drawn of test section is presented in Fig. 5.3. The heat sink with 2 mm wall thickness is made of aluminum by using electric discharge machine, where the length, width and height are $44\ \text{mm} \times 44\ \text{mm} \times 52\ \text{mm}$, respectively. A plate heater with size of $40 \times 40 \times 1\ \text{mm}^3$ is employed to mimic the heat generated by electronic component. The thermal grease is used between the heat sink base and heater to reduce contact resistance. The metal foam and PCM are put in the cavity of heat sink. The insulation block with low thermal conductivity is used for enclosing heat sink to reduce thermal loss. Considering the influence of the mass of PCM on the thermal behavior of heat sinks, the mass of paraffin filled in heat sinks is the same and

40 g for all experiments. A plexiglass sheet is placed at the top of heat sink to survey the experimental evolution and fix the thermocouple. Two small round holes are drilled through the plexiglass sheet, which is used to fix the wires of thermocouples.

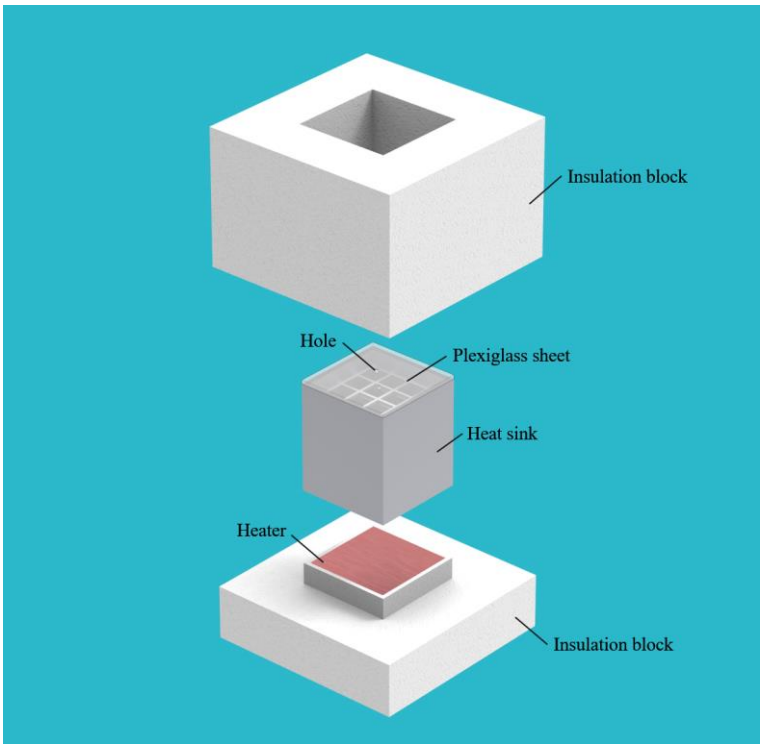

Fig. 5.3. Cross-section drawn of test equipment

5.2.3 Thermocouple positions

Six calibrated K-type thermocouples are employed to trace the temperature variation at various locations of heat sink. The locations of thermocouples are displayed in Fig. 5.4. For obtaining the base temperature, three thermocouples (TC#3, TC#4, TC#5) are evenly attached to the bottom surface of heat sink along the vertical centerline. The internal temperature of heat sink is measured by embedding two thermocouples (TC#1 and TC#2) into two symmetrical locations at height of 20 mm from heat sink base. To fix positions of thermocouples in heat sink, TC#1 and TC#2 were inserted into heat sink through the round holes of plexiglass sheet, and the thermal adhesive is also used. The last thermocouple is used to monitor the ambient temperature.

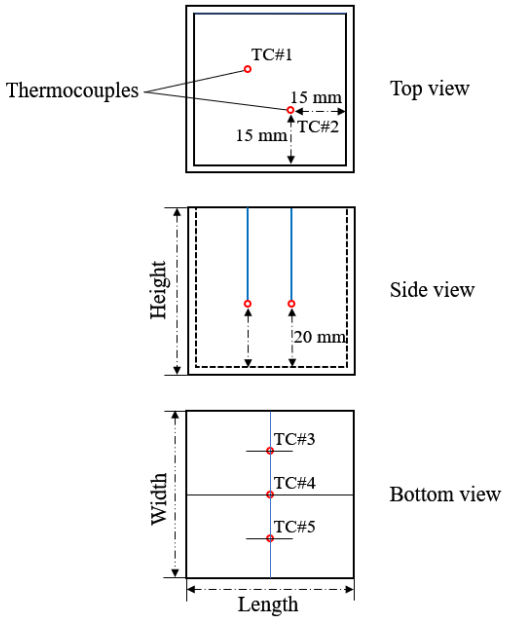

Fig. 5.4. Thermocouple distribution positions

5.2.4 Uncertainty in experiment

The experimental uncertainties are determined in this section. The uncertainties of experiment are caused due to the errors of employed instruments, including DC power, electric heater and thermocouple. The uncertainty of power input supplied by DC power is 1%, which is determined using a standard calibrated multi-meter. The uncertainty of plate heater is 5%, which is provided by the manufacturer. The uncertainty of temperature measurement is evaluated by a standard thermometer. The maximum deviation in the temperature is ± 0.5°C.

5.3 Thermal behavior of heat sink

The base temperature of heat sink acts as the maximum allowable temperature of the electronic component. Considering the allowable operating temperature of electronic devices, the critical temperature of the heat sink base is set to a constant, such as 60 ℃ or 70 ℃, in order to ensure operating efficiency and reliability of electronic devices. Thereby, the time taken to reach the critical temperature can reflect the thermal management performance of heat sink, so it is a primary parameter for evaluating the heat sink effect.

5.3.1 Thermal response of heat sink with PCM

Fig. 5.5 shows a comparison of the base temperature for single heat sink and heat sink with PCM at the power level 8 W. The average value of thermocouples TC#3, TC#4 and TC#5 is employed to represent the base temperature of heat sink. It can be observed that the ambient temperature is about 20 ℃. An allowable operating temperature of electronic device is assumed to 70 ℃. The base temperature of the single heat sink increases quickly to 70 ℃ at 667 s. The operation time taken by heat sink with PCM to reach the critical temperature of 70 ℃ is 2140 s that is 3.2 times as much as that of single heat sink. It indicates that the use of metal foam is conducive to heightening the thermal performance of heat sink.

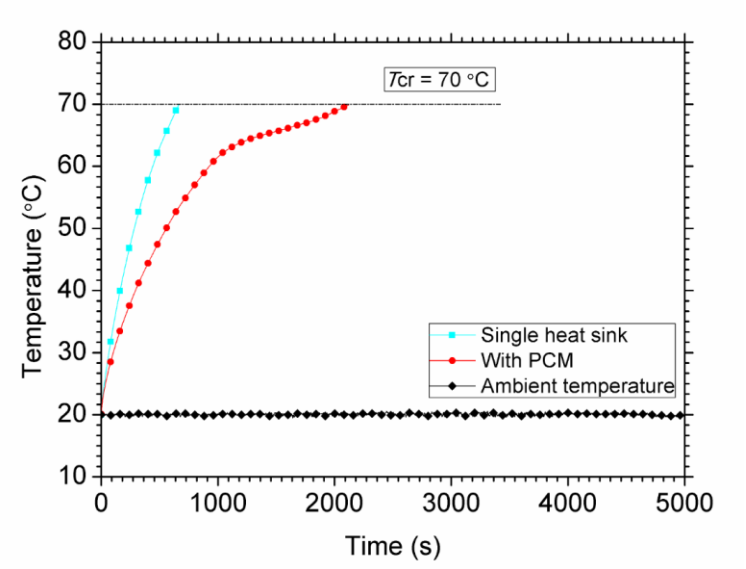

Fig. 5.5. Thermal response of heat sinks with PCM and without PCM

5.3.2 Thermal response of heat sink with PCM and metal foam

To study the role of metal foam on thermal enhancement of PCM based heat sink, the thermal response of heat sinks using metal foam is analyzed, in which the heat sink base is subjected to the power input of 8 W. The comparison of thermal performance for heat sink with PCM and heat sink with PCM and metal foam (a composite) is presented in Fig. 5.6. The comparison experiment is conducted under the same experimental condition. The results show the operation time of heat sink with PCM

and metal foam to reach the critical temperature of 70 ℃ can increase to 4045 s, which is 1.9 times that of heat sink with PCM and 6.1 times that of single heat sink. It reveals that the combined usage of PCM and metal foam in heat sink can obviously improve the thermal performance of heat sink.

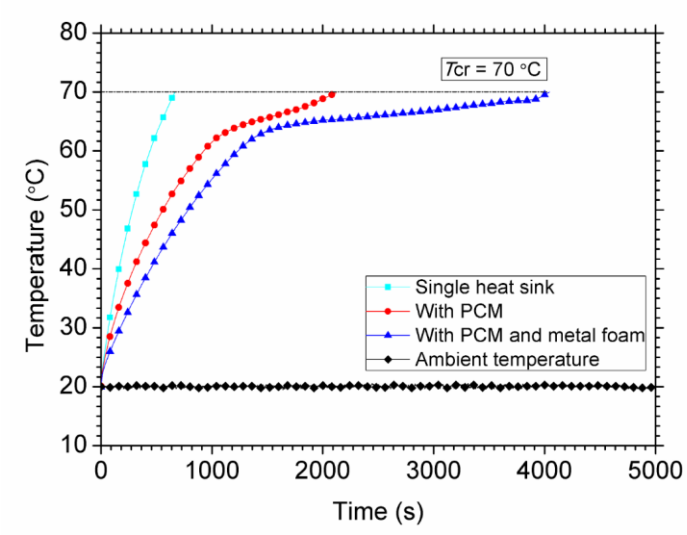

Fig. 5.6. Thermal response of heat sinks with and without metal foam

5.3.3 Temperature variation of heat sink

To examine the thermal performance of heat sink in a whole heating and cooling process, the temperature values at different locations of heat sink are employed to show the temperature variation of the base and inside of heat sink. The temperature profile of heat sink with 80% porosity metal foam is depicted in Fig. 5.7. The whole temperature control process mainly contains two stages, where one is the heating stage, and another is the cooling stage. For the heating process, the rising rate of temperature is high in the pre-sensible heating and post-sensible heating stages. The temperature profile of heat sink is flat in the latent heating stage because a large amount of energy is stored by PCM. For the cooling stage, it is observed that the temperature of heat sink decreases rapidly after input power is stopped. In the latent cooling stage, the temperature variation of heat sink is not apparent. In the post-sensible cooling stage, the decrease rate of temperature becomes larger again.

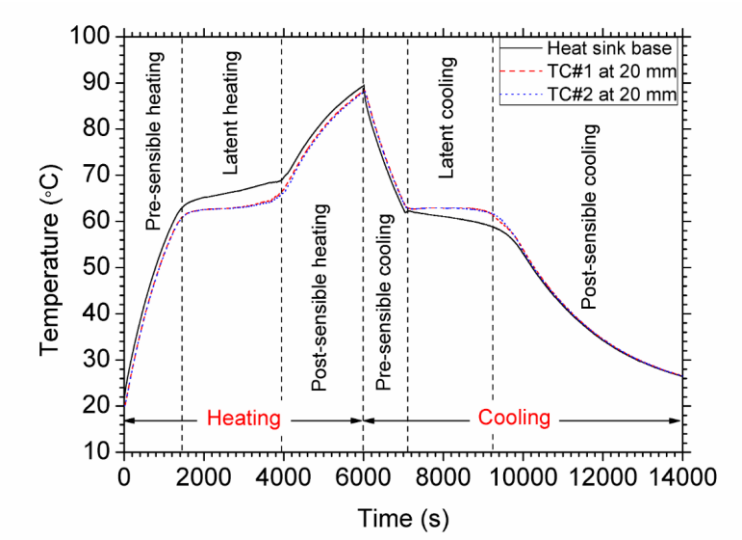

Fig. 5.7 Temperature profile of heat sink at different locations for input power of 8 W

5.4 Role of metal foam in the thermal enhancement of PCM based heat sink

5.4.1 Effect of the porosity of metal foam

A temperature comparison for heat sinks using various porosities metal foam at two power inputs of 8 W and 12 W is displayed in Fig. 5.8. It is found that the trend in temperature variation for all heat sinks is similar. For instance, the base temperature of heat sink rises fast until PCM in heat sink begins to melt. The rising rate of base temperature becomes small when PCM close to the base face of heat sink starts to melt, which is since a large amount of heat is stored in PCM as latent heat. It can be observed that the base temperature of heat sinks with metal foam is lower than that of the heat sink with PCM at the same time. This phenomenon is because heat can be quickly removed from the base to the whole domain of heat sink through high thermal conductivity metal foam. The base temperature of heat sink using metal foam with various porosities is different. It implies that the porosity of metal foam has an influence on the thermal performance of heat sink. The heat sink using 80% porosity metal foam exhibits the minimum rise in base temperature among heat sinks using metal foam.

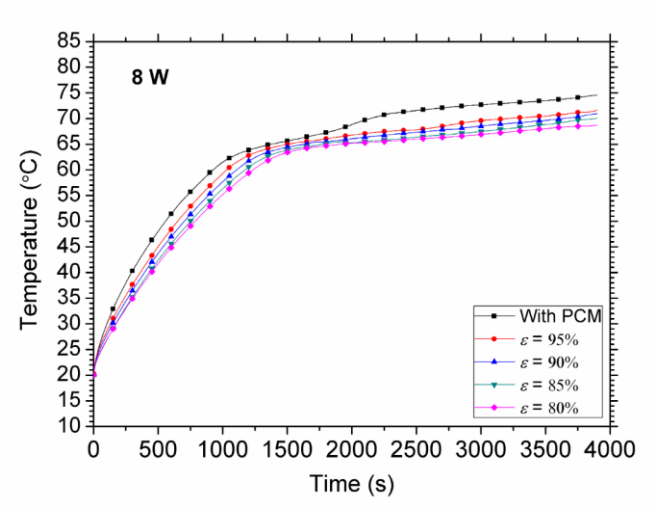

(a)

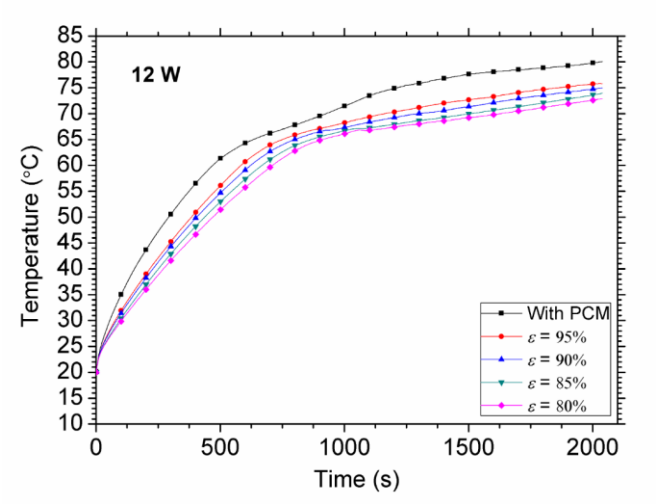

(b)

Fig. 5.8 Temperature response of designed heat sinks at various power levels (a) 8 W and (b) 12 W

5.4.2 Enhancement in operating time

To estimate the enhancement in thermal performance of PCM based heat sink, the time taken by heat sinks using various porosity of metal foam to reach the critical temperatures is obtained at three power levels: 8 W, 10 W, and 12 W. The critical temperatures selected (60°C and 70°C) represent the maximum allowable temperature of the electronic component. Fig. 5.9 (a) and (b) display the time required to the critical temperatures of 60 °C and 70 °C. It is observed that the time taken by heat sinks with metal foam is larger than that of heat sink without metal foam, e.g., the operating time

of heat sink using 95% porosity metal foam for T_{cr} = 70 ℃ is increased by 50% at input power of 8 W compared to heat sink with PCM. It reveals that metal foam has a positive role in the enhancement in thermal performance of heat sink.

A notable feature among heat sinks with metal foam is that the operating time of heat sink using low porosity metal foam is longer. It is seen that more time is taken by the heat sink with 80% porosity metal foam to reach each critical temperature compared to the other heat sinks. This phenomenon indicates that the decrease of porosity can improve the thermal performance of heat sink. Moreover, it is found that the increase in heat generation density of electronic component can result in the reduction of operating time, e.g., the operating time of 80% porosity metal foam heat sink at critical temperature 70 ℃ is 4045 s, 2495 s, and 1622 s for heating power 8 W, 10 W and 12 W, respectively.

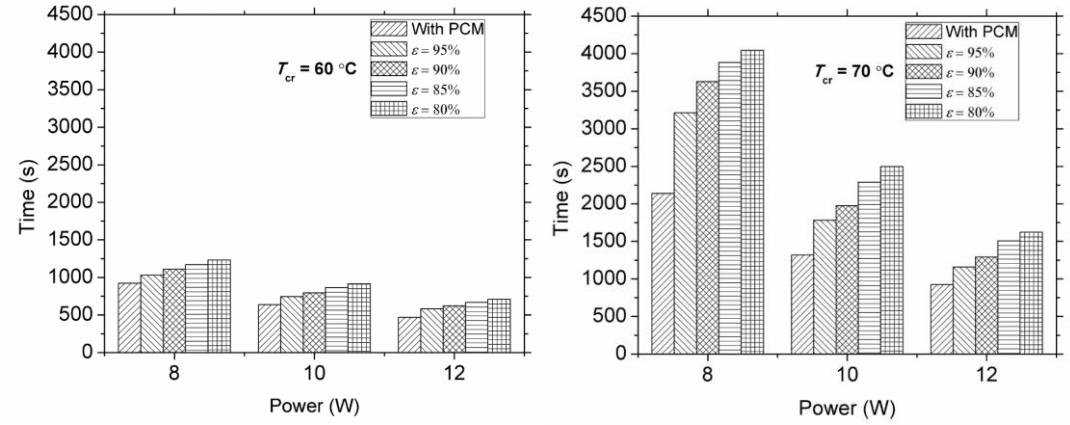

Fig. 5.9. Time taken by various heat sinks to reach critical temperatures of: (a) 60 ℃ and (b) 70 ℃

5.4.3 Enhancement ratio of PCM based heat sink

The enhancement in thermal performance of heat sink can be estimated by the enhancement ratio e_r that is the ratio of time taken by heat sink with metal foam to that of heat sink without metal foam (i.e., With PCM) to reach the critical temperature, as written by:

$$e_r = \frac{t_{cr}(\text{with metal foam})}{t_{cr}(\text{without metal foam})} \tag{5-1}$$

where t_{cr} is the time taken to reach the critical temperature.

The enhancement ratio e_r of heat sinks with various porosities metal foam at the critical temperatures of 60 ℃ and 70 ℃ is presented in Fig. 5.10. It is found that the heat sink using metal foam with 80% porosity shows the highest enhancement ratio against other heat sinks in all cases. The enhancement ratio increases with the reduction of porosity of metal foam in all cases of using metal foam. For instance, for critical temperature 70 ℃, the enhancement ratios of heat sink with 95%, 90%, 85%, and 80% porosities metal foam are 1.35, 1.50, 1.73, and 1.89 at the power level of 10 W. It indicates that the porosity of metal foam (i.e., the volume fraction of enhancer material) plays a significant role in the thermal performance enhancement of PCM based heat sink.

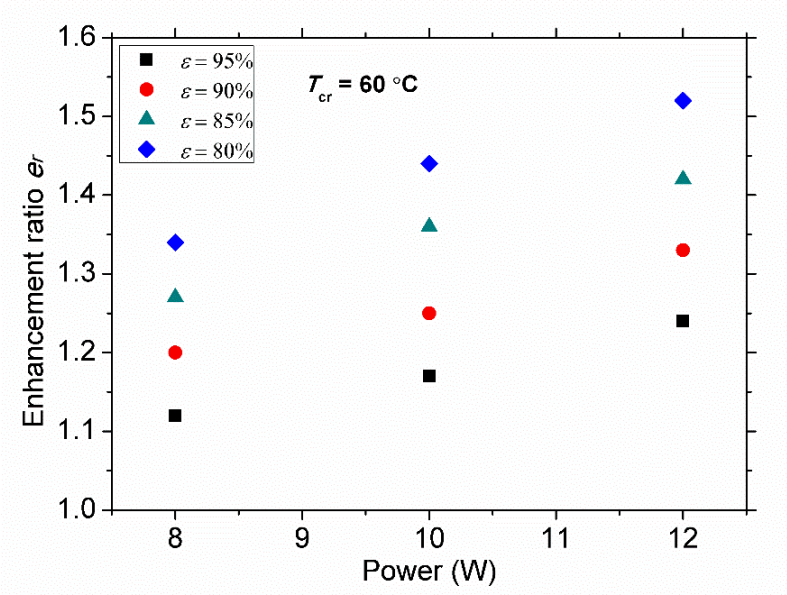

(a)

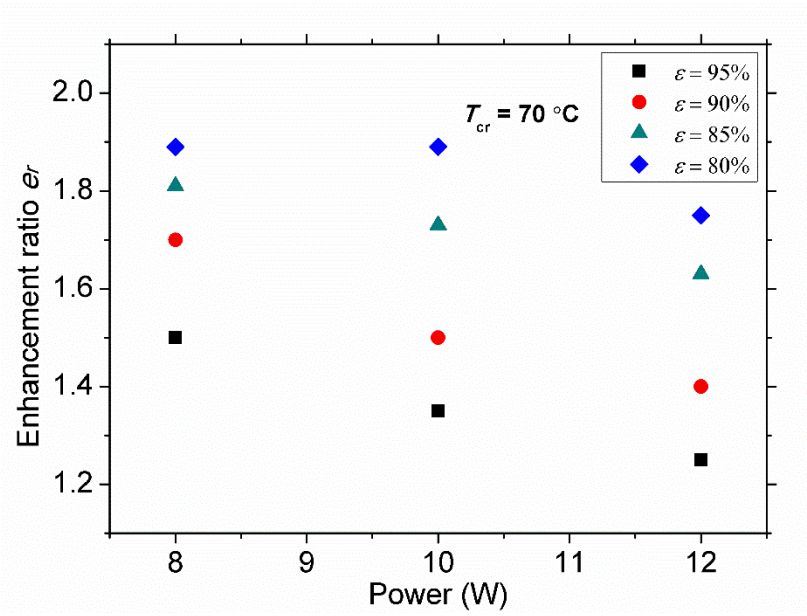

(b)

Fig. 5.10 Enhancement ratio e_r of heat sinks with different porosities metal foam at critical temperatures of: (a) 60 ℃ and (b) 70 ℃.

Fig. 5.11 presents the comparison of enhancement ratios e_r for heat sink with 80% porosity metal foam at two critical temperatures of 60 ℃ and 70 ℃. We can see that the higher ratios are obtained for the critical temperature of 70 ℃ at each input power. This phenomenon is owing to that the critical temperature is higher than the melting point of PCM. In the latent heating stage, heat sink can remain a longer operating time to achieve a more efficient cooling for the higher critical temperature (i.e., 70 ℃). The enhancement ratio of heat sink increases as power density increases for the critical temperatures of 60 ℃. While the enhancement ratio slightly reduces with an increase in input power for the critical temperature of 70 ℃. It implies that the allowable operating temperature and heat generation density have a comprehensive influence on the thermal performance of PCM based heat sink using metal foam.

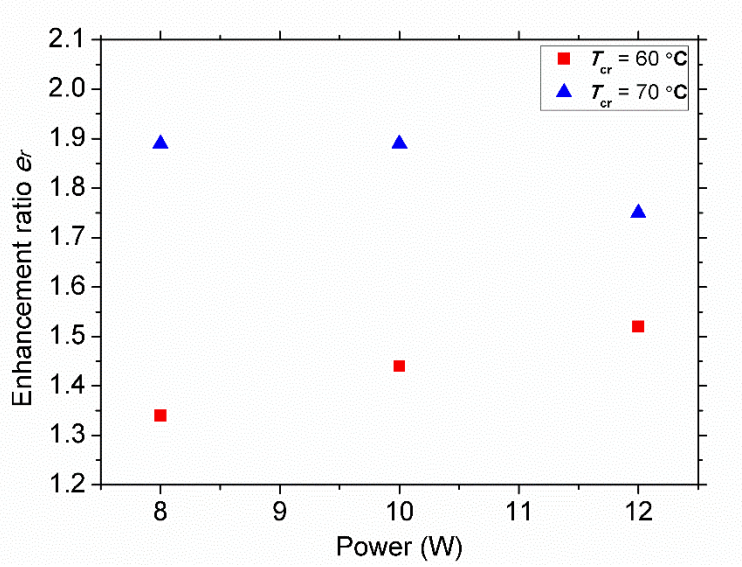

Fig. 5.11 Comparison of enhancement ratio for heat sink with 80% porosity metal foam at two critical temperatures

5.5 Conclusion

In this chapter, the metal foam with a cubic periodic cell is designed, and metal foam with different porosities is fabricated by 3D printing technology. The experiment is carried out to investigate the thermal performance of PCM based heat sink with and without metal foam. Also, the thermal performance of heat sinks with four porosities metal foam is analyzed and compared. The heat sink base is subjected to three power inputs of 8 W, 10 W, and 12 W, and the base temperature of heat sink acts as the maximum temperature of the electronic device.

The experimental results show that the use of metal foam can effectively extend the operation time of PCM based heat sink for electronic device cooling compared to the single heat sink and heat sink with PCM. For instance, the operation time of heat sink with PCM and metal foam (i.e., 80% metal foam) to reach critical temperature 70 °C is 6.1 times and 1.9 times that of the single heat sink and heat sink with PCM. Besides, the temperature distribution is more uniform for the heat sink with metal foam.

It can be found from results that the porosity of metal foam has an important influence on the thermal behavior of PCM based heat sink. The operation time of heat sink increases when the porosity of metal foam decreases at three power inputs. The

enhancement ratios e_r of heat sink using metal foam also increase with the reduction of porosity of metal foam. The heat sink using 80% porosity metal foam presents the best thermal performance in all cases of the experiments. Besides, heating power levels also affect the thermal response of PCM based heat sink. The increase of power level can lead to a decrease in the operating time of PCM based heat sink.

General conclusions and perspectives

General conclusions

Embedding metal foam in phase change material is an effective method for enhancing the thermal performance of PCM. The metal foam as a thermal conductivity enhancer plays a vital role in metal foam/PCM composite. The aim of this thesis is to study the thermal performance of metal foam/PCM composite by using experimental and numerical methods, in which metal foam possesses a cubic cell structure and is fabricated by 3D printing technique. This study is of great significance for the utilization of PCM in thermal energy storage and thermal management system.

To analyze the effects of heating and contact conditions, nine different heating and contact condition cases are considered and used. It is found from the results that the heat transfer mechanism is different under various heating conditions, which can affect the thermal charging performance of PCM composite. For the different contact conditions, it is noted that contact conditions have an evident influence on the thermal behavior of PCM composite under the left and bottom heating conditions. Finally, it is concluded that the heating and contact conditions have a combined effect on the thermal performance of PCM composite for thermal energy storage. The study of heating and contact conditions can provide theoretical guidance for the selection of heating and contact conditions in the thermal storage system using PCM composite, such as solar thermal storage and latent heat storage device.

A visible experiment is implemented to study the melting evolution of PCM embedded in metal foam that is fabricated by 3D printing and used as a heat transfer enhancer. It is indicated that embedding metal foam with a cubic cell structure can improve the thermal behavior of PCM. For instance, the total melting time of paraffin with aluminum foam is shortened by 38% compared to pure paraffin. Metal foam with different materials has a different effect on the heat transfer rate of PCM composite. Besides, the use of high thermal conductivity metal foam can heighten the thermal performance of PCM more obviously, e.g., the maximum enhancement ratio of PCM with metal foam reaches 63%.

Pore-scale numerical method is used to investigate the effects of structure parameters on the thermal characteristics of PCM composite. The role of metal foam on the thermal performance of PCM composite is very apparent. For example, the effective thermal conductivity of PCM composite using metal foam with 95% porosity and 10ppi can be improved about 17 times as much as that of pure paraffin (PCM). In addition, the porosity and pore density of metal foam have a distinct influence on the thermal behavior of PCM composite. For instance, the melting time for PCM composite using the high porosity or low pore density metal foam is longer than that of PCM composite with the low porosity or high pore density metal foam. This phenomenon is attributed to the combined effect of porosity and pore density on the heat conduction and convection heat transfer within PCM composite.

The experimental application on the thermal performance of PCM based heat sink using 3D printed metal foam is also studied at the end of this thesis. We can see that the use of metal foam can effectively prolong the operation time of heat sink for electronic devices cooling in comparison with the heat sink without metal foam. Also, the temperature distribution is more uniform for the heat sink with metal foam. In addition, the porosity of metal foam has a significant influence on the performance of heat sink. The operation time of heat sinks increases when the porosity of metal foam decreases. The heating power level also affects the thermal response of PCM based heat sink. The rise in power level can lead to the reduction of operation time of heat sink.

Perspectives

This thesis focuses on the thermal performance of metal foam/PCM composite for thermal energy storage and thermal management, in which 3D printing technology is used to fabricate the metal foam with periodic cell structure. For future research, the following aspects can be investigated to continue this thesis:

1. The thermal discharging performance of metal foam/PCM composite

For a typical thermal energy storage system, energy can be stored and released through PCM that undergoes a change in phase. The current study mainly focuses on thermal charging performance. The thermal discharging performance of metal foam/PCM composite also needs to be paid more attention.

2. The thermal optimization of metal foam/PCM composite

It is proved from the present study that the porosity and pore density have a combined effect on thermal performance. The thermal optimization of metal foam/PCM composite needs to be further studied, considering different combinations for porosity and pore density of metal foam.

3. The optimal design of morphology structure of metal foam

Metal foam is a promising thermal enhancer for improving the thermal behavior of PCM. With the development of manufacturing technology, 3D printing can achieve a breakthrough in the fabrication of metal foam with a controlled structure. Hence, the optimal design of the morphology structure of metal foam can be further developed and explored.

Résumé en français

Résumé en français

1. Introduction

Le matériau à changement de phase (MCP) est un matériau idéal pour le stockage d'énergie thermique. Il peut absorber et libérer une grande quantité d'énergie thermique pendant le processus de changement de phase avec une faible variation de température. Par conséquent, Ce comportement peut être largement utilisé dans le domaine du stockage et de la gestion d'énergie thermique. Cependant, la plupart des MCP actuels ont une faible conductivité thermique, ce qui diminue leurs taux de stockage et d'extraction de la chaleur, réduit ainsi leur application potentielle dans l'ingénierie. Pour améliorer cet inconvénient, de nombreuses méthodes d'amélioration ont été proposées et étudiées, telles que l'ajout d'additif des nanomatériaux, l'insertion d'une ailette métallique et l'utilisation de mousse métallique.

Parmi les méthodes citées, l'utilisation de la mousse métallique s'avère être une méthode efficace pour améliorer la conductivité thermique du MCP. En raison de la forte conductivité thermique de la mousse métallique, la chaleur peut être transférée rapidement le long du squelette métallique dans le MCP composite. Ainsi, le taux de stockage de la chaleur pendant le processus de changement de phase du MCP incorporé dans la mousse métallique peut être amélioré. Au cours de la dernière décennie, les performances thermiques du MCP composite utilisant la mousse métallique à topologie stochastique ont été largement étudiées, pourtant à notre connaissance, les études concernant le MCP composite utilisant la mousse métallique à structure cellulaire périodique sont relativement rares.

Actuellement, la mousse métallique à topologie stochastique est souvent fabriquée par les méthodes de fabrication conventionnelles, telles que la méthode d'électrodéposition, la méthode de métallurgie des poudres, la méthode de moulage à la cire perdue et la méthode de moulage par infiltration, etc. Cependant, la structure morphologique de la mousse métallique est difficile à contrôler par ces méthodes de fabrication. Lorsqu'on parle de la fabrication avancée, la fabrication additive offre une possibilité de la fabrication rapide et précise de la mousse métallique avec une

structure cellulaire périodique en fonction du modèle de personnalisation ou d'optimisation. Ce genre de mousse métallique à structure cellulaire périodique est prometteur, permettant d'être utilisée pour renforcer/améliorer le comportement thermique du MCP. Ainsi, les performances thermiques du MCP incorporé dans la mousse métallique, fabriquée par impression 3D (donc un MCP composite), sont étudiées dans ce mémoire de thèse de doctorat.

En raison des impacts de l'épuisement progressif des combustibles fossiles et des effets de serre causés par les émissions de dioxyde de carbone, l'énergie a devenu un vrai problème de plus en plus important ces dernières années. Les chercheurs ont porté une attention particulière au développement des ressources énergétiques renouvelables, dans lesquelles le stockage d'énergie thermique (SET) joue un rôle essentiel. Grâce à la forte densité de stockage d'énergie et à la bonne stabilité thermique, le matériau à changement de phase (MCP) est largement utilisé dans les systèmes SET, tels que l'énergie solaire, la récupération de la chaleur résiduelle et les bâtiments économiques en énergie. Actuellement, le composite mousse métallique/MCP pour le stockage d'énergie thermique devient graduellement un sujet d'actualité.

Avec la technique de l'électronique, une grande quantité de chaleur peut être générée par les appareils électroniques. La température de fonctionnement peut réduire directement la durée de vie des appareils électroniques. La dissipation de la chaleur des appareils électroniques et la réduction de monté en température pendant le fonctionnement ont devenu un défi important dans le domaine de l'ingénierie électronique. Par conséquent, la gestion thermique est un problème majeur pendant leur utilisation. Les matériaux à changement de phase (MCP) peuvent être largement utilisés dans le stockage de l'énergie thermique en raison de leur chaleur latente de fusion considérable. Le développement des nouveaux matériaux dans ce domaine de l'énergie est nécessaire pour la gestion thermique. Ces dernières années, de plus en plus de chercheurs ont mené des études sur l'application du MCP composite à la gestion thermique pour le refroidissement des composants électronique.

L'objectif de cette thèse est d'étudier, en utilisant la méthode expérimentale et numérique, les performances thermiques d'un composite à la base d'une mousse métallique + MCP pour le stockage d'énergie thermique et la gestion thermique. La mousse métallique à structure contrôlable a été conçue et fabriquée par la technique d'impression 3D. L'amélioration thermique du MCP à l'aide de mousse métallique imprimée en 3D a été proposée. Ensuite, nous avons étudié les effets des paramètres de structure de la mousse métallique sur le comportement thermique du MCP composite. En plus, les effets dû à la procédure de chauffage et des conditions de contact sur les caractéristiques de transfert de chaleur du MCP composite sont également mis en évidence afin de donner une première information utile pour la conception du stockage d'énergie thermique en ingénierie. Enfin, nous essayons d'utiliser une mousse métallique imprimée en 3D dans une unité de dissipateur thermique pour une future application potentielle.

2. Effets de la chaleur et des conditions de contact

2.1 Description du problème

La Fig. 6.1 montre le statut de contact du MCP composite utilisé dans le stockage d'énergie thermique. Pour faciliter l'assemblage, il peut y avoir un espace libre entre la mousse métallique et la paroi du mur chaud (épaisseur d'espace δ, voir fig. 6.1). L'espace peut être rempli par flux de MCP en phase liquide lorsque MCP fond après chauffage. La résistance thermique supplémentaire provoquée par l'espace δ peut avoir un effet significatif sur les performances de transfert de chaleur du MCP composite. Compte tenu des différents processus de traitement et d'assemblage, cet espace δ peut apparaître dans chaque paire de surfaces de contact. En outre, la position du chauffage de l'unité de stockage d'énergie thermique est différente pour les différentes applications. Par conséquent, l'effet de la condition de chauffage sur les caractéristiques de stockage d'énergie du MCP composite mérite une étude approfondie.

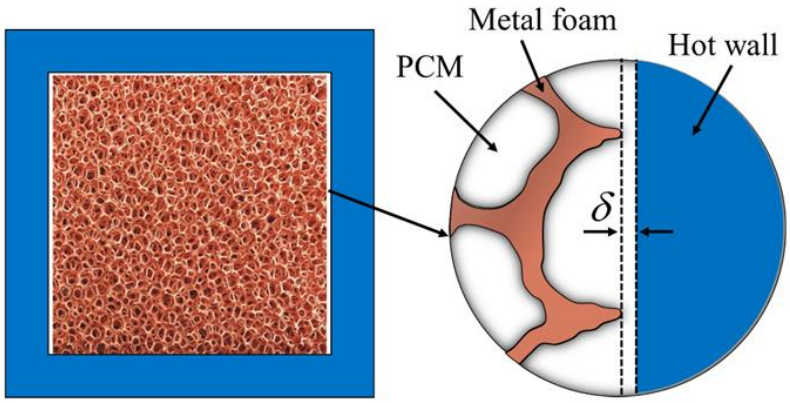

Fig. 6.1. Schéma de l'état des contacts du MCP composite

Pour étudier les effets combinés des conditions de chauffage et de contact sur le comportement thermique du MCP composite, neuf cas de conditions de chauffage et de contact ont été illustrés et résumés dans la Fig. 6.2. Par exemple, Cond. 1, 4 et 7 ont été utilisés pour étudier l'effet de la position de la chaleur (la paroi bleue a été chauffée à une température constante, et les autres parois ont été adiabatiques), et Cond. 4-6 ont été utilisés pour étudier l'effet de la condition de contact sur les performances thermiques lorsque les conditions de chauffage étaient les mêmes. Les dimensions des mousses métalliques sont les mêmes: $50\times50\,\mathrm{mm}^2$ pour ces neuf cas différents. Les espaces de contact δ sont de 0, 0,4 et 0,8 mm. Étant donné que la mousse métallique possède non seulement une conductivité thermique élevée mais également une grande surface spécifique, la mousse métalliques avec une porosité de 95% et une densité de pores de 5ppi a été choisie comme squelette métallique. Comme la paraffine peut stocker une grande quantité de chaleur par chaleur latente et largement appliquée dans le stockage d'énergie thermique, elle est donc utilisée comme Matériaux à Changement de Phase (MCP) dans cette étude.

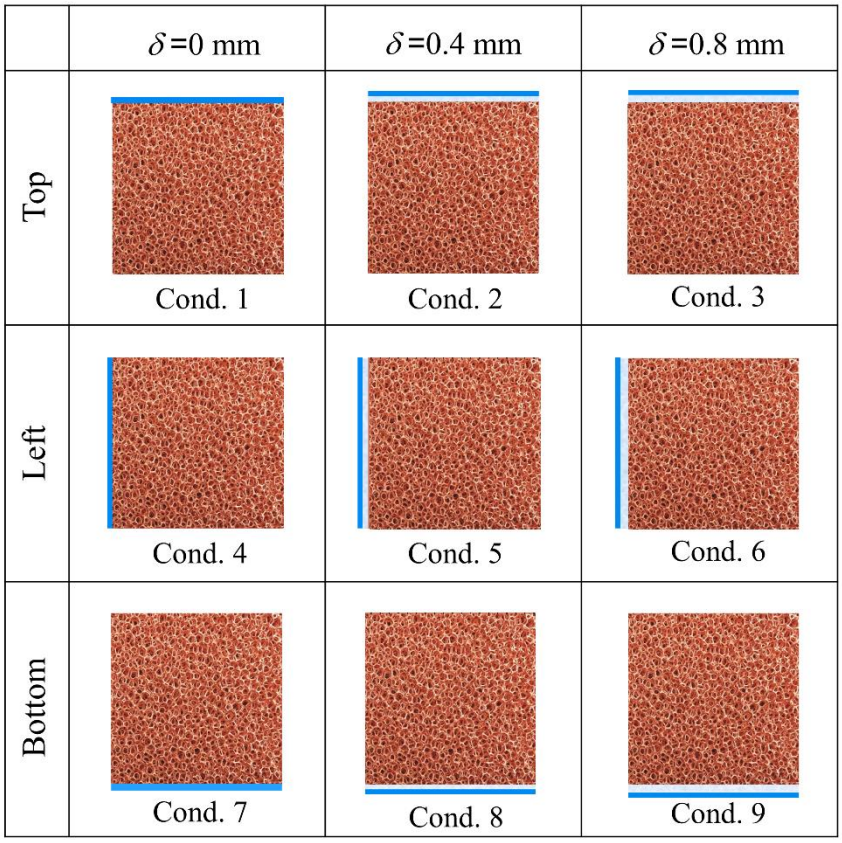

Fig. 6.2. Différentes conditions de chauffage et de contact

2.2 Méthode numérique

Nous avons choisi la méthode de la moyenne volumique pour simuler le transfert de chaleur à changement de phase dans les MCP composites. En se basant sur l'hypothèse d'un équilibre thermique local, un modèle d'équilibre peut être servi pour décrire le transfert de chaleur entre le MCP et le squelette métallique. Le modèle de Darcy-Brinkman-Forchheimer est choisi pour étudier l'effet de la mousse métallique sur le flux de MCP liquide. Sur la base des hypothèses et de la méthode ci-dessus, les équations continues, d'impulsion et d'énergie peuvent être données comme suit:

Équation continue:

$$\frac{\partial \rho_f}{\partial t} + \nabla \cdot (\rho_f \vec{U}) = 0 \qquad (1)$$

Équations de Momentum:

$$\frac{\rho_f}{\varphi}\frac{\partial u}{\partial t}+\frac{\rho_f}{\varphi^2}(\vec{U}\cdot\nabla)u=-\frac{\partial p}{\partial x}+\frac{\mu}{\varphi}\nabla^2 u-\left(\frac{\mu}{K}+\frac{C\rho_f\left|\vec{U}\right|}{\sqrt{K}}\right)u+S(u) \tag{2}$$

$$\frac{\rho_f}{\varphi}\frac{\partial v}{\partial t}+\frac{\rho_f}{\varphi^2}(\vec{U}\cdot\nabla)v=-\frac{\partial p}{\partial y}+\frac{\mu}{\varphi}\nabla^2 v-\left(\frac{\mu}{K}+\frac{C\rho_f\left|\vec{U}\right|}{\sqrt{K}}\right)v+\rho g\gamma(T-T_m)+S(v) \tag{3}$$

Les termes S(u) et S(v) dans les équations (2) et (3) sont les termes sources de la force d'amortissement, et sont définis comme les équations suivantes:

$$S(u)=-\frac{(1-\beta)^2}{\beta^3+\lambda}A_m u \tag{4}$$

$$S(v)=-\frac{(1-\beta)^2}{\beta^3+\lambda}A_m v \tag{5}$$

Où A_m est une constante de la zone de boue et fixée à 10^5, et λ est une petite constante égale à 10^{-3}. β est la fraction liquide à l'intérieur des pores et définie par:

$$\beta=\begin{cases}0 & T_f<T_{m1}\\ \left(T_f-T_{m1}\right)/\left(T_{m2}-T_{m1}\right) & T_{m1}<T_f<T_{m2}\\ 1 & T_f>T_{m2}\end{cases} \tag{6}$$

La relation entre β et φ peut être écrite comme suit:

$$\varphi=\varepsilon\cdot\beta \tag{7}$$

Où φ est la fraction liquide du composite, et ε est la porosité.

Équation énergétique pour MCP et mousse métallique:

$$\frac{\partial T}{\partial t}\left[\varepsilon\rho_f c_f+(1-\varepsilon)\rho_s c_s\right]+\varepsilon\rho_f c_f\left(\vec{U}\cdot\nabla\right)T=k_{eff}\nabla^2 T-\varepsilon\rho_f L\frac{\partial\beta}{\partial t} \tag{8}$$

La taille des pores d_p peut être déterminée de façon suivante, dont ω est la densité de pores:

$$d_p=\frac{22.4\times10^{-3}}{\omega} \tag{9}$$

La perméabilité *K* et le coefficient d'inertie *C* sont nécessaires pour le calcul du débit de liquide en milieu poreux, qui sont des paramètres complexes et difficiles à obtenir par le test expérimental. *K* et *C* sont ainsi déterminés en utilisant le modèle proposé:

$$\frac{K}{d_p} = 0.00073(1-\varepsilon)^{-0.224}\left[1.18\sqrt{\frac{1-\varepsilon}{3\pi}}\left(\frac{1}{1-e^{-((1-\varepsilon)/0.04)}}\right)\right]^{-1.11} \tag{10}$$

$$C = 0.00212(1-\varepsilon)^{-0.224}\left[1.18\sqrt{\frac{1-\varepsilon}{3\pi}}\left(\frac{1}{1-e^{-((1-\varepsilon)/0.04)}}\right)\right]^{-1.63} \tag{11}$$

Pour le modèle d'équilibre, la conductivité thermique effective du MCP composite est un paramètre indispensable pour simuler numériquement le transfert de chaleur. De nombreux modèles ont été utilisés pour déterminer les conductivités thermiques efficaces, cités dans la littérature bibliographique. Nous avons remarqué que le modèle théorique développé par Bhattacharya est très proche de la structure réelle de la mousse métallique et donc choisi dans cette étude. La conductivité thermique effective est calculée par:

$$k_{eff} = 0.35(\varepsilon k_f + (1-\varepsilon)k_s) + \frac{0.65}{(\frac{\varepsilon}{k_f} + \frac{1-\varepsilon}{k_s})} \tag{12}$$

2.3 MCP composite dans différentes conditions de chaleur et de contact

(a) Évolution du changement de phase du MCP composite

La Fig. 6.3 présente l'évolution du changement de phase du MCP composite sous Cond. 4-6 (voir fig. 6.2). L'interface solide-liquide est légèrement inclinée au stade de début de la fusion, ce qui est dû à l'effet de la convection naturelle. La fusion se poursuit avec la hausse de température, la paraffine liquide s'écoule vers le haut et entre en collision avec la paraffine solide à l'interface. Les diagrammes vectoriels montrent que la plus grande vitesse de fusion se trouve au voisinage de la face chaude

et de l'interface pendant le processus de fusion. La fusion du MCP composite dans la zone supérieure est plus rapide que celle de la zone inférieure et que l'interface solide-liquide est inclinée, ce qui résulte de la convection naturelle pendant le chauffage. Il peut être démontré que la convection naturelle joue un rôle dominant dans le processus de transfert de chaleur par changement de phase. On observe également qu'avec la même fraction liquide, la vitesse diminue lorsque l'intervalle de contact augmente. Ce phénomène indique que la convection naturelle peut être restreinte lorsque la taille de l'espace augmente. Par conséquent, le temps de fusion est plus long pour un espace de contact plus grand dans la condition de la même fraction liquide, par exemple, le temps de fusion de Cond. 6 est de 1387 s et se prolonge presque trois fois plus long que celui de Cond. 4 (492 s) avec la même fraction liquide de 80%.

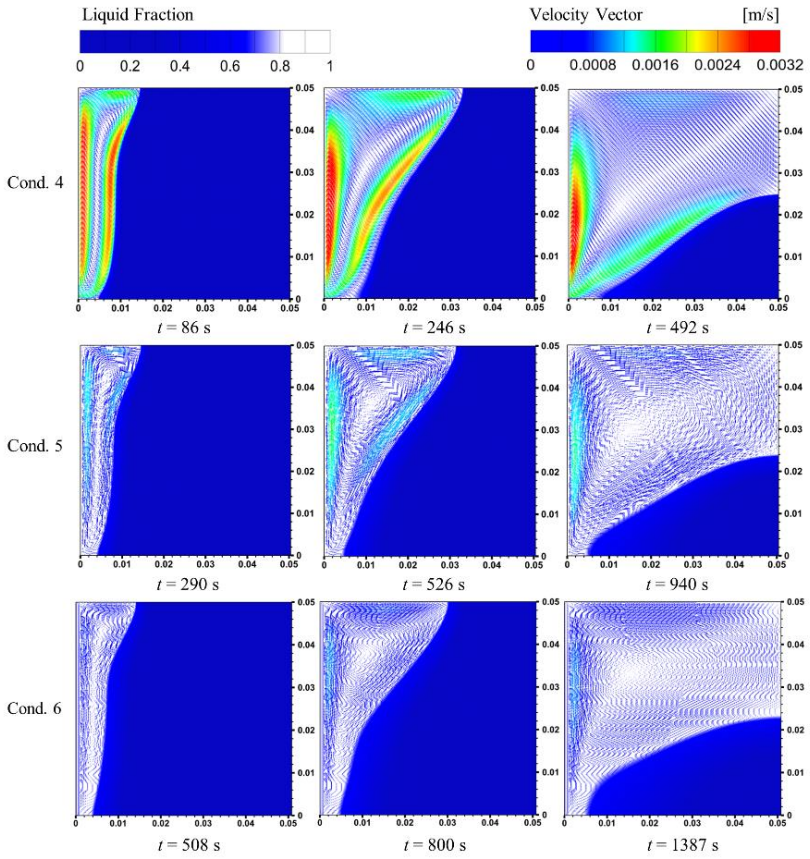

Fig. 6.3. Évolution du changement de phase pour les composites avec chauffage gauche à 20%, 40% et 80% de fraction liquide

(b) Taux de stockage de chaleur

Le taux moyen de stockage de chaleur est un critère essentiel pour estimer les performances thermiques du MCP composite, défini par l'unité de temps par masse du MCP composite qui stocke l'énergie dans l'ensemble du processus de fusion : W/kg. Le taux moyen de stockage de chaleur du MCP composite dans neuf conditions différentes est résumé et comparé dans la Fig. 6.4. On constate que:

1, le taux de stockage de chaleur avec chauffage à gauche (en rouge) et en bas (en vert) diminue en fonction de l'intervalle de contact δ, plus δ est importante, moins ce taux est élevé, ce qui est compréhensible du fait de la convection naturelle.

2, ce taux avec chauffage par le haut (en bleu) reste quasi inchangé (environ 120 W/kg) quelle que soit l'intervalle de contact δ entre 0 et 0,8 mm. Il parait que la condition de contact a un léger effet sur le comportement thermique du composite dans lequel le transfert de chaleur est dominé par la conduction thermique.

Il est à noter, à partir des résultats ci-dessus, que l'influence des conditions de chauffage et de contact sur le taux de stockage thermique n'est pas négligeable, le meilleur taux de stockage de chaleur est bien entendu ceux qui n'ont pas de l'espace de contact, δ = 0 mm.

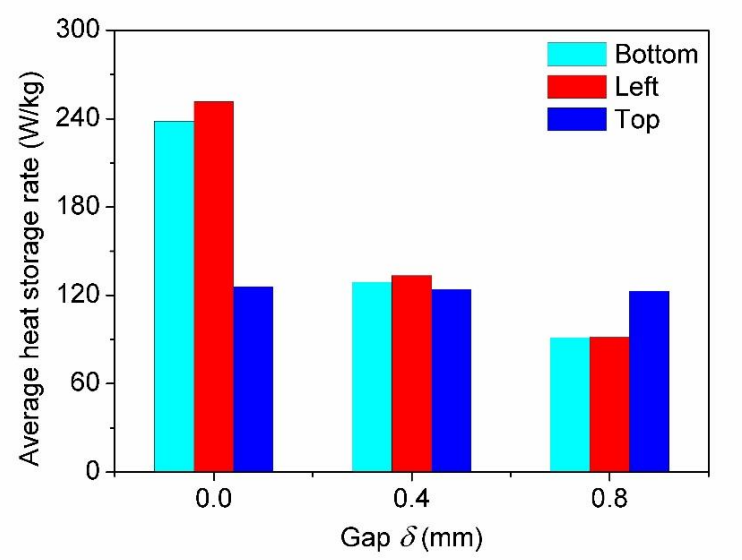

Fig. 6.4. Comparaison du taux moyen de stockage de chaleur en fonction de direction de chauffage et de l'intervalle de contact δ

3. Mousse métallique MCP composite fabriquée par impression 3D

3.1 Fabrication de la mousse métallique

L’avantage de la mousse métallique fabriquée par impression 3D est sa bonne contrôlabilité de la forme et de la taille. De plus, avec le développement de matériaux de fabrication additive, l'impression 3D présente un grand potentiel pour la fabrication de mousse métallique avec divers matériaux, tels que l'alliage d'aluminium, l'alliage de cuivre, l'alliage de titane et l'acier inoxydable, etc. Dans la présente étude, la mousse métallique a été fabriquée par l’alliage d'aluminium à haute conductivité thermique par fusion sélective au laser (FSL), une des méthodes de l’impression 3D, comme le montre la Fig. 6.5. La longueur et l'épaisseur du ligament métallique dans la mousse métallique sont respectivement *l* et *a*.

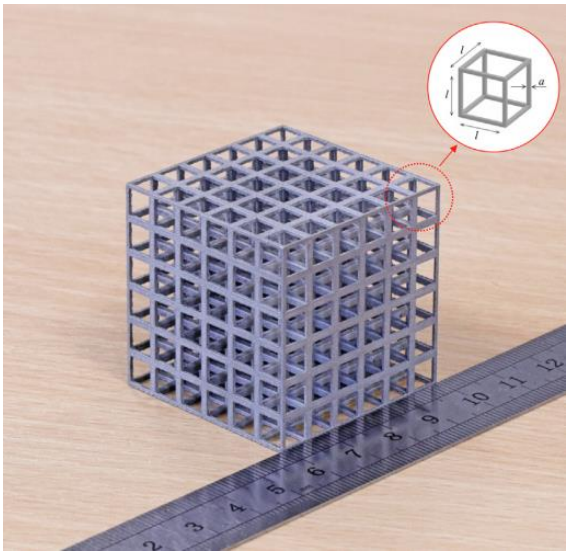

Fig. 6.5. Mousse métallique fabriquée par impression 3D

3.2 Procédure expérimentale

Afin d’étudier la performance thermique, nous avons réalisé une série de mesures expérimentales au sein de notre laboratoire, permettant de retracer la variation de température et l'évolution de la fusion. Le montage expérimental est présenté dans la

Fig. 6.6. La mousse métallique/paraffine MCP composite de taille $40 \times 40 \times 40$ mm est utilisée comme échantillon d'essai, le composite est préparé par imprégnation de la paraffine dans une mousse d'aluminium. Pour comparaison, nous avons aussi préparé une paraffine cubique pure de la même taille. Le matériau isolant (mousse de polyuréthane avec conductivité de 0,02 W/m K) est employé afin d'envelopper le récipient en plexiglas pour minimiser la perte de chaleur. Cependant les dimensions intérieures de la cavité isolante étaient basées sur la taille extérieure du récipient en plexiglas. Nous avons constaté que le matériau de l'isolation joue un rôle significatif sur l'évolution de la fusion du MCP après avoir fait quelques tests. Le plexiglas de conductivité thermique relativement faible (0,2 W/m K) a été recommandé. Ainsi, le conteneur d'enceinte rectangulaire choisi est en plexiglas d'une épaisseur de 3 mm. Un espace d'environ 5 mm entre la face supérieure du MCP et la surface interne du plexiglas est donné pour l'expansion volumique de la paraffine pendant le processus de changement de phase. Quatre petits trous ronds sont percés à travers la paroi supérieure de plexiglas, pour relâcher la pression dans le conteneur de l'enceinte ainsi pour la fixation des fils de thermocouples et de chauffage. La face avant de la cavité d'isolation est retirée pendant environ 20 s pour tracer l'interface de fusion instantanée à un intervalle de temps sélectionné. Les températures à différents endroits sont enregistrées toutes les secondes via un enregistreur informatisé pour une étude plus approfondie par la suite.

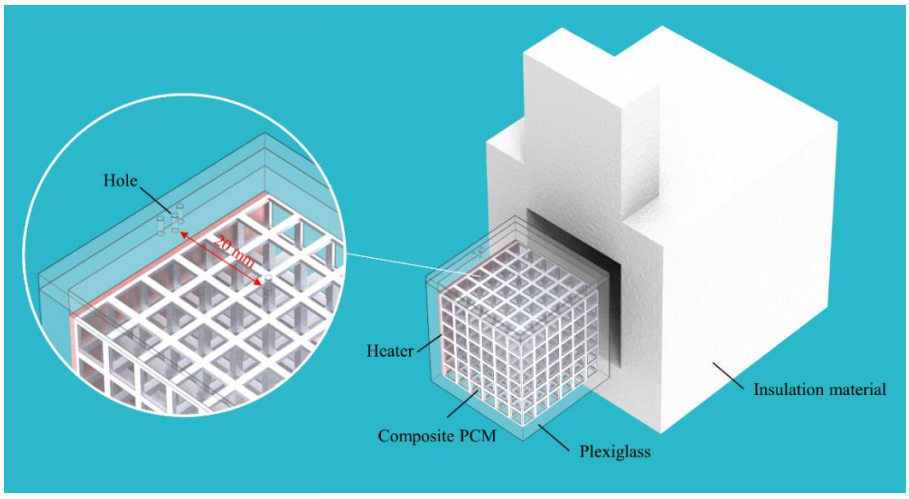

Fig. 6.6. Illustration schématique du montage expérimental

3.3 Amélioration de la performance thermique du MCP

La Fig. 6.7 montre les résultats expérimentaux de l'interface de fusion de la paraffine pure à trois instants : 15 min, 25 min et 35 min. On peut voir que l'interface de fusion est légèrement tordue à 15 min, ce qui indique que la convection naturelle et la conduction thermique ont un effet global sur le transfert de chaleur de fusion. Lorsque la fusion progresse au fur et à mesure, l'inclinaison de l'interface de fusion de la paraffine est de plus en plus évidente à 25 min, ce qui prouve que la convection naturelle se développe et domine progressivement le transfert de chaleur. Dans la dernière étape de la fusion à 35 min, la courbure de l'interface de fusion devient plus importante, et la fusion de la paraffine pure dans la partie « solide » est plus lente jusqu'à ce que la paraffine devienne complètement liquide après environ 68 minutes.

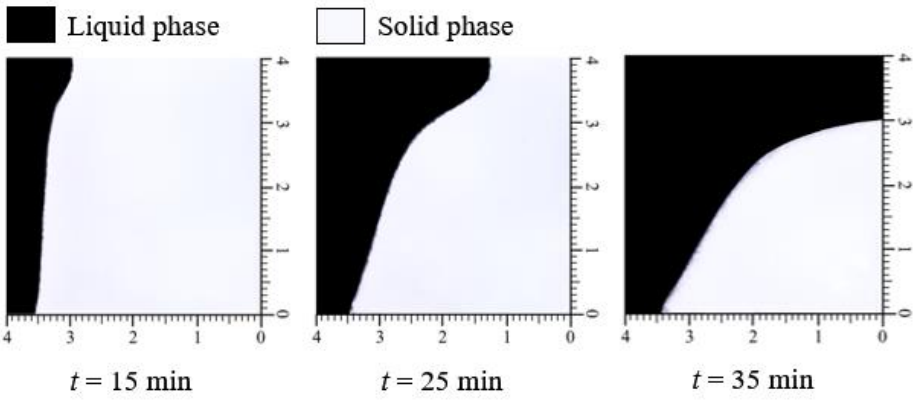

Fig. 6.7. Évolution de l'interface de fusion de la paraffine pure en fonction du temps

Maintenant, nous avons mis cette paraffine (MCP) dans la mousse métallique, l'évolution de l'interface de fusion de ce MCP composite est illustrée à la Fig. 6.8, également en fonction du temps à 15, 25 et 35 min. Au premier stade de la fusion à 15 min, l'interface de fusion du MCP composite est parallèle à la paroi chauffée, ce qui est expliqué par le fait que la conduction thermique joue un rôle important dans cette période du transfert de chaleur de fusion. La fusion continue, l'interface solide-liquide reste presque droite à 25 min, ce qui est différent par rapport à la fusion de la paraffine seule. Ce phénomène révèle que le transfert de chaleur de fusion au sein du MCP composite est encore dominé par la conduction thermique. L'interface de fusion

s'incline légèrement au stade de 35 min, ce qui représente que la convection naturelle au sein du MCP composite devient plus importante, et une forte influence de la convection naturelle sur l'évolution de la fusion du MCP composite est observée jusqu'à ce que la paraffine se fond complètement après environ 42 min.

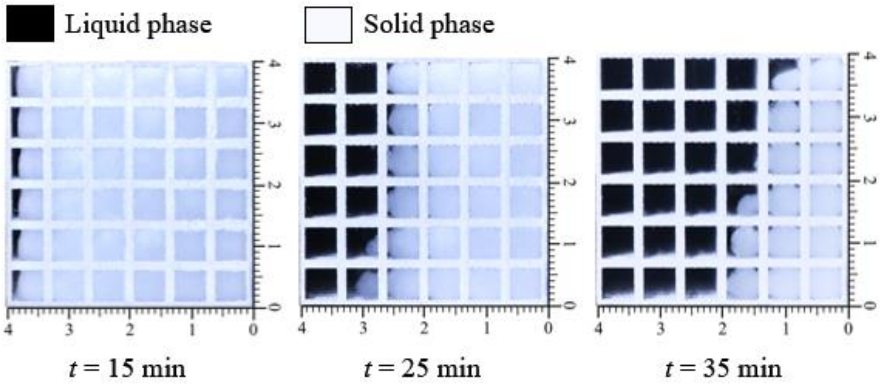

Fig. 6.8. Évolution de l'interface de fusion du MCP composite en fonction du temps

4. Paramètres de structure et les performances thermiques du MCP composite

4.1 Mousse métallique à structure cellulaire cubique

Une mousse métallique avec structure cellulaire cubique est schématisée dans la Fig. 6.9. Cette structure peut être fabriquée par la technologie de fabrication additive. Elle possède toutes les caractéristiques souhaitées d'une mousse métallique conventionnelle. La cellule élémentaire de la mousse métallique est idéale en forme de cube, dans laquelle des entretoises métalliques sont reliées ensemble à 90 ° à chaque sommet. La structure périodique de cette mousse est modélisée en 3D, avec la longueur ligamentaire l et la section transversale carrée du côté a (épaisseur). Avec ces deux paramètres géométriques l et a, la porosité ε de la mousse métallique peut être déterminée par:

$$\varepsilon = \frac{l^3 - 12a^2 l + 16a^3}{l^3} \tag{13}$$

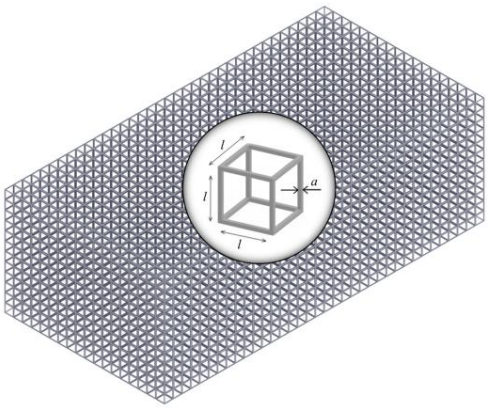

Fig. 6.9. Schéma d’une mousse métallique avec cellule périodique cubique.

4.2 Modèle numérique à l'échelle des pores

Pour réduire le temps de calcul, une mousse d'aluminium cubique avec les dimensions de $15\ \text{mm} \times 15\ \text{mm} \times 15\ \text{mm}$ a été sélectionnée, comme le montre la Fig. 6.10. Le comportement thermique des MCP composites avec différents paramètres de morphologie est étudié en deux états : stable et instable. De plus, les résultats obtenus sont comparés à ceux de la paraffine seule. En régime permanent (état stable), la conductivité thermique effective du MCP composite peut être calculée sur la base de l'équation de Fourier pour étudier afin de mettre en évidence les effets de la porosité et de la densité des pores sur la conductivité thermique effective des MCP composites. Les températures des parois gauche/droite sont respectivement de 290K/310K lorsque tous les autres murs sont isolés. Le flux thermique peut être obtenu en régime permanent, dans lequel il n'y a que la conduction thermique entre la paraffine et la mousse d'aluminium, car la paraffine est en phase solide entre 290K et 310K.

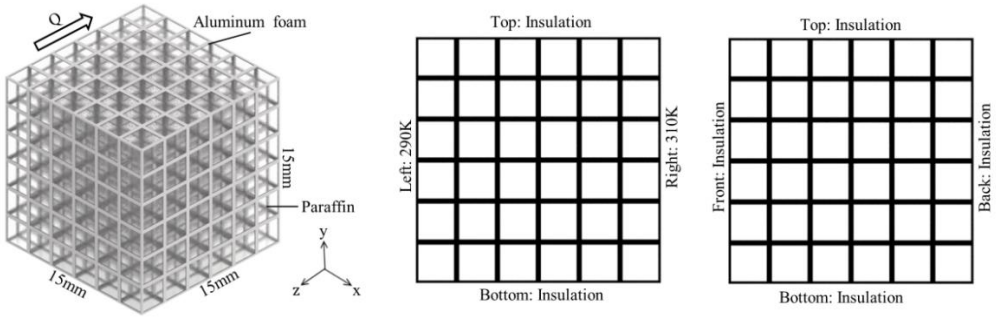

Fig. 6.10. Modèle numérique de MCP composite en état stable

Pour étudier l'évolution de la fusion et les caractéristiques de transfert de chaleur

du MCP composite au cours des processus de fusion, la simulation numérique est réalisée à l'état instable. Il est très important de prendre en compte l'influence combinée de la conduction de la chaleur et de la convection du transfert de chaleur entre la paraffine et la mousse d'aluminium. La paraffine d'une température initiale de 293,15 K est chauffée par la paroi chaude gauche d'une température constante de 350 K. De plus, les autres murs sont isolés. Afin d'obtenir les variations de température à l'intérieur du MCP composite pendant le processus de changement de phase, neuf points de surveillance de la température (T1, T2…T9) ont été sélectionnés dans les composites, comme le montre la Fig. 6.11.

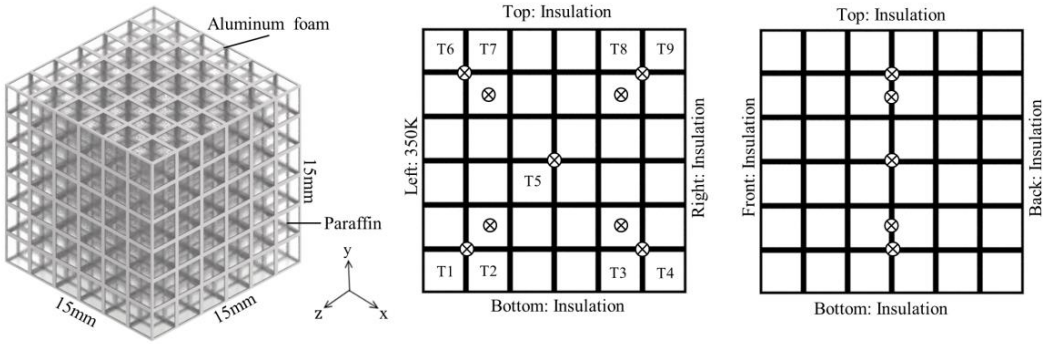

Fig. 6.11. Modèle numérique de MCP composite mousse en état instable

4.3 Comparaison des performances thermiques

(a) Temps de fusion totaux

Les temps de fusion totaux pour les MCP composites avec différents paramètres géométriques sont comparés dans la Fig. 6.12. On constate que le temps de fusion des MCP composites ayant la même densité de pores augmente avec la porosité. De plus, le temps de fusion total des MCP composites à 10ppi est inférieur à celui des MCP composites à 5ppi lorsque nous avons la même porosité des MCP composites. Le temps de fusion total de la paraffine seule sans la mousse d'aluminium est de 1216s. Les temps de fusion des MCP composites avec mousse d'aluminium de 5ppi et 10ppi sont considérablement réduits, respectivement à 6,6%-24,1% et 3,7 %-19,7% par rapport à ceux de la paraffine seule. Cela signifie que la densité des pores et la porosité ont une influence considérable sur le temps de fusion des MCP composites. Cela

indique également que le comportement thermique des MCP composites dépend de la densité des pores et de la porosité. Il est donc nécessaire de prendre en compte les effets combinés de la densité des pores et de la porosité, lorsque la mousse métallique est utilisée dans le stockage d'énergie thermique ou le système de gestion thermique. Dans tous les cas, le MCP composite avec 70% de porosité et 10ppi présente les meilleures performances thermiques. Cette étude peut fournir les informations importantes pour l'optimisation des performances thermiques du MCP composite.

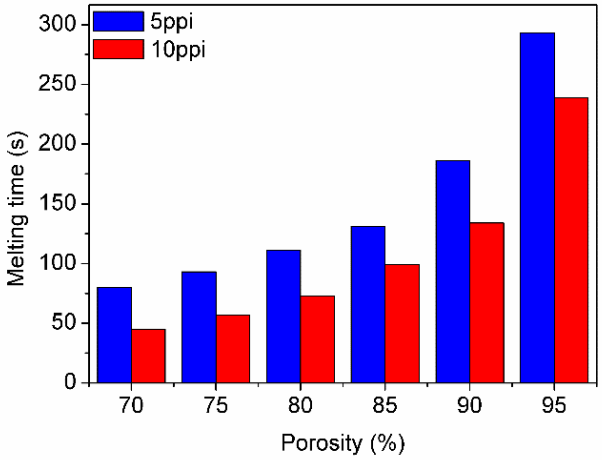

Fig. 6.12. Comparaison du temps de fusion des MCP composites avec différents paramètres géométriques

(b) Conductivité thermique effective

La Fig. 6.13 présente une comparaison des conductivités thermiques effectives des MCP composites avec différentes porosités et densités. Pour les porosités 70% et 95% avec une densité de pores de 10ppi, les conductivités thermiques efficaces sont de 24,6 W/(m K) et de 3,3 W/(m K), soit environ 123 et 17 fois plus que celle de la paraffine pure (0,2 W/m K). On remarque que la conductivité thermique effective du MCP composite est nettement améliorée. De plus, les conductivités thermiques effectives des MCP composites diminuent avec l'augmentation des porosités, alors que les conductivités thermiques effectives des composites de 5ppi et de 10ppi avec la même porosité sont presque identiques, ce qui signifie qu'il n'y a pas d'effet évident de la densité des pores sur la conductivité thermique effective. Les résultats numériques (nos calculs de 5ppi et 10 ppi) des MCP composites avec les porosités 90% et 95%

correspondent bien avec la prédiction théorique (modèles Xu et Bhattacharya et al). Les résultats numériques (nos calculs de 5ppi et 10 ppi) des MCP composites avec faibles porosités sont supérieurs aux résultats de prédiction théoriques (modèles Xu et Bhattacharya et al). Cela peut être dû au fait que ces modèles de prédiction sont recommandés pour calculer théoriquement les conductivités thermiques efficaces des composites avec une porosité supérieure à 90%, ce qui entraîne un écart de la simulation numérique lors de nos calculs sur une porosités inférieure à 90%.

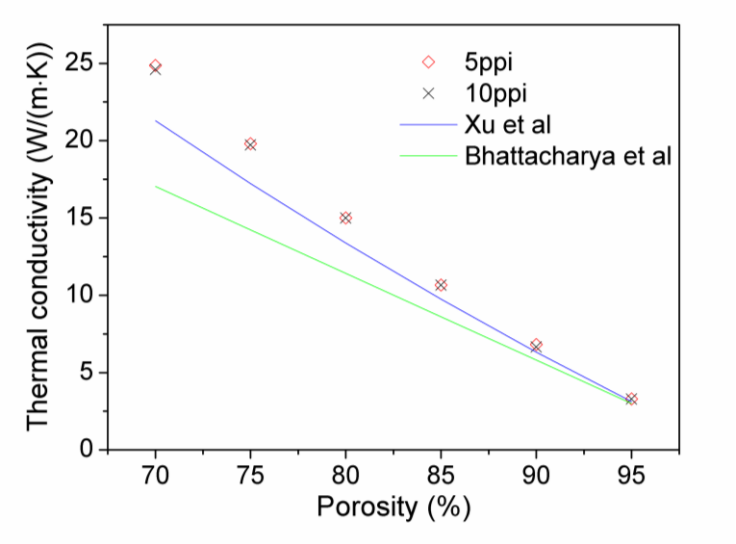

Fig. 6.13. Comparaison de nos calculs de 5ppi et 10 ppi
et prédiction théorique selon les modèles Xu, Bhattacharya et al

5. Dissipateur thermique à base de MCP

5.1 Échantillon d'essai

La mousse métallique à structure cellulaire cubique peut être développée pour être utilisée comme par exemple un dissipateur thermique. La mousse métallique possède une structure de cellules unitaires cubiques, dans laquelle les ligaments métalliques de la mousse métallique se sont connectés à un angle de 90 °. La longueur et l'épaisseur du ligament métallique sont respectivement l et a. Selon l'équation 13, la porosité ε peut être calculée en fonction de la valeur de l et a. Sur la base du modèle conçu ci-dessus, un échantillon de dimensions $40\times40\times40$ mm^3 a été fabriqué par

impression 3D (la technique de fusion sélective au laser FSL), comme illustré par la Fig. 6.14. L'alliage d'aluminium est choisi comme dissipateur thermique en raison de sa conductivité thermique élevée, de sa faible densité et coût, de sa résistance à la corrosion et de sa large utilisation dans le domaine de l'industrie électronique. Dans cette étude, nous étudions les effets de la mousse métallique et son MCP composite comme dissipateur thermique lors d'un appareil électronique sur leurs performances thermiques.

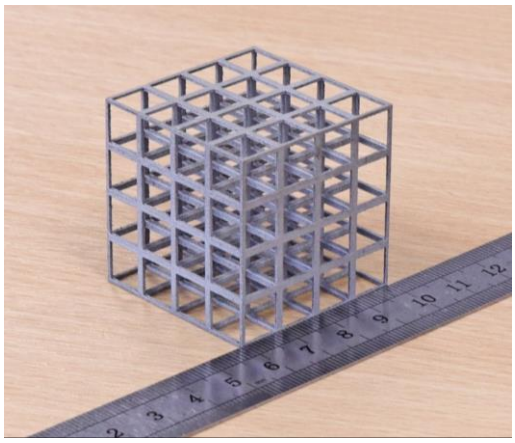

Fig. 6.14. Mousse métallique imprimée en 3D et utilisée comme dissipateur thermique

La coupe transversale de la section du montage avec l'échantillon est présentée sur la Fig. 6.15. Le bloc d'isolation à faible conductivité thermique est utilisé pour enfermer le dissipateur afin de réduire la perte de chaleur. Le dissipateur avec une épaisseur de paroi de 2 mm est constitué d'une plaque d'aluminium (AL-T6-6061). Une plaque chauffante de $40 \times 40 \times 1$ mm^3 est utilisée pour simuler la chaleur générée par le composant électronique. Une couche de graisse thermique est appliquée entre le dissipateur et le composant chauffant pour réduire la résistance thermique de contact. La mousse métallique et le MCP sont placés dans la cavité du dissipateur thermique. Pour éviter l'influence de la masse de MCP sur le comportement thermique des dissipateurs, la masse de paraffine remplie dans les dissipateurs est identique de 40 g pour toutes les expériences. Une plaque en plexiglas est aussi utilisée en haut du dissipateur pour observer l'évolution d'essais, et aussi pour fixer les thermocouples avec deux petits trous ronds percés à travers la plaque de plexiglas.

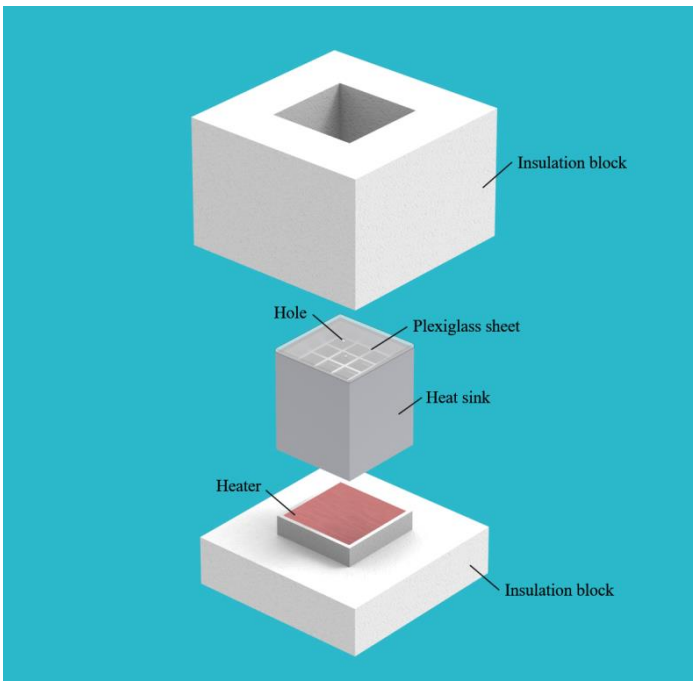

Fig. 6.15 Coupe transversale du montage et l'échantillon d'essai

5.2 Performances thermiques des dissipateurs

La température de base du dissipateur thermique agit comme la température maximale admissible du composant électronique. Compte tenu de la température de fonctionnement admissible des appareils électroniques, la température critique de la base du dissipateur est une constante, telles que 60 ℃ ou 70 ℃ selon la norme des produits, pour garantir l'efficacité de fonctionnement et la fiabilité des appareils électroniques. Ainsi, le temps nécessaire pour atteindre la température critique peut refléter les performances de gestion thermique du dissipateur thermique, est donc un paramètre principal d'évaluation de l'effet de dissipateur thermique.

La Fig. 6.16 montre une comparaison de la variation de température en fonction du temps, pour un dissipateur simple (sans MCP et mousse métallique), un dissipateur avec MCP, et un dissipateur avec composite (MCP+mousse métallique) avec une puissance de chauffage à 8 W. Les valeurs moyennes sont prises par les thermocouples TC#3, TC#4 et TC#5. Tous les essais sont réalisés dans les mêmes conditions expérimentales afin que la comparaison soit correcte. On sait bien que la température ambiante est d'environ 20 ℃ et la température de fonctionnement admissible d'un

appareil électronique est supposée à 70 ℃.

La comparaison de performance thermique pour (1) un dissipateur simple (sans MCP et mousse métallique), (2) un dissipateur avec MCP et (3) MCP composite; est illustrée par la Fig. 6.16. La température du dissipateur simple augmente rapidement à 70 ℃ pour 667s; le temps de fonctionnement pris par le dissipateur avec MCP à la même température est de 2140 s, soit 3,2 fois plus que celui d'un dissipateur simple; en ce qui concerne MCP composite, le temps de chauffage à 70°C est encore mieux que celui de MCP, jusqu'à 4045 s, soit 1,9 fois plus que celui du MCP dissipateur et 6,1 fois que celui du dissipateur simple. Il est évident que l'utilisation du MCP améliore déjà la performance thermique du dissipateur, et le MCP composite met en évidence encore plus la performance thermique du dissipateur.

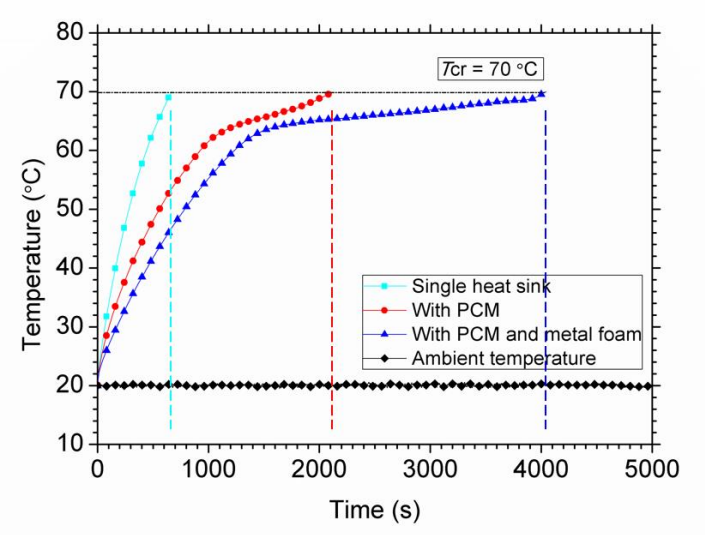

Fig. 6.16 Temps atteint à 70°C pour différents types de dissipateurs thermique

5.3 Amélioration des performances thermiques des dissipateurs

Pour étudier le rôle d'une mousse métallique dans l'amélioration thermique des dissipateurs à base de MCP, les temps nécessaires pour atteindre à des températures critiques de dissipateurs sont résumés dans les Figs. 6.17 (a) (b), les mousses métalliques possèdent cependant différente porosité ε, de 80% à 95%, pour trois niveaux de puissance de chauffage 8 W, 10 W et 12 W. Les températures critiques T_{cr} sélectionnées (60°C ou 70°C) représentent la température maximale admissible des composants électroniques pour assurer sa fiabilité opérationnelle, selon la norme des

produits. On observe à partir de ces résultats que le temps de fonctionnement des dissipateurs avec mousse métallique est plus long que celui des dissipateurs avec MCP seul. Par exemple lorsque T_{cr} = 70 °C et la puissance de chauffage est de 8W (voir Fig. 6.17(b)), le temps de fonctionnement d'un dissipateur avec une mousse métallique de porosité ε = 95% augmente de 50% par rapport à celle de dissipateur sans mousse métallique. Il révèle que la mousse métallique a un rôle positif non négligeable sur l'amélioration de la performance thermique d'un dissipateur thermique.

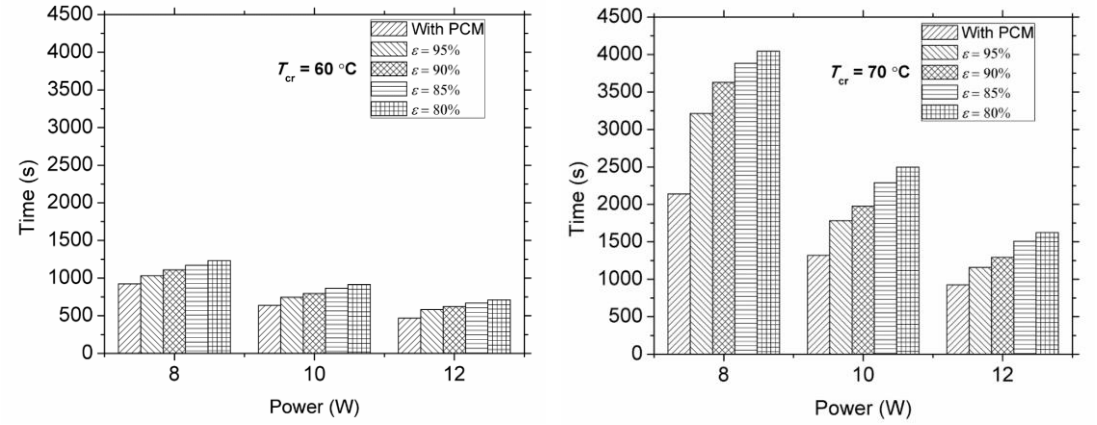

Fig. 6.17 Temps nécessaires par différents dissipateurs pour atteindre la température critique de: (a) 60 °C et (b) 70 °C. (selon différentes normes)

Une caractéristique intéressante est que pour les dissipateurs avec mousse métallique, plus la porosité est faible, plus le temps de fonctionnement du dissipateur est long, donc l'effet de dissipateur est meilleur. Il est évident que le dissipateur avec une mousse métallique de porosité à 80% prend plus de temps pour atteindre à une température critique par rapport à ceux qui ont les porosités plus importantes. Ce phénomène signifie que la diminution de la porosité peut améliorer la performance thermique du dissipateur. De plus, il ressort des résultats que l'augmentation de la densité de chaleur du composant électronique peut conduire à la réduction du temps de fonctionnement, par exemple pour atteindre à une température critique de 70°C, le temps de fonctionnement d'un dissipateur avec mousse métallique à porosité 80% est de 4045s, 2495 s et 1622 s, correspondant à une puissance de chauffage de 8 W, 10 W et 12 W, respectivement.

6. Conclusions générales

Le matériau à changement de phase (MCP) introduit dans une mousse métallique pour former un nouveau matériau composite s'avère être une méthode efficace pour améliorer les performances thermiques par rapport à un MCP seul. La mousse métallique permettant de renforcer la conductivité thermique joue un rôle important dans le MCP composite. L'objectif de cette thèse est d'étudier les performances thermiques d'un composite en base de mousse métallique+MCP avec les méthodes expérimentales et numériques. La mousse métallique possède une structure cellulaire cubique et fabriquée par impression 3D. Les résultats obtenus dans cette étude peuvent être servis pour l'application du MCP dans le stockage de l'énergie thermique et le système de gestion thermique.

Afin d'étudier les effets des conditions de chauffage et de contact sur la performance thermique des MCP composites dans le domaine de stockage d'énergie thermique, neuf cas de conditions de chauffage et de contacts ont été analysés. Il ressort des résultats que le mécanisme de transfert de chaleur est différent dans des conditions de chauffage différentes. Les conditions de contact ont une influence significative sur les performances thermiques du MCP composite dans des conditions de chauffage à gauche et à l'inférieure. Nous avons aussi constaté que les conditions de chauffage et de contact ont un effet combiné sur les performances thermique du MCP composite. Cette partie d'étude peut fournir des informations utiles pour le choix des conditions de chauffage et de contact du système de stockage d'énergie thermique en utilisant le MCP composite, comme par exemple le stockage d'énergie solaire thermique et le dispositif de stockage de chaleur latente.

Nous avons ensuite réalisé les tests expérimentaux pour étudier le transfert de chaleur du MCP incorporé dans une mousse métallique fabriquée par impression 3D. Les résultats obtenus ont montré que l'incorporation de mousse métallique à structure cellulaire cubique dans le matériau MCP (donc un composite) peut améliorer nettement le transfert thermique du MCP seul. Par exemple, le temps de fusion total

de la paraffine avec la mousse d'aluminium est réduit de 38% par rapport à MCP seul. Le rapport d'amélioration maximal du MCP composite atteint à 63%.

La méthode numérique à l'échelle des pores a été utilisée pour mettre en évidence les effets des paramètres de structure sur la performance thermique du MCP composite. Les résultats numériques ont montré que les effets de la mousse métallique sur les performances thermiques du MCP composite sont très significatifs. Par exemple, la conductivité thermique effective du MCP composite, utilisant une mousse métallique avec une porosité de 95% et 10ppi, peut être améliorée environ 17 fois de plus par rapport à celle de la paraffine seule. La porosité et la densité des pores de la mousse métallique ont aussi un effet évident sur le comportement thermique du composite MCP. Par exemple, pour un MCP composite utilisant la mousse métallique à porosité élevée ou à faible densité de pores, le temps de fusion est plus long par rapport au MCP composite avec la mousse métallique à faible porosité ou à haute densité de pores. Ceci est dû à l'effet combiné de la porosité et de la densité des pores sur le transfert de chaleur par la conduction et la convection au sein du composite.

Nous avons étudié à la fin de cette thèse une application potentielle : le dissipateur thermique. Les résultats montrent que la distribution de température est plus uniforme pour le dissipateur thermique avec de la mousse métallique. De plus, la porosité de la mousse métallique a une influence importante sur l'efficacité du dissipateur thermique à base de MCP. Le temps de fonctionnement des dissipateurs augmente lorsque la porosité de la mousse métallique diminue. Le niveau de puissance de chauffage affecte également la performance thermique des dissipateurs thermiques à base de MCP. L'augmentation du niveau de puissance peut réduire le temps de fonctionnement du dissipateur thermique.

Publications

International journal papers:

- **X.S. Hu,** X.L. Gong*,
  Pore-scale numerical simulation of the thermal performance for phase change material embedded in metal foam with cubic periodic cell structure
  Applied Thermal Engineering 151 (2019) 231-239

- **X.S. Hu**, F. Zhu, X.L. Gong*,
  Experimental and numerical study on the thermal behavior of phase change material infiltrated in low porosity metal foam
  Journal of Energy Storage 26 (2019) 101005

- **X.S. Hu**, X.L. Gong*,
  Experimental and numerical investigation on thermal performance enhancement of phase change material embedding porous metal structure with cubic cell
  Applied Thermal Engineering 175 (2020) 115337

- **X.S. Hu**, F. Zhu, X.L. Gong*,
  Numerical investigation of the effects of heating and contact conditions on the thermal charging performance of composite phase change material
  Journal of Energy Storage 30 (2020) 101444

- Feng ZHU, **Xusheng HU**, Xuecai WANG, Chuan ZHANG, Xiaolu GONG*
  Experimental and numerical investigation of the melting process of aluminum foam/paraffin composite with low porosity
  Numerical Heat Transfer Part A 77 (2020) 998-1013.

- **X.S. Hu**, X.L. Gong*,
  Experimental study on the thermal response of PCM-based heat sink using structured porous material fabricated by 3D printing
  Case Studies in Thermal Engineering 24 (2021) 100844.

References

[1] B. Sosnick, Process for making foamlike mass of metal, U.S. Patent 2434775,1948.

[2] E.J. Cookson, D.E. Floyd, A.J. Shih, Design, manufacture, and analysis of metal foam electrical resistance heater, International Journal of Mechanical Sciences, 48(11) (2006) 1314-1322.

[3] L.Q. Ma, D.P. He, Fabrication and pore structure control of new type aluminum foams, Chinese journal of materials research, 8(1) (1994) 11-17.

[4] K. Boomsma, D. Poulikakos, F. Zwick, Metal foams as compact high performance heat exchangers, Mechanics of Materials, 35(12) (2003) 1161-1176.

[5] E. Furman, A. Finkelstein, M. Cherny, Permeability of Aluminium Foams Produced by Replication Casting, Metals, 3(1) (2012) 49-57.

[6] A. Mustaffar, D. Reay, A. Harvey, The melting of salt hydrate phase change material in an irregular metal foam for the application of traction transient cooling, Thermal Science and Engineering Progress, 5 (2018) 454-465.

[7] A. Ejlali, A. Ejlali, K. Hooman, H. Gurgenci, Application of high porosity metal foams as air-cooled heat exchangers to high heat load removal systems, International Communications in Heat and Mass Transfer, 36(7) (2009) 674-679.

[8] O. Losito, An Analytical Characterizzation of Metal Foams for Shielding Applications, PIERS Online, 4(8) (2008) 805-810.

[9] J. Hohe, V. Hardenacke, V. Fascio, Y. Girard, J. Baumeister, K. Stöbener, J. Weise, D. Lehmhus, S. Pattofatto, H. Zeng, H. Zhao, V. Calbucci, F. Rustichelli, F. Fiori, Numerical and experimental design of graded cellular sandwich cores for multi-functional aerospace applications, Materials & Design, 39 (2012) 20-32.

[10] M. Odabaee, K. Hooman, Application of metal foams in air-cooled condensers for geothermal power plants: An optimization study, International Communications in Heat and Mass Transfer, 38(7) (2011) 838-843.

[11] G.F. Yang, J.S. Song, H.Y. Kim, S.K. Joo, Metal Foam as Positive Electrode Current Collector for LiFePO4-Based Li-Ion Battery, Japanese Journal of Applied Physics, 52(10S) (2013) 10MB13.

[12] P.S. Liu, H.B. Qing, H.L. Hou, Primary investigation on sound absorption performance of highly porous titanium foams, Materials & Design, 85 (2015) 275-281.

[13] I. Dincer, Renewable energy and sustainable development: a crucial review, Renewable & Sustainable Energy Reviews, 4 (2000) 157-175.

[14] E. Cuce, D. Harjunowibowo, P.M. Cuce, Renewable and sustainable energy saving strategies for greenhouse systems: A comprehensive review, Renewable and Sustainable Energy Reviews, 64 (2016) 34-59.

[15] P. Zhang, X. Xiao, Z.W. Ma, A review of the composite phase change materials: Fabrication, characterization, mathematical modeling and application to performance enhancement, Applied Energy, 165 (2016) 472-510.

[16] Z.X. Liu, Z. Yu, T.T. Yang, D. Qin, S.S. Li, G.Q. Zhang, F. Haghighat, M.M. Joybari, A review on macro-encapsulated phase change material for building envelope applications, Building and Environment, 144 (2018) 281-294.

[17] N.I. Ibrahim, F.A. Al-Sulaiman, S. Rahman, B.S. Yilbas, A.Z. Sahin, Heat transfer

enhancement of phase change materials for thermal energy storage applications: A critical review, Renewable & Sustainable Energy Reviews, 74 (2017) 26-50.
[18] Z.A. Qureshi, H.M. Ali, S. Khushnood, Recent advances on thermal conductivity enhancement of phase change materials for energy storage system: A review, International Journal of Heat and Mass Transfer, 127 (2018) 838-856.
[19] J.P. Veale, Investigation of the behaviour of open cell aluminum foam (Master thesis), University of Massachusetts Amherst, 2014.
[20] P. Liu, Introduction to porous materials, 2th ed., Beijing, Tsinghua University Press, 2012.
[21] F. Zhu, Experimental and numerical study of metal foam composite in innovative application of thermal ennergy storage (P.h.D thesis), University of Technology of Troyes, 2017.
[22] C. Zhang, Aluminum foams composite:elaboration and thermal propoties for energy storage (P.h.D thesis), University of Technology of Troyes, 2017.
[23] X. Wang, S. Xu, S. Zhou, W. Xu, M. Leary, P. Choong, M. Qian, M. Brandt, Y.M. Xie, Topological design and additive manufacturing of porous metals for bone scaffolds and orthopaedic implants: A review, Biomaterials, 83 (2016) 127-141.
[24] D. Jafari, W.W. Wits, The utilization of selective laser melting technology on heat transfer devices for thermal energy conversion applications: A review, Renewable and Sustainable Energy Reviews, 91 (2018) 420-442.
[25] C. Yan, L. Hao, A. Hussein, D. Raymont, Evaluations of cellular lattice structures manufactured using selective laser melting, International Journal of Machine Tools and Manufacture, 62 (2012) 32-38.
[26] B. Zalba, J.M. Marin, L.F. Cabeza, H. Mehling, Review on thermal energy storage with phase change: materials, heat transfer analysis and applications, Applied Thermal Engineering, 23(3) (2003) 251-283.
[27] J. Chen, S. Kang, J. E, Z. Huang, K. Wei, B. Zhang, H. Zhu, Y. Deng, F. Zhang, G. Liao, Effects of different phase change material thermal management strategies on the cooling performance of the power lithium ion batteries: A review, Journal of Power Sources, 442 (2019) 227228.
[28] I. Sarbu, A. Dorca, Review on heat transfer analysis in thermal energy storage using latent heat storage systems and phase change materials, International Journal of Energy Research, 43(1) (2018) 29-64.
[29] L.K. Liu, D. Su, Y.J. Tang, G.Y. Fang, Thermal conductivity enhancement of phase change materials for thermal energy storage: A review, Renewable & Sustainable Energy Reviews, 62 (2016) 305-317.
[30] X. Hu, F. Zhu, X. Gong, Experimental and numerical study on the thermal behavior of phase change material infiltrated in low porosity metal foam, Journal of Energy Storage, 26 (2019) 101005.
[31] N.R. Jankowski, F.P. McCluskey, A review of phase change materials for vehicle component thermal buffering, Applied Energy, 113 (2014) 1525-1561.
[32] A. Elgafy, K. Lafdi, Effect of carbon nanofiber additives on thermal behavior of phase change materials, Carbon, 43(15) (2005) 3067-3074.
[33] S. Ramakrishnan, X. Wang, J. Sanjayan, Effects of various carbon additives on the thermal storage performance of form-stable PCM integrated cementitious composites, Applied Thermal Engineering, 148 (2019) 491-501.

[34] C.J. Ho, J.Y. Gao, Preparation and thermophysical properties of nanoparticle-in-paraffin emulsion as phase change material, International Communications in Heat and Mass Transfer, 36(5) (2009) 467-470.
[35] K.P. Venkitaraj, S. Suresh, Effects of Al2O3, CuO and TiO2 nanoparticles son thermal, phase transition and crystallization properties of solid-solid phase change material, Mechanics of Materials, 128 (2019) 64-88.
[36] Z. Yin, Z. Huang, R. Wen, X. Zhang, B. Tan, Y.g. Liu, X. Wu, M. Fang, Preparation and thermal properties of phase change materials based on paraffin with expanded graphite and carbon foams prepared from sucroses, Rsc Advances, 6(97) (2016) 95085-95091.
[37] X. Wang, Q. Guo, Y. Zhong, X. Wei, L. Liu, Heat transfer enhancement of neopentyl glycol using compressed expanded natural graphite for thermal energy storage, Renewable Energy, 51 (2013) 241-246.
[38] S. Wu, T.X. Li, T. Yan, Y.J. Dai, R.Z. Wang, High performance form-stable expanded graphite/stearic acid composite phase change material for modular thermal energy storage, International Journal of Heat and Mass Transfer, 102 (2016) 733-744.
[39] T. Xu, Q. Chen, G. Huang, Z. Zhang, X. Gao, S. Lu, Preparation and thermal energy storage properties of D-Mannitol/expanded graphite composite phase change material, Solar Energy Materials and Solar Cells, 155 (2016) 141-146.
[40] H. Tian, W. Wang, J. Ding, X. Wei, M. Song, J. Yang, Thermal conductivities and characteristics of ternary eutectic chloride/expanded graphite thermal energy storage composites, Applied Energy, 148 (2015) 87-92.
[41] X. Xiao, P. Zhang, M. Li, Thermal characterization of nitrates and nitrates/expanded graphite mixture phase change materials for solar energy storage, Energy Conversion and Management, 73 (2013) 86-94.
[42] Z.G. Zhang, X.M. Fang, Study on paraffin/expanded graphite composite phase change thermal energy storage material, Energy Conversion and Management, 47(3) (2006) 303-310.
[43] X. Py, R. Olives, S. Mauran, Paraffin/porous-graphite-matrix composite as a high and constant power thermal storage material, International Journal of Heat and Mass Transfer, 44(14) (2001) 2727-2737.
[44] S. Pincemin, X. Py, R. Olives, M. Christ, O. Oettinger, Elaboration of Conductive Thermal Storage Composites Made of Phase Change Materials and Graphite for Solar Plant, Journal of Solar Energy Engineering, 130(1) (2008).
[45] X. Xiao, P. Zhang, M. Li, Experimental and numerical study of heat transfer performance of nitrate/expanded graphite composite PCM for solar energy storage, Energy Conversion and Management, 105 (2015) 272-284.
[46] Y.B. Tao, Y.-L. He, A review of phase change material and performance enhancement method for latent heat storage system, Renewable & Sustainable Energy Reviews, 93 (2018) 245-259.
[47] S.K. Saha, K. Srinivasan, P. Dutta, Studies on Optimum Distribution of Fins in Heat Sinks Filled With Phase Change Materials, Journal of Heat Transfer, 130(3) (2008).
[48] C.Z. Ji, Z. Qin, S. Dubey, F.H. Choo, F. Duan, Simulation on PCM melting enhancement with double-fin length arrangements in a rectangular enclosure induced by natural convection, International Journal of Heat and Mass Transfer, 127 (2018) 255-265.

[49] S. Gharbi, S. Harmand, S. Ben Jabrallah, Experimental comparison between different configurations of PCM based heat sinks for cooling electronic components, Applied Thermal Engineering, 87 (2015) 454-462.
[50] L.-L. Tian, X. Liu, S. Chen, Z.-G. Shen, Effect of fin material on PCM melting in a rectangular enclosure, Applied Thermal Engineering, 167 (2020) 114764.
[51] S. Tiari, S. Qiu, M. Mahdavi, Discharging process of a finned heat pipe–assisted thermal energy storage system with high temperature phase change material, Energy Conversion and Management, 118 (2016) 426-437.
[52] T. Sathe, A.S. Dhoble, Thermal analysis of an inclined heat sink with finned PCM container for solar applications, International Journal of Heat and Mass Transfer, 144 (2019) 118679.
[53] B. Kamkari, H. Shokouhmand, Experimental investigation of phase change material melting in rectangular enclosures with horizontal partial fins, International Journal of Heat and Mass Transfer, 78 (2014) 839-851.
[54] K.C. Nayak, S.K. Saha, K. Srinivasan, P. Dutta, A numerical model for heat sinks with phase change materials and thermal conductivity enhancers, International Journal of Heat and Mass Transfer, 49(11-12) (2006) 1833-1844.
[55] R. Baby, C. Balaji, Experimental investigations on phase change material based finned heat sinks for electronic equipment cooling, International Journal of Heat and Mass Transfer, 55(5-6) (2012) 1642-1649.
[56] S.F. Hosseinizadeh, F.L. Tan, S.M. Moosania, Experimental and numerical studies on performance of PCM-based heat sink with different configurations of internal fins, Applied Thermal Engineering, 31(17-18) (2011) 3827-3838.
[57] C. Zhang, F. Zhu, H. Badreddine, X. Gong, A Modified Kelvin Model for Thermal Performance Simulation of High Mechanical Property Open-Cell Metal Foams, Journal of Materials Science and Chemical Engineering, 03(07) (2015) 113-118.
[58] C.Y. Zhao, Review on thermal transport in high porosity cellular metal foams with open cells, International Journal of Heat and Mass Transfer, 55(13-14) (2012) 3618-3632.
[59] C.Y. Zhao, W. Lu, Y. Tian, Heat transfer enhancement for thermal energy storage using metal foams embedded within phase change materials (PCMs), Solar Energy, 84(8) (2010) 1402-1412.
[60] C.Y. Zhao, Z.G. Wu, Heat transfer enhancement of high temperature thermal energy storage using metal foams and expanded graphite, Solar Energy Materials and Solar Cells, 95(2) (2011) 636-643.
[61] K. Lafdi, O. Mesalhy, S. Shaikh, Experimental study on the influence of foam porosity and pore size on the melting of phase change materials, Journal of Applied Physics, 102(8) (2007).
[62] X. Xiao, P. Zhang, M. Li, Preparation and thermal characterization of paraffin/metal foam composite phase change material, Applied Energy, 112 (2013) 1357-1366.
[63] X. Yang, W. Wang, C. Yang, L. Jin, T.J. Lu, Solidification of fluid saturated in open-cell metallic foams with graded morphologies, International Journal of Heat and Mass Transfer, 98 (2016) 60-69.
[64] F. Zhu, C. Zhang, X. Gong, Numerical analysis on the energy storage efficiency of phase change material embedded in finned metal foam with graded porosity, Applied Thermal Engineering, 123 (2017) 256-265.

[65] A. Horibe, H. Jang, N. Haruki, Y. Sano, H. Kanbara, K. Takahashi, Melting and solidification heat transfer characteristics of phase change material in a latent heat storage vessel: Effect of perforated partition plate, International Journal of Heat and Mass Transfer, 82 (2015) 259-266.
[66] M.M.A. Khan, N.I. Ibrahim, I.M. Mahbubul, H.M. Ali, R. Saidur, F.A. Al-Sulaiman, Evaluation of solar collector designs with integrated latent heat thermal energy storage: A review, Solar Energy, 166 (2018) 334-350.
[67] D. Zhou, C.Y. Zhao, Y. Tian, Review on thermal energy storage with phase change materials (PCMs) in building applications, Applied Energy, 92 (2012) 593-605.
[68] R.J. Warzoha, A.S. Fleischer, Improved heat recovery from paraffin-based phase change materials due to the presence of percolating graphene networks, International Journal of Heat and Mass Transfer, 79 (2014) 314-323.
[69] N.L. Panwar, S.C. Kaushik, S. Kothari, Role of renewable energy sources in environmental protection: A review, Renewable and Sustainable Energy Reviews, 15(3) (2011) 1513-1524.
[70] W. Zhao, D.M. France, W. Yu, T. Kim, D. Singh, Phase change material with graphite foam for applications in high-temperature latent heat storage systems of concentrated solar power plants, Renewable Energy, 69 (2014) 134-146.
[71] A.M. Khudhair, M.M. Farid, A review on energy conservation in building applications with thermal storage by latent heat using phase change materials, Energy Conversion and Management, 45(2) (2004) 263-275.
[72] S.Y. Kee, Y. Munusamy, K.S. Ong, Review of solar water heaters incorporating solid-liquid organic phase change materials as thermal storage, Applied Thermal Engineering, 131 (2018) 455-471.
[73] Y. Tian, C.Y. Zhao, A review of solar collectors and thermal energy storage in solar thermal applications, Applied Energy, 104 (2013) 538-553.
[74] E. Oro, A. de Gracia, A. Castell, M.M. Farid, L.F. Cabeza, Review on phase change materials (PCMs) for cold thermal energy storage applications, Applied Energy, 99 (2012) 513-533.
[75] F. Cheng, R. Wen, Z. Huang, M. Fang, Y.g. Liu, X. Wu, X. Min, Preparation and analysis of lightweight wall material with expanded graphite (EG)/paraffin composites for solar energy storage, Applied Thermal Engineering, 120 (2017) 107-114.
[76] J. Prakash, H.P. Garg, G. Datta, A solar water heater with a built-in latent heat storage, Energy Conversion and Management, 25(1) (1985) 51-56.
[77] S.A. Kalogirou, Solar thermal collectors and applications, Progress in Energy and Combustion Science, 30(3) (2004) 231-295.
[78] R. Rabie, M. Emam, S. Ookawara, M. Ahmed, Thermal management of concentrator photovoltaic systems using new configurations of phase change material heat sinks, Solar Energy, 183 (2019) 632-652.
[79] X. Huang, G. Alva, Y. Jia, G. Fang, Morphological characterization and applications of phase change materials in thermal energy storage: A review, Renewable & Sustainable Energy Reviews, 72 (2017) 128-145.
[80] A. Sharma, V.V. Tyagi, C.R. Chen, D. Buddhi, Review on thermal energy storage with phase change materials and applications, Renewable & Sustainable Energy Reviews, 13(2) (2009) 318-345.

[81] G. Evola, L. Marletta, F. Sicurella, A methodology for investigating the effectiveness of PCM wallboards for summer thermal comfort in buildings, Building and Environment, 59 (2013) 517-527.
[82] M. Pomianowski, P. Heiselberg, Y. Zhang, Review of thermal energy storage technologies based on PCM application in buildings, Energy and Buildings, 67 (2013) 56-69.
[83] L. Royon, L. Karim, A. Bontemps, Optimization of PCM embedded in a floor panel developed for thermal management of the lightweight envelope of buildings, Energy and Buildings, 82 (2014) 385-390.
[84] B. Duraković, PCM-based building envelope system: innovative energy solutions for passive design. Switzerland: Springer; 2020.
[85] L. Royon, L. Karim, A. Bontemps, Thermal energy storage and release of a new component with PCM for integration in floors for thermal management of buildings, Energy and Buildings, 63 (2013) 29-35.
[86] M. Ahmad, A. Bontemps, H. Sallée, D. Quenard, Thermal testing and numerical simulation of a prototype cell using light wallboards coupling vacuum isolation panels and phase change material, Energy and Buildings, 38(6) (2006) 673-681.
[87] M.M. Farid, A.M. Khudhair, S.A.K. Razack, S. Al-Hallaj, A review on phase change energy storage: materials and applications, Energy Conversion and Management, 45(9-10) (2004) 1597-1615.
[88] F. Agyenim, N. Hewitt, The development of a finned phase change material (PCM) storage system to take advantage of off-peak electricity tariff for improvement in cost of heat pump operation, Energy and Buildings, 42(9) (2010) 1552-1560.
[89] M. M. Farid, R.M. Husian, An electrical storage heater using the phase-change method of heat storage, Energy Conversion and Management, 30(3) (1990) 219-230.
[90] F. Bruno, N.H.S. Tay, M. Belusko, Minimising energy usage for domestic cooling with off-peak PCM storage, Energy and Buildings, 76 (2014) 347-353.
[91] C. Wang, L. Hua, H. Yan, B. Li, Y. Tu, R. Wang, A Thermal Management Strategy for Electronic Devices Based on Moisture Sorption-Desorption Processes, Joule, 4(2) (2020) 435-447.
[92] A.L. Moore, L. Shi, Emerging challenges and materials for thermal management of electronics, Materials Today, 17(4) (2014) 163-174.
[93] W.Q. Li, Z.G. Qu, Y.L. He, Y.B. Tao, Experimental study of a passive thermal management system for high-powered lithium ion batteries using porous metal foam saturated with phase change materials, Journal of Power Sources, 255 (2014) 9-15.
[94] A. Hussain, I.H. Abidi, C.Y. Tso, K.C. Chan, Z. Luo, C.Y.H. Chao, Thermal management of lithium ion batteries using graphene coated nickel foam saturated with phase change materials, International Journal of Thermal Sciences, 124 (2018) 23-35.
[95] K. Lafdi, O. Mesalhy, A. Elgafy, Merits of employing foam encapsulated phase change materials for pulsed power electronics cooling applications, Journal of Electronic Packaging, 130(2) (2008).
[96] A. Bhattacharya, R.L. Mahajan, Finned Metal Foam Heat Sinks for Electronics Cooling in Forced Convection, Journal of Electronic Packaging, 124(3) (2002) 155-163.
[97] J. Li, G.P. Peterson, P. Cheng, Three-dimensional analysis of heat transfer in a micro-

heat sink with single phase flow, International Journal of Heat and Mass Transfer, 47(19-20) (2004) 4215-4231.
[98] F.L. Tan, C.P. Tso, Cooling of mobile electronic devices using phase change materials, Applied Thermal Engineering, 24(2-3) (2004) 159-169.
[99] M. Hodes, R.D. Weinstein, S.J. Pence, J.M. Piccini, L. Manzione, C. Chen, Transient Thermal Management of a Handset Using Phase Change Material (PCM), Journal of Electronic Packaging, 124(4) (2002) 419-426.
[100] Tauseef-ur-Rehman, H.M. Ali, Experimental investigation on paraffin wax integrated with copper foam based heat sinks for electronic components thermal cooling, International Communications in Heat and Mass Transfer, 98 (2018) 155-162.
[101] Z.-Q. Zhu, Y.-K. Huang, N. Hu, Y. Zeng, L.-W. Fan, Transient performance of a PCM-based heat sink with a partially filled metal foam: Effects of the filling height ratio, Applied Thermal Engineering, 128 (2018) 966-972.
[102] S.F. Tie, C.W. Tan, A review of energy sources and energy management system in electric vehicles, Renewable and Sustainable Energy Reviews, 20 (2013) 82-102.
[103] J.T. Zhao, Z.H. Rao, Y.T. Huo, X.J. Liu, Y.M. Li, Thermal management of cylindrical power battery module for extending the life of new energy electric vehicles, Applied Thermal Engineering, 85 (2015) 33-43.
[104] Z. Rao, Y. Huo, X. Liu, G. Zhang, Experimental investigation of battery thermal management system for electric vehicle based on paraffin/copper foam, Journal of the Energy Institute, 88(3) (2015) 241-246.
[105] N. Javani, I. Dincer, G.F. Naterer, G.L. Rohrauer, Modeling of passive thermal management for electric vehicle battery packs with PCM between cells, Applied Thermal Engineering, 73(1) (2014) 307-316.
[106] J. Yan, K. Li, H. Chen, Q. Wang, J. Sun, Experimental study on the application of phase change material in the dynamic cycling of battery pack system, Energy Conversion and Management, 128 (2016) 12-19.
[107] S. Al Hallaj, J.R. Selman, A novel thermal management system for electric vehicle batteries using phase-change material, Journal of the Electrochemical Society, 147(9) (2000) 3231-3236.
[108] N. Javani, I. Dincer, G.F. Naterer, B.S. Yilbas, Heat transfer and thermal management with PCMs in a Li-ion battery cell for electric vehicles, International Journal of Heat and Mass Transfer, 72 (2014) 690-703.
[109] D. Zou, X. Ma, X. Liu, P. Zheng, Y. Hu, Thermal performance enhancement of composite phase change materials (PCM) using graphene and carbon nanotubes as additives for the potential application in lithium-ion power battery, International Journal of Heat and Mass Transfer, 120 (2018) 33-41.
[110] W. Wu, W. Wu, S. Wang, Thermal optimization of composite PCM based large-format lithium-ion battery modules under extreme operating conditions, Energy Conversion and Management, 153 (2017) 22-33.
[111] J. Zhang, X. Li, F. He, J. He, Z. Zhong, G. Zhang, Experimental Investigation on Thermal Management of Electric Vehicle Battery Module with Paraffin/Expanded Graphite Composite Phase Change Material, International Journal of Photoenergy, (2017).
[112] M. Pan, W. Lai, Cutting copper fiber/paraffin composite phase change material

discharging experimental study based on heat dissipation capability of Li-ion battery, Renewable Energy, 114 (2017) 408-422.
[113] M. Pan, Y. Zhong, Experimental and numerical investigation of a thermal management system for a Li-ion battery pack using cutting copper fiber sintered skeleton/paraffin composite phase change materials, International Journal of Heat and Mass Transfer, 126 (2018) 531-543.
[114] Z. Wang, Z. Zhang, L. Jia, L. Yang, Paraffin and paraffin/aluminum foam composite phase change material heat storage experimental study based on thermal management of Li-ion battery, Applied Thermal Engineering, 78 (2015) 428-436.
[115] G. Zhang, W. Zhang, Y. Zhang, J. Zhang, Thermal characteristics of power battery based on copper foam/paraffin wax, Journal of Thermal Science and Technology, 12(1) (2013) 42-46.
[116] Z. Wang, X. Li, G. Zhang, Y. Lv, J. He, J. Luo, C. Yang, C. Yang, Experimental study of a passive thermal management system for three types of battery using copper foam saturated with phase change materials, Rsc Advances, 7(44) (2017) 27441-27448.
[117] W. Wu, X. Yang, G. Zhang, X. Ke, Z. Wang, W. Situ, X. Li, J. Zhang, An experimental study of thermal management system using copper mesh-enhanced composite phase change materials for power battery pack, Energy, 113 (2016) 909-916.
[118] A. Greco, X. Jiang, A coupled thermal and electrochemical study of lithium-ion battery cooled by paraffin/porous-graphite-matrix composite, Journal of Power Sources, 315 (2016) 127-139.
[119] G. Jiang, J. Huang, Y. Fu, M. Cao, M. Liu, Thermal optimization of composite phase change material/expanded graphite for Li-ion battery thermal management, Applied Thermal Engineering, 108 (2016) 1119-1125.
[120] E. Oró, L. Miró, M.M. Farid, V. Martin, L.F. Cabeza, Energy management and CO2 mitigation using phase change materials (PCM) for thermal energy storage (TES) in cold storage and transport, International Journal of Refrigeration, 42 (2014) 26-35.
[121] K. Azzouz, D. Leducq, D. Gobin, Enhancing the performance of household refrigerators with latent heat storage: An experimental investigation, International Journal of Refrigeration, 32(7) (2009) 1634-1644.
[122] E. Oró, L. Miró, M.M. Farid, L.F. Cabeza, Improving thermal performance of freezers using phase change materials, International Journal of Refrigeration, 35(4) (2012) 984-991.
[123] F. Wang, G. Maidment, J. Missenden, R. Tozer, The novel use of phase change materials in refrigeration plant. Part 2: Dynamic simulation model for the combined system, Applied Thermal Engineering, 27(17-18) (2007) 2902-2910.
[124] B. Gin, M.M. Farid, P.K. Bansal, Effect of door opening and defrost cycle on a freezer with phase change panels, Energy Conversion and Management, 51(12) (2010) 2698-2706.
[125] M. Cheralathan, R. Velraj, S. Renganarayanan, Performance analysis on industrial refrigeration system integrated with encapsulated PCM-based cool thermal energy storage system, International Journal of Energy Research, 31(14) (2007) 1398-1413.
[126] Y. Zhao, X. Zhang, X. Xu, Application and research progress of cold storage technology in cold chain transportation and distribution, Journal of Thermal Analysis

and Calorimetry, 139(2) (2019) 1419-1434.
[127] H. Tan, Y. Li, H. Tuo, M. Zhou, B. Tian, Experimental study on liquid/solid phase change for cold energy storage of Liquefied Natural Gas (LNG) refrigerated vehicle, Energy, 35(5) (2010) 1927-1935.
[128] B. Michel, P. Glouannec, A. Fuentes, P. Chauvelon, Experimental and numerical study of insulation walls containing a composite layer of PU-PCM and dedicated to refrigerated vehicle, Applied Thermal Engineering, 116 (2017) 382-391.
[129] X.H. Yang, Z.X. Guo, Y.H. Liu, L.W. Jin, Y.L. He, Effect of inclination on the thermal response of composite phase change materials for thermal energy storage, Applied Energy, 238 (2019) 22-33.
[130] G. Ferrer, A. Solé, C. Barreneche, I. Martorell, L.F. Cabeza, Corrosion of metal containers for use in PCM energy storage, Renewable Energy, 76 (2015) 465-469.
[131] X. Hu, F. Zhu, X. Gong, Numerical investigation of the effects of heating and contact conditions on the thermal charging performance of composite phase change material, Journal of Energy Storage, 30 (2020) 101444.
[132] V.V. Calmidi, Transport Phenomena in High Porosity Fibrous Metal Foams, University of Colorado,, 1998.
[133] A. Bhattacharya, V.V. Calmidi, R.L. Mahajan, Thermophysical properties of high porosity metal foams, International Journal of Heat and Mass Transfer, 45(5) (2002) 1017-1031.
[134] H. Zheng, C. Wang, Q. Liu, Z. Tian, X. Fan, Thermal performance of copper foam/paraffin composite phase change material, Energy Conversion and Management, 157 (2018) 372-381.
[135] T.D. Ngo, A. Kashani, G. Imbalzano, K.T.Q. Nguyen, D. Hui, Additive manufacturing (3D printing): A review of materials, methods, applications and challenges, Composites Part B: Engineering, 143 (2018) 172-196.
[136] A. Merabtine, N. Gardan, J. Gardan, H. Badreddine, C. Zhang, F. Zhu, X.-L. Gong, Experimental and numerical thermal analysis of open-cell metal foams developed through a topological optimization and 3D printing process, The European Physical Journal Applied Physics, 83(1) (2018) 10904.
[137] K.S. Gopalan, V. Eswaran, Numerical investigation of thermal performance of PCM based heat sink using structured porous media as thermal conductivity enhancers, International Journal of Thermal Sciences, 104 (2016) 266-280.
[138] G. Righetti, G. Savio, R. Meneghello, L. Doretti, S. Mancin, Experimental study of phase change material (PCM) embedded in 3D periodic structures realized via additive manufacturing, International Journal of Thermal Sciences, 153 (2020) 106376.
[139] X. Hu, X. Gong, Experimental and numerical investigation on thermal performance enhancement of phase change material embedding porous metal structure with cubic cell, Applied Thermal Engineering, 175 (2020) 115337.
[140] ANSYS fluent software package: user's manual, 18.0, 2017.
[141] J.L. Yang, L.J. Yang, C. Xu, X.Z. Du, Numerical analysis on thermal behavior of solid-liquid phase change within copper foam with varying porosity, Int. J. Heat Mass Transfer 84 (2015) 1008-1018.
[142] X. Yang, S. Feng, Q. Zhang, Y. Chai, L. Jin, T.J. Lu, The role of porous metal foam on the unidirectional solidification of saturating fluid for cold storage, Applied

Energy, 194 (2017) 508-521.
[143] S.S. Feng, M. Shi, Y.F. Li, T.J. Lu, Pore-scale and volume-averaged numerical simulations of melting phase change heat transfer in finned metal foam, International Journal of Heat and Mass Transfer, 90 (2015) 838-847.
[144] S. Yang, W. Tao, Heat transfer, 4th ed., Beijing, Higher Education Press, 2006.
[145] X. Xiao, P. Zhang, M. Li, Effective thermal conductivity of open-cell metal foams impregnated with pure paraffin for latent heat storage, International Journal of Thermal Sciences, 81 (2014) 94-105.
[146] W.Q. Li, Z.G. Qu, Y.L. He, W.Q. Tao, Experimental and numerical studies on melting phase change heat transfer in open-cell metallic foams filled with paraffin, Applied Thermal Engineering, 37 (2012) 1-9.
[147] X. Hu, X. Gong, Pore-scale numerical simulation of the thermal performance for phase change material embedded in metal foam with cubic periodic cell structure, Applied Thermal Engineering, 151 (2019) 231-239.
[148] W.Q. Xu, X.G. Yuan, Z. Li, Study on effective thermal conductivity of metal foam matrix composite phase change materials, Journal of Functional Materials, 40(8) (2009) 1329-1332,1337.
[149] A. Vassighi, M. Sachdev, Thermal and power management of integrated circuits, 2006 ed., Springer, New York, 2006.
[150] S. Mancin, A. Diani, L. Doretti, K. Hooman, L. Rossetto, Experimental analysis of phase change phenomenon of paraffin waxes embedded in copper foams, International Journal of Thermal Sciences, 90 (2015) 79-89.
[151] A. Arshad, H.M. Ali, W.M. Yan, A.K. Hussein, M. Ahmadlouydarab, An experimental study of enhanced heat sinks for thermal management using n-eicosane as phase change material, Applied Thermal Engineering, 132 (2018) 52-66.
[152] A. Arshad, H.M. Ali, S. Khushnood, M. Jabbal, Experimental investigation of PCM based round pin-fin heat sinks for thermal management of electronics: Effect of pin-fin diameter, International Journal of Heat and Mass Transfer, 117 (2018) 861-872.
[153] R. Baby, C. Balaji, Experimental investigations on thermal performance enhancement and effect of orientation on porous matrix filled PCM based heat sink, International Communications in Heat and Mass Transfer, 46 (2013) 27-30.
[154] S. Mahmoud, A. Tang, C. Toh, R. AL-Dadah, S.L. Soo, Experimental investigation of inserts configurations and PCM type on the thermal performance of PCM based heat sinks, Applied Energy, 112 (2013) 1349-1356.
[155] Rubitherm GmbH, Data sheet, Rubitherm Technologies GmbH, Berlin, Germany, 2018.
[156] X. Hu, X. Gong, Experimental study on the thermal response of PCM-based heat sink using structured porous material fabricated by 3D printing, Case Studies in Thermal Engineering, 24 (2021) 100844.

Xusheng HU

Doctorat : Matériaux, Mécanique, Optique, Nanotechnologie

Année 2021

Etude de performance thermique de mousse métallique et de MCP composite pour le stockage d'énergie thermique

Le but de cette thèse est d'étudier les performances thermiques d'une mousse métallique ainsi que de ses composites avec un matériau à changement de phase (MCP) en utilisant des méthodes expérimentales et numériques. La mousse métallique étudiée possède une structure cellulaire cubique. Les effets des conditions de contact et de chaleur sur le taux de stockage de chaleur dans le composite MCP sont d'abord simulés numériquement. Ensuite, la mousse métallique avec une structure cellulaire cubique est conçue et fabriquée par impression 3D. L'étude expérimentale permet par la suite d'observer l'évolution de la fusion du MCP introduit dans la mousse métallique. Parallèlement, une méthode numérique à l'échelle des pores est utilisée pour simuler les caractéristiques de transfert thermique dans le composite MCP. Il ressort des résultats que la mousse métallique d'enrobage peut réduire le temps total de fusion du matériau MCP. Compte tenu de l'influence des paramètres de morphologie de la mousse métallique, nous avons étudié numériquement le comportement thermique de la mousse métallique en variant la porosité et la densité de pores. La dernière partie de cette thèse consiste à explorer une application de la mousse métallique dans les dissipateurs thermiques à base de MCP. Les essais expérimentaux sur composite MCP permettent d'obtenir la réponse thermique des dissipateurs thermiques. Les effets de la porosité de la mousse métallique et de la puissance du chauffage sur la réponse thermique du dissipateur thermique sont également mis en évidence.

Mots clés : mousses métalliques – composites à matrice métallique – impression 3D – analyse thermique – chaleur, stockage – simulation, méthodes de.

Study of the Thermal Performance of Metal Foam and PCM Composite for Thermal Energy Storage

The aim of this Ph.D. thesis is to study the thermal performance of metal foam and phase change material (PCM) composite by using experimental and numerical methods, in which metal foam possesses a cubic cell structure and is fabricated by 3D printing technique. Firstly, the effects of contact and heat conditions on heat storage rate of PCM composite are investigated to provide theoretical guidance for the practical application of PCM composite in thermal energy storage (TES) system. Then the metal foam with a cubic cell structure is designed and fabricated by 3D printing. The experimental investigation is carried out to examine the melting evolution of PCM embedded in metal foam. Meanwhile, the pore-scale numerical method is also proposed and used to investigate heat transfer characteristics inside the PCM composite. It is found from the results that the embedding metal foam can short the total melting time of PCM. Considering the influence of morphology parameters of metal foam, the thermal behavior of metal foam with different porosities and pore densities is numerically studied. The last part of this thesis explores the application of metal foam in PCM based heat sink. The thermal response of heat sinks using PCM composite is obtained by experimental tests, including base temperature, temperature variation, operating time and enhancement ratio of operating time. Also, the effects of the porosity of metal foam and the power level of the heater on the thermal response of heat sink are investigated.

Keywords: metal foams – metallic composites – three-dimensional printing – thermal analysis – heat storage – simulation methods.

Thèse réalisée en partenariat entre :